MICROFLUIDIC SYSTEM TO DETECT SELECT DNA FRAGMENTS USING AGGLUTINATION PROCESS

by

Sumanpreet K. Chhina
Bachelor of Technology, Punjab Technical University, 2007

THESIS SUBMITTED IN PARTIAL FULFILLMENT OF
THE REQUIREMENTS FOR THE DEGREE OF

MASTER OF APPLIED SCIENCE

In the
School of Engineering Science

© Sumanpreet K. Chhina 2011

SIMON FRASER UNIVERSITY

Summer 2011

APPROVAL

Name:	**Sumanpreet K. Chhina**
Degree:	**Master of Applied Science**
Title of Thesis:	**Microfluidic system to detect select DNA fragments using agglutination process**

Examining Committee:

> **Chair:** **Michael Sjoerdsma, Lecturer, EIT.**
>
> School of Engineering Science

_____

Dr. Ash M Parameswaran, P. Eng
Senior Supervisor
Professor, School of Engineering Science

_____

Dr. Paul C. H. Li
Supervisor
Professor, Department of Chemistry

_____

Dr. Carlo Menon, P. Eng
Internal Examiner
Assistant Professor, School of Engineering Science

Date Defended/Approved: ___24 June 2011_____

Declaration of
Partial Copyright Licence

The author, whose copyright is declared on the title page of this work, has granted to Simon Fraser University the right to lend this thesis, project or extended essay to users of the Simon Fraser University Library, and to make partial or single copies only for such users or in response to a request from the library of any other university, or other educational institution, on its own behalf or for one of its users.

The author has further granted permission to Simon Fraser University to keep or make a digital copy for use in its circulating collection (currently available to the public at the "Institutional Repository" link of the SFU Library website <www.lib.sfu.ca> at: <http://ir.lib.sfu.ca/handle/1892/112>) and, without changing the content, to translate the thesis/project or extended essays, if technically possible, to any medium or format for the purpose of preservation of the digital work.

The author has further agreed that permission for multiple copying of this work for scholarly purposes may be granted by either the author or the Dean of Graduate Studies.

It is understood that copying or publication of this work for financial gain shall not be allowed without the author's written permission.

Permission for public performance, or limited permission for private scholarly use, of any multimedia materials forming part of this work, may have been granted by the author. This information may be found on the separately catalogued multimedia material and in the signed Partial Copyright Licence.

While licensing SFU to permit the above uses, the author retains copyright in the thesis, project or extended essays, including the right to change the work for subsequent purposes, including editing and publishing the work in whole or in part, and licensing other parties, as the author may desire.

The original Partial Copyright Licence attesting to these terms, and signed by this author, may be found in the original bound copy of this work, retained in the Simon Fraser University Archive.

Simon Fraser University Library
Burnaby, BC, Canada

ABSTRACT

This thesis investigates the design, fabrication, and testing of an easy-to-use, disposable and portable microfluidic system for DNA amplification detection; this is suitable for point-of-care testing (POCT) applications. The microfluidic system utilizes biotin-labelled DNA to agglutinate streptavidin-coated microspheres. The microfluidic system is designed to retain aggregates of cross-linked microspheres as opposed to single microspheres, indicating the detection of biotin-labelled DNA. The microfluidic platform is composed of a filter design and inlet/outlet reservoirs, which was fabricated using microfabrication techniques. This research demonstrates that the microfluidic system is an improvement on the current DNA detection technique utilizing particle agglutination. Such a system may in turn form the basis of future hand-held, compact, point-of-care biosensors for disease screening and identification.

Keywords: Point-of-care testing; Microfluidics; DNA amplification; Microsphere agglutination

DEDICATION

I would like to dedicate this thesis to my loving parents, Manjit Kaur and Harpal Singh Bath, without whom I would not be who I am today.

ACKNOWLEDGEMENTS

TABLE OF CONTENTS

LIST OF FIGURES

LIST OF TABLES

LIST OF ACRONYMS

bp   Base pair

ddH_2O Doubly distilled water

DI   De-ionized

DNA   Deoxyribonucleic acid

ds-DNA   Double stranded-DNA

DUV   254nm Deep Ultra Violet

IPA   Isopropyl Alcohol

LOC   Lab-on-chip

µ-TAS   Micro-Total Analysis System

PBS/BSA   Phosphate Buffered Saline with Bovine Serum Albumin

PCR   Polymerase Chain Reaction

PDMS   Polydimethylsiloxane

PMMA   Poly(methyl methacrylate)

POCT   Point-of-care-Testing

RNA   Ribonucleic acid

SFC   Scanning flow cytometry

TE   Tris-EDTA buffer

UV   Ultra Violet

1: INTRODUCTION

1.1 Point-of-care testing

In terms of testing, current laboratory medicine can be categorized into centralized testing and point-of-care testing (POCT) [1]. Centralized laboratory medicine provides high quality and reliability in results, as assured by the application of quality control programs and the expertise of highly trained staff [2]. On the other hand, POCT is executed by clinical staff (occasionally by the patient themselves), and it is performed at or near the site of patient care [3].

POCT protocol moves the testing and, perhaps, the first level of diagnosis closer to the patient. POCT has the benefit of decreasing the turnaround time, which directly affects the treatment decision. Furthermore, POCT does not require highly qualified personnel to perform the testing, but, at the same time, the quality and reliability of results totally depends upon the device employed [2]. Consequently, when deciding which part of testing should be performed in central laboratories and which part as POCT, a trade-off between quality and urgency should be considered. If satisfactory quality can be guaranteed, POCT is preferable because its timeliness and cost-effectiveness can lessen the burden to the health care system. It is also preferred in resource limited or remote settings, where the possibility of having a centralized laboratory is limited. In hospitals where a full-fledged centralized laboratory is operational, many test

results for critical diagnosis cannot be performed within minutes. To address this deficiency POCT is being explored for many diagnostic tests [2].

The advancement of lab-on-a-chip (LOC)[1] devices for biochemical laboratory analysis has caused a tremendous growth in the POCT over the past decade [4, 5]. Preliminary studies in LOC focused on developing micro-total analysis systems (μTAS), an analogous term to LOC. μTAS readily found applications in various biochemical analysis steps; for example, clinical analyses (blood glucose), proteomics analyses (proteins and peptides), DNA analyses (including nucleic acid sequence analysis), immunoassays[2], and forensic analyses [6-8]. In other words, μTAS/LOC is as an ideal technology for clinical diagnostics.

An early, fast, and sensitive detection of a disease condition is the fundamental goal of clinical diagnosis. The biochemical changes in a patient's body fluids (blood, urine, saliva) can serve as an indicator of organ dysfunction or damage before any noticeable microscopic cellular damages or other symptoms appears. Therefore, there has been a tremendous demand for easy-to-use, minimally invasive, low-cost clinical diagnostic chips that can provide fast and reliable results. Most POCT diagnostic applications have concentrated on detecting nucleotides and peptides that are early markers of disease [8-10]. For example, Zoiber *et al.* [11] describe an LOC based oral cancer screening. The

---

[1] Lab-on-a-chip (LOC) is a term for devices that incorporate one or multiple laboratory processes onto a chip with dimensions in the range of millimetres to a few centimetres.

[2] An immunoassay is a biochemical test that determines the concentration or presence of a substance in solutions that, often, contain a complex mixture of substances.

handheld I-Stat analyzer provides POCT for monitoring a variety of clinically relevant parameters of blood [12]. The range of applications for LOC systems for POCT is growing as more and more researchers are becoming aware of the imperative benefits of this technology. Most of these advantages are derived from the base of μTAS/LOC, the so-called "microfluidics" technology.

1.2 Microfluidics

Microfluidics is the science and technology of systems that manipulate or process small volumes (in microlitres) of fluids, utilizing fluid handling channels with dimensions of tens to hundreds of micrometres [13] . The advantages of using microfluidics for fluid manipulation and processing include low sample/reagent volume, faster response times, low-sample wastage, cost efficacy, and the possibility of developing disposable devices [13]. One of the most significant challenges in developing a microfluidic, biochemical analysis system has been the development of dependable microfluidic manipulation methods. Many researchers have investigated active control[3] devices for fluidic flow control, for example, microvalves and micropumps [14-17]. In spite of the advantages, active microfluidic control has many inherent drawbacks, for example, high cost, complex fabrication/assembly, and complicated control circuitry [18].

---

[3] Active control indicates applying external forces (magnetic field, electric field, optical force, heat, etc.) to control the flow movement in microchannels.

Therefore, in order to eliminate these drawbacks, attention has shifted towards the use of passive[4] microfluidic components for fluid control. A large variety of passive microfluidic devices has been successfully demonstrated, including passive mixers/valves [19-21], passive membranes [22], filters [23], and also several passive actuation schemes [24, 25]. Passive microfluidic devices provide several distinct advantages, especially for portable LOCs, such as no external power requirement, ease of integration, low cost, rapid prototyping, and the possibility of operating without complex control electronics [4, 5]. Some of the disadvantages of passive microfluidic devices are that they are highly application-specific; their performance strongly depends upon the fabrication process, and they are unsuitable for a wide range of fluidic media. Regardless of these challenges, the merits of passive fluidic control make it a realistic approach for developing compact and low cost microfluidic chips for numerous biochemical analyses.

The choice of material is the most critical decision for a μTAS/LOC platform [5]. Earlier, most of the microfluidic devices were fabricated using silicon (Si) or glass substrates because the fabrication processes for these two materials were well established [13, 26, 27]. However, each of these two materials has disadvantages that restrict their use in microfluidic applications. Silicon is opaque in visible and UV wavelengths, and hence it is rendered useless for UV detection or visual monitoring. Although glass is transparent, it is amorphous, so etching vertical side walls is extremely difficult [28]. In addition, microdevices fabricated

---

[4] Passive control indicates that the fluidic movement is controlled by channel geometries and/or liquid flow rates.

with silicon or glass require fabrication in a cleanroom facility, entailing significant

processing infrastructure and technology. Consequently, Si- or glass-based

microfluidics systems can be expensive for many applications [29]. Therefore,

attention has shifted to plastics and polymers as the materials of choice, due to

their much lower fabrication costs and less complex process technology [29, 30].

Plastic substrates, such as poly(methamethylacrylate) (PMMA),

poly(dimethylsiloxane) (PDMS), polyethylene, polyimide or polycarbonate,

provide a broad range of physical and chemical material properties for fabricating

microfluidic chips for biochemical analyses [29]. Polymers offer various

advantages, such as low cost, ease of fabrication, and rapid prototyping [29]. A

major advantage of employing polymer substrates is the wide range of surface

properties that they can provide. The surface properties of polymers can be

customized to meet the biocompatibility and/or fluidic requirements in a miniature

biochemical analysis system [31],[32]. In addition, polymer processing is an

established field, and hence polymers can be utilized to fabricate multifunctional,

disposable, cost-effective microfluidic modules.

1.3 Motivation

Advancement in µTAS/LOC that combines molecular biology, microfabrication,

and bioinformatics are advancing the nucleic acid detection technologies, for

example, DNA hybridization, from standard laboratory techniques to rapid

disease diagnostics. DNA detection technologies has been utilized in a wide

range of applications: forensic and genetic identification; gene expression

analysis; screening samples for single nucleotide polymorphisms; infectious and genetic diseases; and cancer diagnostics [33].

DNA detection along with DNA amplification, integrated onto a microfluidic system (as shown in Figure 1) can offer broad potential in field applications. This detection technique can be potentially used to develop diagnostic devices for detecting specific human pathogens for various diseases, including sexually transmitted diseases (STDs), viral infections (e.g., HBV, HCV, H1N1), bacterial based enteric disease (e.g., *Salmonella*, *Campylobacter jejuni*, *Clostridium diffile*, *E. coli* O157:H7, *Shigella dysenteriae* type 1), and hospital associated infections [HAIs; e.g., *C. diffile*, methicillin resistant *Staphylococcus aureus* (MRSA)]. Additionally, similar devices can be used in veterinary applications (e.g., porcine and equine diarrhea) and to detect pathogens in food sources (e.g., *Salmonella*, *E. coli* O157:H7) during factory processing.
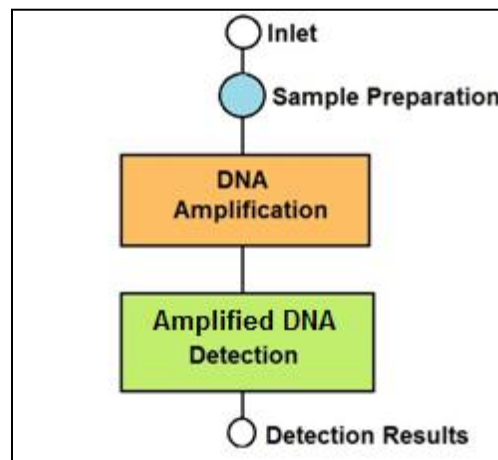
Figure 1: Schematic illustration of the potential microfluidic diagnostic device.

Developing a diagnostic system as illustrated in Figure 1 is a two-step process —DNA amplification and amplified DNA detection. There are several

chip-level DNA amplification implementations in literature and Asiello *et al.* [34] presents a review of these microfluidic implementations. Therefore, in this thesis research we have concentrated on developing amplified DNA (amplicon[5]) detection using microfluidics technology.

Although, direct DNA detection has been popularly used, these procedures employed for detection are time consuming, complex, and laborious. For example, gel electrophoresis coupled with dye staining--commonly used for the visual detection of DNA [35]—typically takes around 3.5 hours and requires staining, de-staining, and disposing of dye-containing buffer. Some electrochemical DNA detection techniques have been reported that are fast and efficient, but these techniques involve complex chemistry and require sophisticated, expensive and customized optics and/or circuits [36-40]. These techniques are unsuitable for inexpensive, hand-held diagnostic devices. Therefore, the motivation for the research and development work presented in this thesis is developing a portable, easy-to-use, inexpensive and disposable device for detecting amplified DNA. Using the philosophy of low-cost, simple solutions for complex problems, research presented in this thesis, explores a novel microfluidic unit capable of detecting DNA amplicons — using passive polymer microfluidics approach.

---

[5] An amplicon is a piece of DNA that is the product of DNA amplification.

1.4 Approach

1.4.1 Agglutination based detection

Microsphere agglutination along with polymer microfluidics is employed to achieve DNA amplicon detection. Agglutination is an old (since 1896) technique, that is prevalent in immunological diagnostics [41]. The test is performed by mixing the suspension of target DNA (usually after amplification and ligand labeling) with receptor-immobilized microspheres binding probes specific for the target DNA under study. After 1-2 minutes, in contrast, to the control samples, clumping is observed in a positive reaction [41] (as illustrated in Figure 2). Agglutination is usually observed with the naked eye or *via* microscopy, making this detection technique highly subjective.

Therefore, in this research, a microfluidic chip for detecting ligand-labeled DNA amplicons was designed to discriminate between individual or cross-linked receptor-modified microspheres, indicating the absence or presence of amplified target DNA, respectively. The goal of this microfluidic system is to provide results that can be easily visualized within 2 minutes without the aid of a specialized optics or any other expensive hardware. The straightforwardness and portability of this microfluidic discrimination approach is ideal in field applications where portability is of paramount importance.
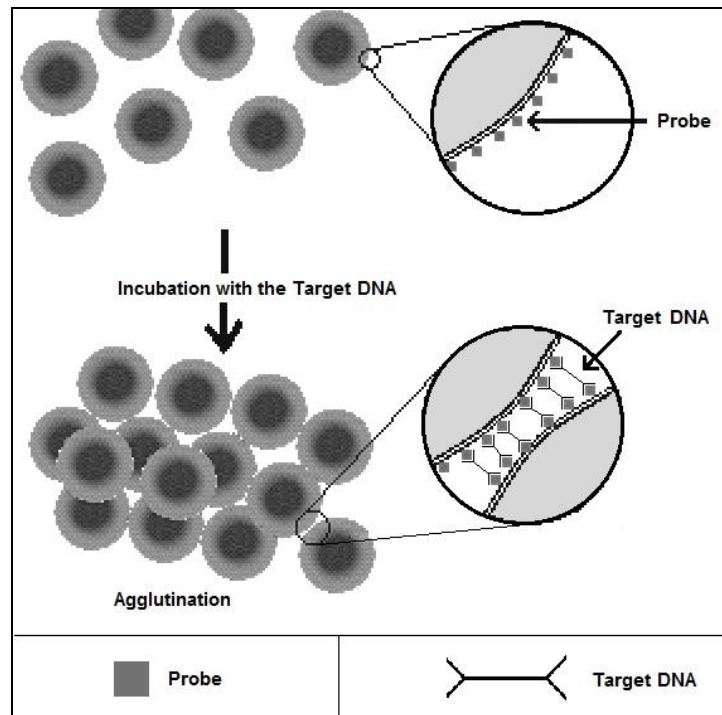
Figure 2: Illustration of the agglutination process

1.4.2 Why use microspheres?

Polymer microspheres have been a popular choice for a number of LOC applications as the quality and functionality of the microspheres can be tailored according to particular specifications [42]. Microsphere surfaces are easily modified with molecules providing biological specificity and function. Polymer microspheres in low-millimetre to sub-millimetre diameters have been prevalently employed as solid supports in surface-binding assays for years. For example, in 1956, an agglutination based test for rheumatoid arthritis in serum employed latex beads with diameter <1mm [43]. Today, a wide assortment of microspheres is obtainable, including beads in the nanometre range with a selection of organic and inorganic polymer core compositions.

Numerous types of surface coatings are available, either for attaching molecules or with molecules already attached [44-47]. The availability of these enhancements is due to the increasing demand from assay developers, who have implemented microsphere surfaces as sensing platforms for different applications. Accordingly, the range of tests and assays using microspheres is extremely broad and include affinity assays, immunoassays, DNA hybridization assays, protein–DNA, protein–protein and enzymological studies. The clinical diagnostic and high throughput screening fields have been immensely benefited [44-47] by microsphere utilization. The reasons for the attractiveness of microspheres are: (1) effective ratios of reactive surface to volume are increased when using small microspheres; (2) conducting reactions in much smaller volumes; (3) increased concentrations of bound analyte/probe on bead surfaces as compared to solution produce higher signals than for the same reaction in solution. Microspheres thus can efficiently amplify signal [44].

1.5 Research objectives and goals

This thesis explores a microfluidic system that discriminates between the agglutinated and individual microspheres from a disease diagnostic device perspective. The focus of the research was to design a microfluidic discriminator by employing computer simulation of hydrodynamic conditions and testing various microfluidic designs. With the aid of agglutination test (streptavidin-coated polystyrene microspheres and biotin-labelled target DNA) the microfluidic discriminator effectiveness was evaluated. Computer simulations were performed to study the fluid flow in the microfluidic channels. The computer simulation

results determined the system design, which, in turn, provided the ideal fluid flow rates for effective discrimination. Finally, with the study of microfluidic discriminator design, the reagent concentrations for the agglutination test, and fluid velocities and corresponding agglutinate physical characteristics, a microfluidic DNA amplicon detection device was developed.

1.6 Organization of the thesis

Chapter 2 presents the literature research on agglutination detection and highlights the importance of the research described in this thesis. This chapter introduces the idea of a microfluidic system for discriminating between agglutinated and individual microspheres.

Chapter 3 is an in-depth explanation of the fabrication techniques utilized to fabricate microfluidic devices. This chapter describes the process flow of the fabrication techniques for PMMA and PDMS as substrate materials.

Chapter 4 covers the theory of nucleic acid DNA detection and reasons for the strong interaction between biotin and streptavidin. Furthermore, this chapter explains the development of the agglutination protocol that is utilized in microfluidic discriminator in the next phase of this research

Chapter 5 presents various PMMA microfluidic discriminator designs and their results. This chapter identifies key requirements and methods to achieve successful discrimination.

Chapter 6 provides the computer simulation results for the different designs that are based on the recommendations from the previous chapter. These

simulation results validate the recommendations and assist in the development of a final microfluidic system design.

Chapter 7 presents the implementation of the simulation results from the previous chapter by using the soft lithography technique for fabricating the microfluidic discriminator.

Finally, Chapter 8 gives an insight into the future work and presents the contribution of this research.

2: SIGNIFICANCE OF RESEARCH

Hybridization-based detection of target DNA is currently the most prevalent technique available. Typically, either the target DNA fragment or the probe DNA fragment is tagged with a fluorescent molecule; therefore, hybridization is detected by fluorescence. Alternatively, there are electrochemical techniques, which replace the optical detection. Still, both these techniques, although they serve as reference standards for central laboratory testing, have not been available to resource-limited countries. Primarily, fluorescence-based optical techniques require special excitation light sources and photon detectors, while electrochemical techniques require complex electronic circuits. Therefore, the area of rapid target DNA detection is open for interdisciplinary research teams to explore and to develop. This chapter presents the literature review on agglutination based DNA detection techniques and highlights the problems and challenges with the present techniques. Finally, the chapter proposes a new detection technique and emphasizes the significance of the research and proposed detection technique.

2.1 Literature review of present agglutination detection techniques

Normally, in the agglutination-based assays, the test sample is mixed with derivatized particles and spread on a glass slide to facilitate visual inspection of particle agglutination, which requires subjective scoring to discriminate the extent

of agglutinated particles in the presence of single particles. Attar et al. [48] describes one such criterion that determines the extent of agglutination. If the majority of the agglutinates move to the edges, the maximum level of agglutination is observed. If the agglutinates resemble "chalk dust" then the agglutination is scored a level below maximum. The minimum scoring level is presumed if the agglutination can just be noticed as compared to the negative control. Similarly, if the clear agglutination is seen against the background of negative control, the agglutination is a level higher than the minimum level. Clearly, visual inspection is very subjective and it provides ambiguous results. Figure 3 shows the results of an agglutination test (details of the test will be discussed later in chapter 4 and page 38). It is evident from Figure 3 that it is difficult to distinguish between positive and negative agglutination by visual inspection.
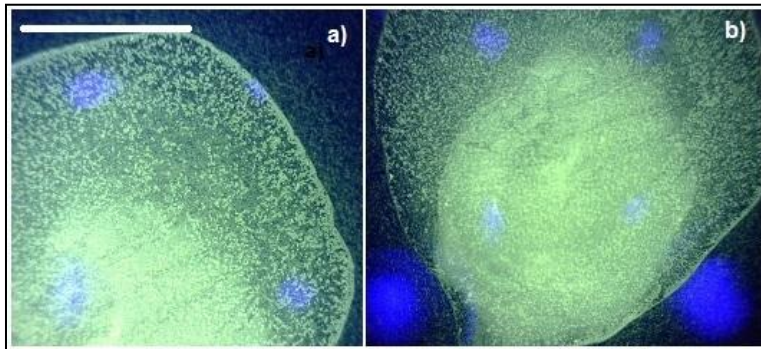
Figure 3: Illustration of visual inspection of agglutination. a) Positive agglutination of microspheres due to the presence of target DNA; b) Negative agglutination (individual microspheres). The scale bar represents 0.5 cm.

To improve upon this limitation, a microscope is typically used [49]. Although the use of microscope enhances the observation, determining the

extent of the agglutination still remains subjective. Furthermore, the use of a microscope limits the use of "agglutination assay" in field applications. To eliminate the problems of subjective analysis of agglutination and non-portability, many attempts have been reported [50-54].

Typically, for latex beads agglutination tests, light scattering or absorbance [55, 56] detection methods are utilized when the particle size is between 10 nm – 200 nm. However, these detection mechanisms require the formation of large aggregates and have limited sensitivity. Thus, to improve the sensitivity, detection has mostly been performed in flow-through systems. In Ramasubramanian *et al.* [50], an integrated fiberoptic–microfluidic device for agglutination-based blood typing has been described. The microfluidic device comprises of a straight microfluidic channel through which a reacted red blood cell (RBC) suspension is pumped with the aid of a syringe pump. The flow traverses an optical path produced by an emitter-receiver fiber-optic pair incorporated into the microfluidic device. A 650-nm laser diode is utilized as the light source, and a silicon photodiode is used to measure the light intensity. The scattering of the light is used to determine agglutination level. An agglutination strength factor is calculated from the collected data. Although this sensing mechanism (laser diode and Si photodiode) correctly identifies the agglutination for all the blood types, the device relies upon the integrated detection mechanism, resulting in a non-disposable and expensive device. Hence, this detection scheme is costly and limits its use in resource-limited settings.

Similarly, Pamme *et al.* [51] present a microfluidic device for counting, sizing, and particle agglutination based on laser light scattering. The particles are focussed hydrodynamically and passed through a focussed laser beam. Scattering at two different angles, 15° and 45°, is observed. To detect particle scattering, the microfluidic chip is first mounted on an inverted microscope. Fluid flow is generated with a syringe pump. The laser beam is focussed on the examination point in the microchannel with a beam splitter and objective lens. Two optical fibers are placed above the microchip at 15° and 45° angles in reference to the incident laser beam. Then the light signal is pre-amplified by a photomultiplier tube and processed by a computer. The use of specialized equipment limits the portability and usefulness of this detection mechanism in remote or field applications.

In addition, flow cytometry is a powerful and versatile tool commonly used for analysis and/or separation of cells, but it can also be useful for sensitive and multiplexed sized particle assays [52]. Flow cytometry is based on the same principle as Ramasubramanian *et al.* [50] and Pamme *et al.* [51], with the exception that fluorescent chemicals attached to the particle is excited to emit light at a longer wavelength than the source. The detectors collect this combination of scattered and fluorescent light. By studying fluctuations in brightness at each detector, information about the shape and size of agglutinates is obtained. Scanning flow cytometry (SFC) has recently been employed for investigated the initial immunoagglutination process [53]. SFC technology offers more detailed information about the shape and size of agglutinates than classical

flow cytometry, and it can be utilized for distinguishing between agglutinates consisting of singlets, doublets, and triplets. Although flow cytometry can measure small amount of agglutination, it requires image processing to retrieve and interpret data. Therefore, this process may be highly reliable, but it is extremely expensive and complex in terms of resources required.

Non-optical detection of particle agglutination is described by Chunara et al. [54]. The authors report a technique for particle counting where initial stage agglutination is quantified by measuring mass with the suspended microchannel resonator or cantilever. In this detection mechanism, the weight of each agglutinate is measured in real time by associating it with transient changes in the resonant frequency as the agglutinate flows through a vibrating microchannel embedded in the cantilever. The paper claims that the results are comparable to earlier test results accomplished by conventional flow cytometry and image analysis; however, the device fabrication is complex and the device is not portable.

2.2 Proposed design

To overcome the limitations observed in the existing agglutination detection techniques, this research proposes a novel, precisely designed, microfluidic flow channel that will **retain agglutinated particles while allowing individual particles to flow through.** Hence, the retention of the agglutinated particles will provide non-subjective positive result. The flow channel was designed with an engineered constriction in the flow path. When the contents of the microfluidic chamber are transported through the constriction, the individual detector particles

and unbound analytes pass through the flow channel; in contrast, the agglutinated complexes are retained. If the detector particles are pigmented, the retention can be easily visualized, indicating the presence of the target DNA. Figure 4 illustrates the visual detection scheme (simplified) for negative and positive agglutination.
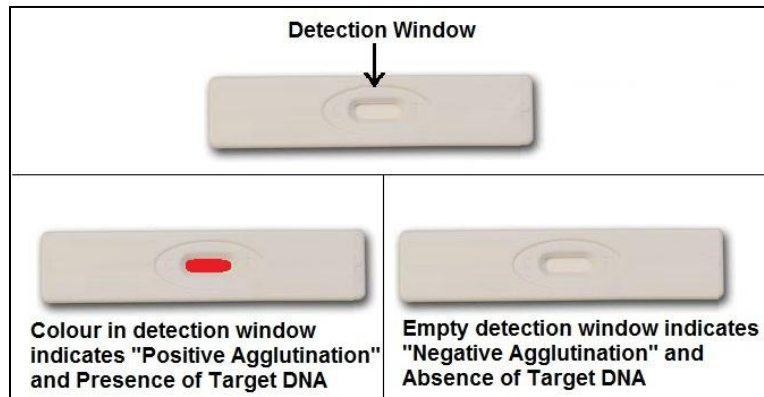
Figure 4: Detection scheme of the proposed design.

Table 1 compares different agglutination detection techniques discussed in this chapter, in terms of reliability, simplicity and portability of device.

Table 1: Summary of the literature research.

Reference	Technique for detection	Reliable	Simple	Portable
[48]	Visual inspection by naked eye	NO	YES	YES
[49]	Microscope	YES	YES	NO
[50]	Optical- integrated fiberoptic	YES	NO	NO
[51]	Laser light scattering	YES	NO	NO
[52]	Flow cytometry	YES	NO	NO
[53]	Scanning flow cytometry	YES	NO	NO
[54]	Mass based	YES	NO	NO
Present research	Visual detection: Engineered constrictions in the flow path	YES	YES	YES

3: FABRICATION PROCESS

This chapter presents the fabrication materials and techniques utilized in this research. The chapter is divided into two parts based on the two fabrication materials used in the research. The first part presents poly (methyl methacrylate) (PMMA) and the fabrication process for the PMMA-based microfluidics. The second part explains the material polydimethylsiloxane (PDMS), and it presents the soft lithography process for fabricating PDMS microfluidic devices.

3.1 Poly (methyl methacrylate): PMMA

PMMA has potential for extensive use in microfluidic fabrication because it is bio-compatible, the least hydrophobic among the popularly used polymers, cost effective, has excellent optical properties [57], and is readily available in a range of chemical and physical properties. The chemical composition of PMMA is shown in Figure 5.
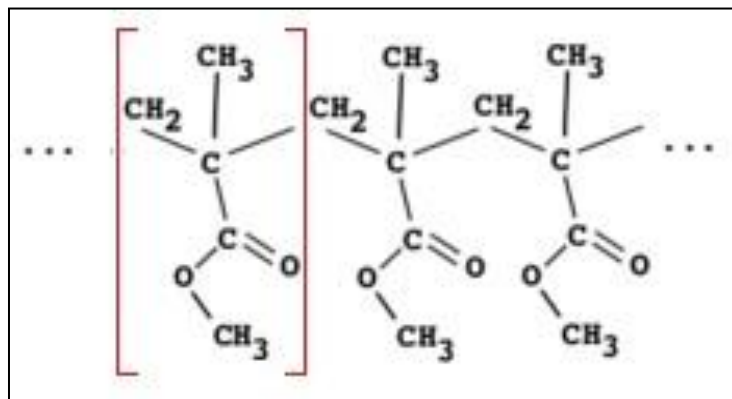
Figure 5: Chemical composition of PMMA.

When PMMA is irradiated with deep-UV, it undergoes a change in its chemical structure [58]: the molecular bonds in the polymer main-chain and pendent methyl-ester groups break down, decreasing the average molecular weight of the polymer. Hence, this process increases its solubility in solvents, such as isopropyl alcohol (IPA) [30, 57].

3.1.1 PMMA fabrication steps

In this project, PMMA with the brand name, Plaskolite's Optix®, was used. The PMMA sheets were first cut into 30 cm x 30 cm squares by the supplier. For ease of handling, these pieces were then cut into 75 mm x 75 mm squares using a CO_2 laser cutter [59]. After being cut, the PMMA squares were cleaned using de-ionized (DI) water. The samples were immersed in methanol solution for 5 minutes to rid any surface contamination, before the subsequent DI water rinse and N_2 gas blow drying. In the next step, a 100-nm thick layer of gold was sputtered on the PMMA substrate using a Corona Vacuum Coater. This gold layer, which was patterned by photo lithography, acts as a photo-mask during the subsequent deep-UV exposure.

The photolithographic step was performed using a positive photoresist. Shipley 1813 photoresist (Shipley Company, Marlborough, USA) was spun on the gold layer at 4000 rpm for 30 seconds. The photoresist was then soft baked at $100°C$ for 8 minutes in the oven to remove the majority of the solvent. The substrates were allowed to cool to room temperature, helping to eliminate any warping that may have occurred during the soft baking process.

To pattern this photoresist layer, the sample was exposed through a contact chrome mask (from FineLine imaging, Colorado Springs, USA with a resolution of 65K dpi.) using an i-line UV source from a mask aligner. The sample was then hard baked on a hotplate at 100°C for 3 minutes. Next, the sample was developed in Microposit MF-319 developer (Shipley Company, Marlborough, USA). Subsequently, the gold on the sample was etched using TFA gold etchant (Transene Company Inc., Danvers, USA). The photoresist was removed using a 60-second UV exposure followed by development in Microposit MF-319. The sample was then exposed to 254 nm Deep-UV(DUV) for 20 hours [60]. Figure 6 shows the sample ready for DUV exposure.

Figure 6: Patterned gold to be used as photo mask during the DUV exposure. The scale bar represents 2.54 cm.

After DUV exposure, the gold layer was etched in TFA gold etchant, and the sample was developed in a bath containing the developer solution, a mixture of IPA and DI H_2O (IPA: H_2O, ratio of 7:3 by volume at 28 °C). In order to increase the dissolution rate, a magnetic stirring rod set to 250 rpm was added to the developer bath to maintain a constant agitation. The development time for the sample depends upon the channel depth required; for example, 3 minutes of

development creates 35±5 μm deep channels [60]. Next, the developed sample was placed in an ultrasonic IPA bath at room temperature for 10 seconds, and then it was rinsed in fresh IPA and DI H_2O. The sample was then dried with N_2 gas. Finally, the input/output access ports were drilled, and the sample was cut into 7.62 cm by 2.54 cm pieces using a CO_2 laser cutter. The channels were sealed by microwave bonding the patterned piece of PMMA to another blank piece of PMMA. The fabrication process is illustrated in Figure 7.

1. Clean PMMA

2. Gold sputtering

3. Photoresist Spinning

4. Exposing (mask aligner)

5. Photoresist Development

6. Gold Etching

7. 254nm Deep UV Exposure

8. Gold Etch

9. PMMA Development

10. Access Hole Drilling

11. Microwave Bonding

Blank PMMA

Unexposed Photoresist

Exposed Photoresist

Gold

Exposed PMMA

254 nm Deep-UV
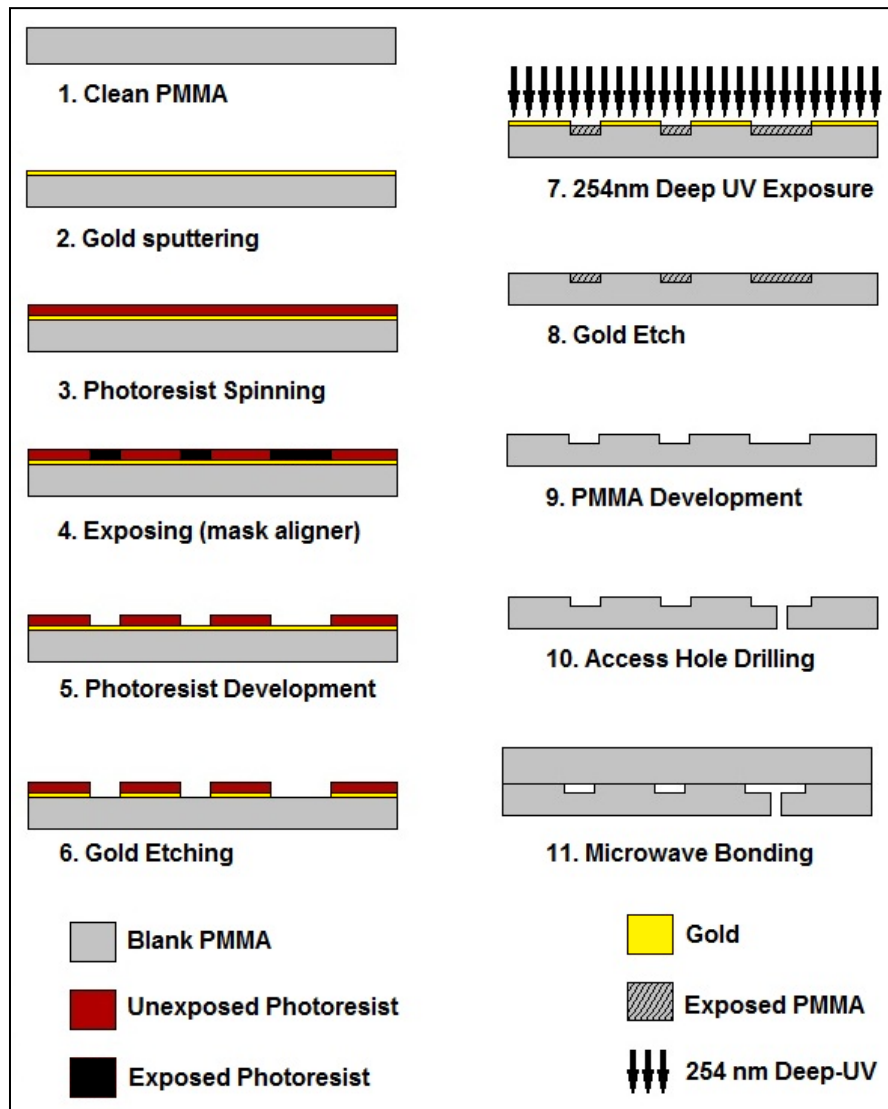
Figure 7: 254 nm DUV fabrication process flow.

3.1.2 Microwave bonding

The patterned and blank PMMA pieces were entirely coated with ethanol. Then, the blank PMMA piece was placed on top of the patterned side of the other PMMA piece. After the ethanol was uniformly distributed between the two PMMA pieces without any trapped air bubbles, the outside was wiped off with a Kimwipe (lintless tissue paper). Then, a total of eight mini binder clips (3/5" size) [61] were placed around the perimeter of the PMMA pieces to hold the two pieces in place. If required, the pieces could be crudely aligned at this point by repositioning the clips. After alignment, a tightly rolled Kimwipe was placed in the access hole at the end of the channel to draw out excess ethanol by capillary action. The clamped PMMA pieces were then placed in a commercial microwave (Danby®, Model-DMW607W) set inside a fume hood. The microwave was operated at full power (700W) for 90 seconds. A small quantity of water (~200 ml) was also placed in the corner of the microwave to absorb excess energy. After the applied time in the microwave, the bonded PMMA microfluidic chip was removed, and polyethylene tubes were connected to the reservoirs using Loctite 495 glue. Figure 8 shows the final PMMA microfluidic device after the microwave bonding.
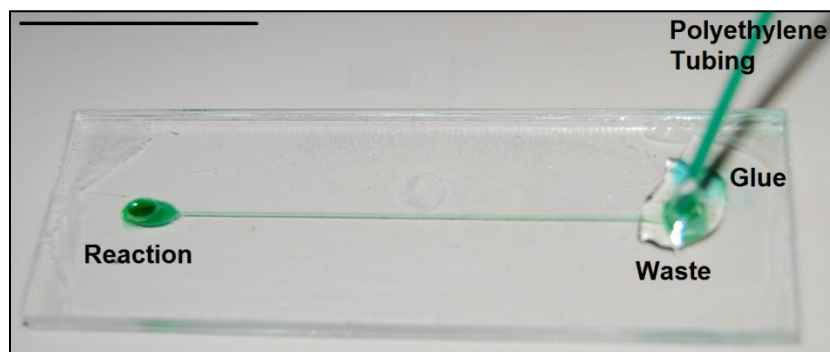
Figure 8: The final PMMA microfluidic device, green ink inserted to demonstrate the microchannel. The scale bar represents 2.54 cm.

3.2 Polydimethylsiloxane (PDMS)

PDMS is a flexible polymer that is prevalently used for microfluidic device fabrication [62]. In this research, Sylgard® 184 Silicone Elastomer Kit from Dow Corning® (Midland, USA) was used. Sylgard is a two part resin system containing vinyl groups and hydrosiloxane groups. Mixing of the two resin components produces a cross-linked network of dimethyl siloxane groups. Because PDMS is flexible, it can be easily removed from the master mold, leaving the master mold undamaged and ready to generate more devices. Figure 9 illustrates the chemical composition of PDMS.
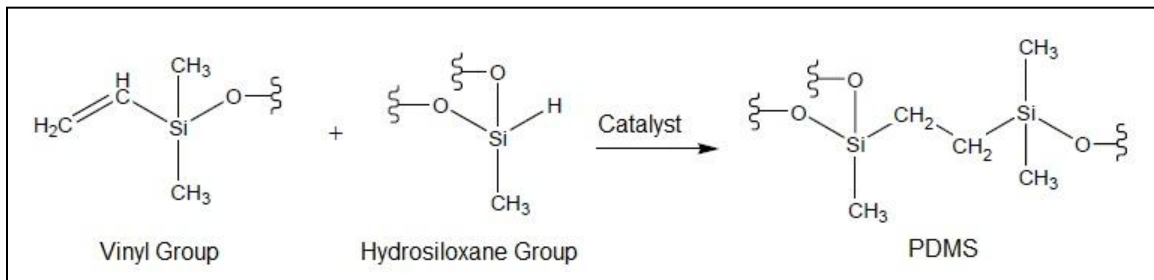
Figure 9: Chemical composition of PDMS.

Additionally, the surface of PDMS can be chemically modified to obtain interfacial properties of interest [63]. Consequently, the PDMS substrate can be easily bonded to PDMS, PMMA, and glass substrates using oxygen plasma or corona surface activation techniques [64].

3.2.1 PDMS fabrication steps

The master mold was fabricated using conventional photolithography technology. The layout of the design was drawn using a computer-aided design program, L-Edit. The design was then printed onto chrome mask (FineLine

imaging, Colorado Springs, USA) with a resolution of 65k dpi. The chrome mask was utilized in contact photolithography in order to transfer the pattern onto the negative-tone UV photoresist (MicroChem Corporation SU-8 2010, Newton, MA). Earlier, SU-8 was spun on a silicon wafer (4 inch in diameter) and was patterned by following the manufacturers guidelines [65]. Figure 10 shows an SU-8 master mold created using a silicon wafer. The design of the SU-8 structure will be explained in chapter 7 and section 7.1.
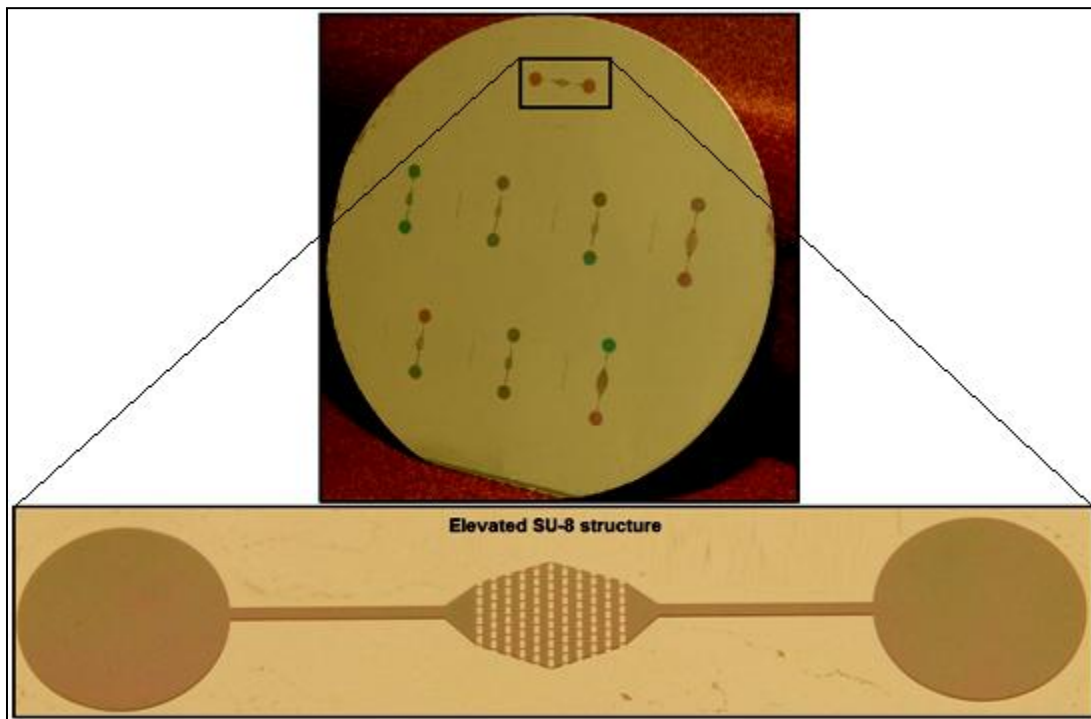
Figure 10: SU-8 master for the PDMS fabrication process (above). Picture below shows the magnified SU-8 feature.

A curing agent and PDMS prepolymer (SYLGARD 184 Silicone Elastomer Kit, Dow Corning, Midland, USA) were thoroughly mixed in a 1:10 weight ratio. The pre-polymer mixture was poured onto the master mold, and was degassed in a desiccator for 1 hour to remove any air bubbles in the mixture. The PDMS was

cured for 3 hours at 80°C in a convection oven. After curing, the PDMS replicas were peeled off from the master mold. Finally, the devices were cut to size (2 cm by 1cm) with a standard surgical steel blade, and the access holes were punched in the reaction and waste reservoirs using gauge 14 (0.069"-0.070") and 17 (0.045"-0.047") blunt needles (Zephyrtronics, Pomona, CA, USA), respectively.

3.2.2 Bonding

The PDMS substrate was thoroughly cleaned with IPA. Bonding was achieved by a hand-held corona device (model BD-20AC, Electro-Technic Products Inc., Chicago, USA) that generates a high-voltage potential across the electrodes at the tip of the unit, ionizing the air to create the localized corona discharge. Bonding was performed by placing a clean glass slide (Premiere Microscope slides) and the PDMS substrate feature side up on a non-conducting surface. Figure 11 shows the experimental setup for bonding using the corona device.
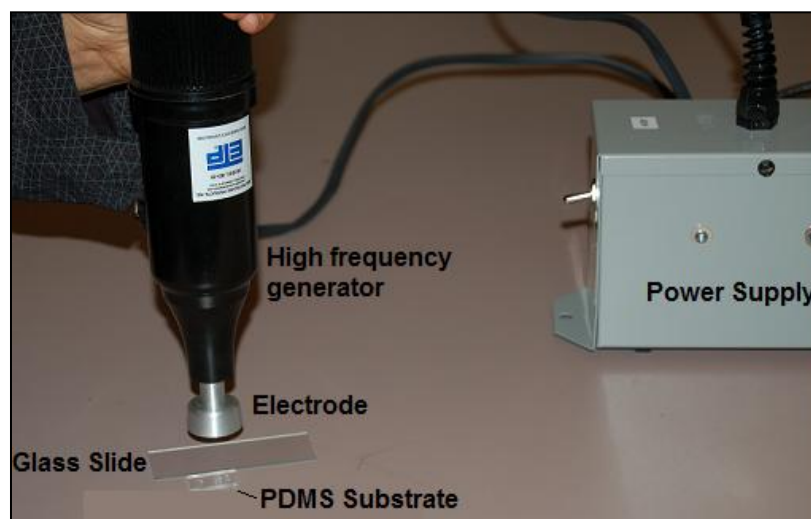
Figure 11: Experimental setup for bonding PDMS substrate to glass slide using the corona device.

The corona was adjusted such that it produced a stable and soft corona with minimal crackling and sparking. Depending on the size of the substrate, the one-inch disc electrode was passed back and forth approximately half an inch above each bonding surface for 40-60 seconds. To ensure a strong bond, the treated surfaces were then gently pressed together and left undisturbed for an hour. After the bonding, the polyethylene tubes (0.045") were connected to the reservoirs using epoxy (Hobbytown, Redmond, WA). In order to minimize or prevent any possible nonspecific binding of the streptavidin coated microspheres to the channel walls, once the epoxy sets, channels were filled with PBS/BSA buffer and were put into in a refrigerator for 24 hours. Figure 12 shows the final PDMS microfluidic device; the microchannel was filled with green dye to facilitate easy visualization.
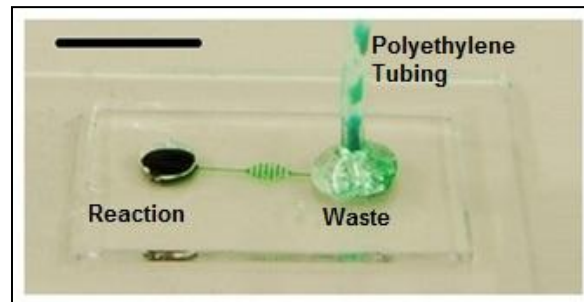
Figure 12: The final PDMS device. The scale bar represents 1cm.

Figure 13 shows the fabrication process flow for fabricating microfluidic devices by using PDMS as the substrate material.

1. RCA Clean Silicon Wafer

2. Spin SU-8 & Soft Bake

3. Expose SU-8

4. SU-8 Development & Hard Bake

5. Pour Uncured PDMS

6. Peel Cured PDMS (Inverted)

7. Punch Access Holes

8. Bonding

Silicon Wafer

SU-8

Exposed SU-8

Uncured PDMS

Glass

Cured PDMS
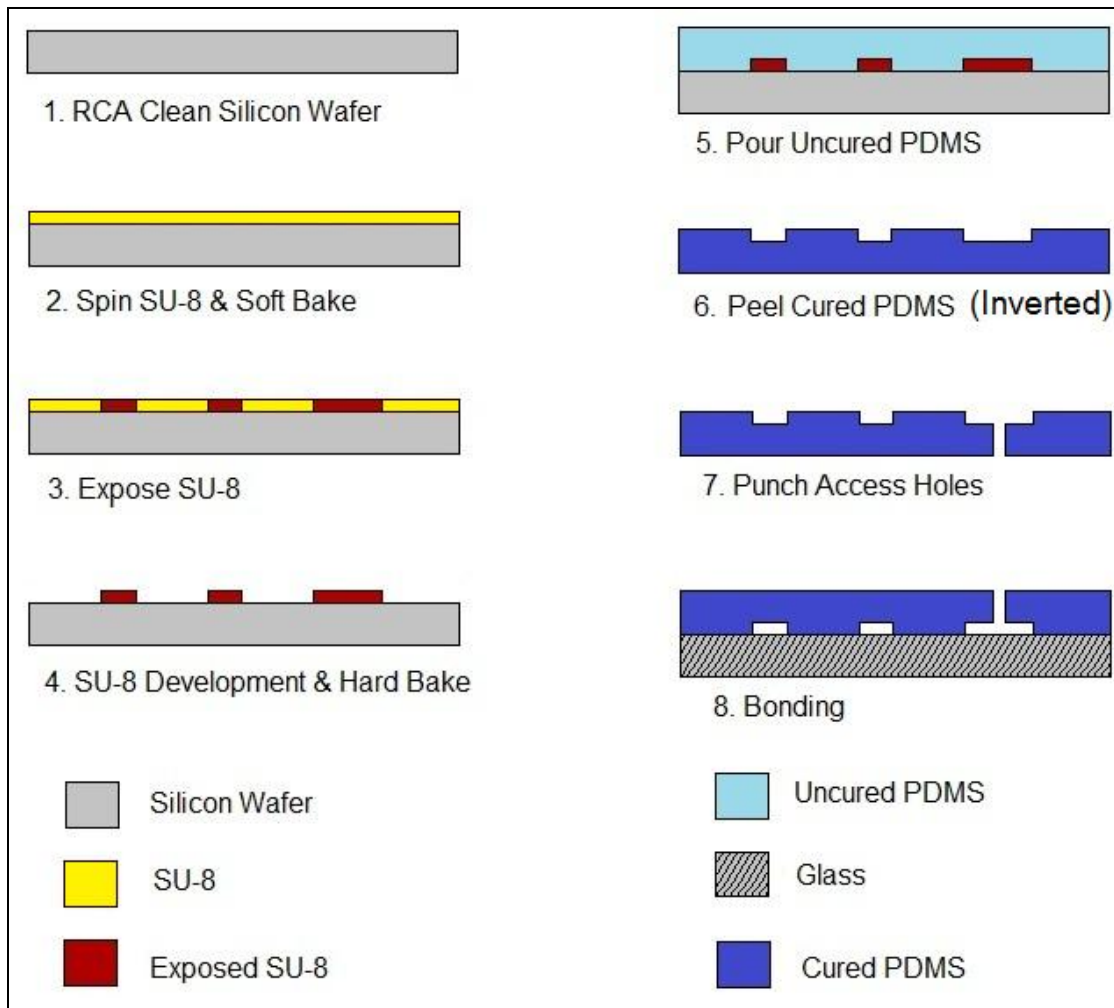
Figure 13: Fabrication process flow for PDMS microfluidic devices.

4: AGGLUTINATION EXPERIMENT: THEORY AND PREPARATION OF REAGANTS

For the development of the agglutination assay, this research utilized the technique of nucleic acid hybridization to produce dual-biotin labelled (biotinylated) DNA fragment. This dual-biotin labelled DNA fragment was used to cross-link the streptavidin-coated microspheres, thereby producing agglutination. This agglutination scheme takes advantage of the strong interaction between biotin and streptavidin. This chapter reviews the theory behind the synthesis of biotin-labelled DNA fragments and potential reasons for the strong interaction between biotin and streptavidin. Furthermore, this chapter explains the development of the agglutination protocol that was utilized in microfluidic discriminator device in next phase of this research.

4.1 DNA structure

DNA consists of long polymers (strands) of nucleotides with backbones composed of sugars and phosphate groups connected by ester bonds [66]. These two strands are opposite in directions to each other and are consequently anti-parallel. To each sugar, one of four types of molecules called bases [thymine (T) and cytosine (C), guanine (G) and adenine (A)] is attached. Each type of base on one strand bonds with only one type of base on the other strand; adenine (A) bonds only to thymine (T), and cytosine (C) bonds only to guanine (G). This arrangement of two nucleotides binding as one is termed as a base pair (bp). These bonds are not covalent; they can be broken (either by a mechanical

force or high temperature) and re-established easily [66]. Additionally, the percentage of GC content and the total length of a DNA double helix determine the strength of the bond between the two strands of DNA. Long DNA helix with a high GC content have stronger-association between the strands, while short helices with high AT content have weaker-association between the strands [66].

In the laboratory, the strength of the association between the DNA strands can be measured by the melting temperature (T_m), which is the temperature at which half of the DNA double helix will dissociate into single strands [66].

4.1.1 Oligonucleotide

Oligonucleotide (oligo) refers to a nucleic acid polymer, which was traditionally used to describe a "short polymer" of 50-nucleotides or less because, in 1970's-80's, the first synthetic nucleic acids were synthesized chemically by hand, and only short ones could be created relatively efficiently. However, with improved chemistry, technology, and automation, oligonucleotides with lengths greater than 200 nucleotides can be easily synthesized. Furthermore, an oligonucleotide may be composed of deoxyribonucleotide acids (DNA); or it may be composed of ribonucleotide acids (RNA). All RNAs (natural or synthetic) are sensitive to degradation. RNA degrades easily by the oils in hands due to large quantities of ribonuclease. Therefore, the oligonucleotides composed of DNA are more stable than the ones made from RNA. Hence, DNA oligonucleotides have been the popular choice for research.

4.2 Nucleic acid hybridization

Hybridization is a process of establishing a sequence-specific and non-covalent association between two or more complementary oligonucleotides or strands of nucleotides into a single hybrid [66]. Under normal conditions, oligonucleotides bind to their complement, and to obtain the most stable hybrids. Figure 14 illustrates the process of hybridization. Hybridization can be achieved by a process called annealing, which consists of two stages: *denaturation* and *renaturation.*
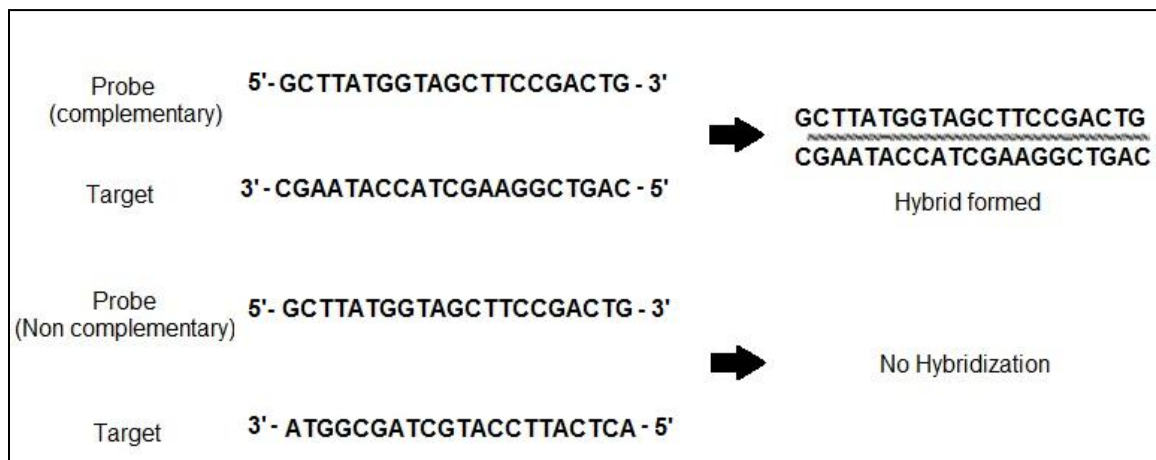
Figure 14: The process of hybridization.

4.2.1 DNA Denaturation

When DNA is dissolved in saline solution, and the solution is gradually warmed, a temperature is reached when strand separation begins. Within a few degrees, the process is completed, and the solution contains single-stranded molecules that are entirely separated from each other [66].

4.2.2 DNA Renaturation

In the process of DNA renaturation, the thermally denatured single strand solution is slowly cooled. The complementary single-stranded DNA molecules re-associate to produce a hybrid; this event is termed as renaturation, or reannealing [66].

4.3 Streptavidin-Biotin interaction

Biotin is a water soluble B-complex vitamin with a strong affinity for streptavidin, a protein found in the bacteria *Streptomyces avidinii* [67]. The association between biotin and streptavidin is one of the strongest non-covalent biological interactions, and it has an association constant (K_a) of approximately 10^{15} M^{-1} [67]. Due to the strong affinity of biotin for streptavidin, this interaction is often used as a diagnostic tool in biochemical assays [67].

The non-covalent binding of biotin and streptavidin is the epitome of high-affinity supramolecular interactions [68]. Several crystal structures of the streptavidin-biotin complex have helped explain the origins of this extraordinarily strong bond. Firstly, the shape of the binding pocket of streptavidin is highly complementary to biotin. Secondly, a large network of hydrogen bonds binds to the biotin when it is in the pocket. Eight hydrogen bonds are directly made to residues in the binding site ("first shell' of hydrogen bonding), and a 'second shell' of hydrogen bonding also engages residues that mesh with the first shell residues. Furthermore, the streptavidin-biotin affinity surpasses the affinity that is predicted from the hydrogen-bonding interactions only, indicating that another mechanism contributes towards the high affinity [68]. The biotin-binding pocket is

hydrophobic, and various van der Waals contacts and hydrophobic interactions occur with the biotin when it is in the pocket [68]. Lastly, biotin binding is accompanied by the formation of a flexible loop that seals the bound biotin by acting like a 'lid' over the binding pocket.

Therefore, the strong streptavidin-biotin bond can be utilized for the agglutination experiments in this research. Figure 15 shows the single streptavidin-coated microspheres agglutinated by the dual-biotinylated DNA fragments. The dual biotinylated DNA fragments act as bridges between two or more streptavidin-coated microspheres, causing cross-linking and the agglutination.
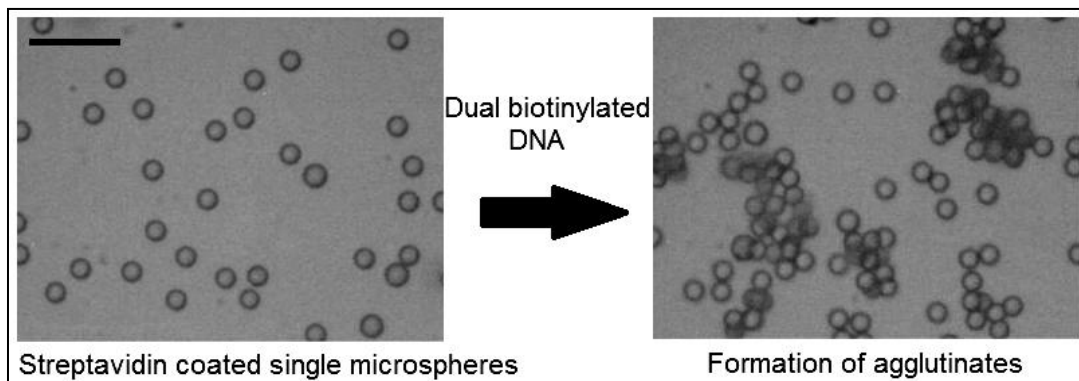
Figure 15: Formation of agglutinates due to the streptavidin and biotin binding. The scale bar represents 24 µm. Note: microsphere size is 6.22 µm.

4.4 Producing dual-biotin labeled duplex oligonucleotide

For the agglutination experiment, a pair of complementary 40-nucleotide oligonucleotides (oligos) was utilized to generate a dual biotinylated 40-basepair DNA fragment. This product was used to agglutinate streptavidin-coated microspheres.

4.4.1 Materials

In this research, fluorescent latex microspheres with diameters of ~6.22 µm were utilized. These microspheres were coated with streptavidin by the vendor, which facilitated the cross-linking of microspheres when bound to dual-biotinylated oligos. Table 2 tabulates the information about the oligonucleotides, streptavidin-coated microspheres and other reagents used in the agglutination experiments.

Table 2: Information about the material utilized in the agglutination experiment.

Reagent	Vendor	Details
Streptavidin Fluoresbrite YG microspheres	Polysciences	1.36% solids-latex, biotin binding capacity: 0.7 µg/ml, diameter: 6.22 µm, SD: 0.129 µm.
Oligo A	UCDNA Services DNA/RNA Synthesis Laboratory	Type: desalted; Length: 40 nt, ODU 531 nmoles, mol wt.:12448, 5'-biotin-GGTCAAGTTATTAAGGGTGCAGGGCGGATGCCTTGGCACT-3'
Oligo B	UCDNA Services DNA/RNA Synthesis Laboratory	Type: desalted; Length: 40 nt, ODU 335 nmoles, mol wt.:12146, 5'-biotin-AGTGCCAAGGCATCCGCCCTGCACCCTTAATAACTTGACC-3'
Tris–EDTA buffer (TE)	In house	Refer to appendix A
PBS/BSA	In house	Refer to appendix A
1 M NaCl	In house	Refer to appendix A

4.4.2 Annealing the oligos: Hybridization procedure

For annealing the oligos, the annealing mixture (as described in Table 3) was aliquoted into a 1.5-ml screw-capped microfuge tube.

Table 3: The volumes of different reagents in the annealing mixture.

Reagent	Quantity (in µl)
Oligo A (0.5 nmoles/µl)	10
Oligo B (0.5 nmoles/µl)	10
10x TE	10
1 M NaCl	10
Distilled water	60

The bottom half of the microfuge tube was immersed in boiling water for 4 minutes. In the next step, the beaker was taken off the hot plate to cool to room temperature. This step enabled slow annealing (free fall ~ 1 hour) that enabled the two oligos to hybridize, thereby generating the dual-biotinylated 40-basepair DNA fragment.

The temperature for annealing process was selected by calculating the melting temperature(T_m) and percentage GC (GC%) content of the oligonucleotides. T_m was calculated by,

$$T_m(in\ °C) = 2(A + T) + 4(C + G) \qquad \text{Equation 1}$$

where, (A+T) is the sum of the A and T residues in the oligo, and (C+G) is the sum of G and C residues in the oligo.

The T_m and GC% content for both oligo A and B was calculated as 71°C and 55%, respectively [69]. Hence, using a temperature higher than the T_m for the annealing ensures that all natural occurring duplex DNA (GC content less

than 60%) denature or "melt." Figure 16 shows the setup for annealing the oligos.

Figure 16: Setup for annealing the oligos.

Figure 17 depicts the formation of the hybrid. Note that the hybrid is a double stranded DNA (ds-DNA) fragment (40 base pairs) with biotin on both ends.
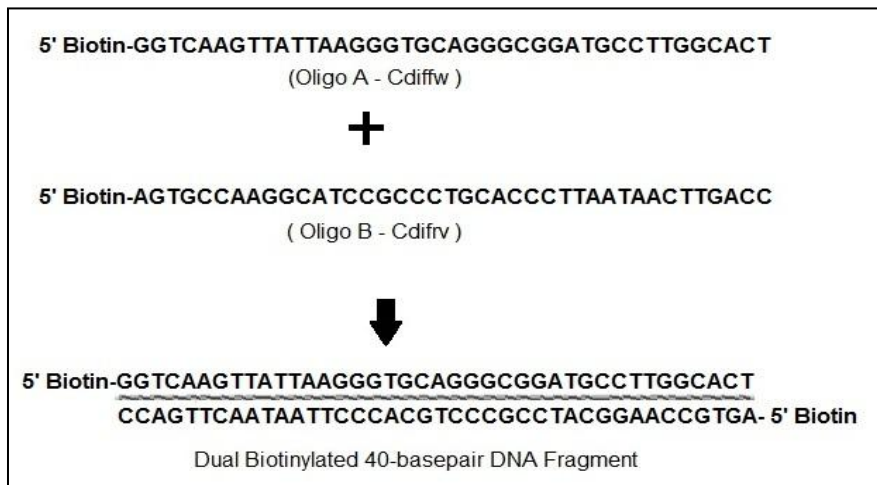
Figure 17: Formation of the dual biotinylated DNA after the annealing process.

In the total volume of the annealing mixture (100 µl), the final concentration of each oligo was 0.050 nmoles/µl (or 50 µM). Thus, the concentration of the biotinylated DS-DNA product was also 50 µM. So, the concentration of molecules was calculated as;

$$(0.050 \ \frac{nmoles}{\mu l}) \ X \ (10^{-9} \ \frac{moles}{nmoles}) \ X \ (6.02 \ X \ 10^{23} \frac{molecules}{mole})$$

$$= \ 3 \ X \ 10^{13} \ \frac{molecules}{\mu l}$$

This concentration of molecules was labelled as *"Tube A".* A series of dilutions were performed using Tris–EDTA buffer (TE) to obtain different concentrations of the DS-DNA. Table 4 gives the concentration of the DS-DNA after the serial dilutions, and the various labels given to the different concentrations of the DS-DNA.

Table 4: Serial dilutions of the DS-DNA product.

Label	Dilutions	Concentration (molecules/µl)
Tube A	3 x 10^{13} molecules/µl	3 x 10^{13}
Tube B	1:100 dilution (10 µl from Tube A+ 990 µl of TE) of Tube A	3 x 10^{11}
Tube C	1:100 dilution (10 µl from Tube B+ 990 µl of TE) of Tube B	3 x 10^9
Tube D	1:100 dilution (10 µl from Tube C+ 990 µl of TE) of Tube C	3 x 10^7
Tube E	1:10 dilution (10 µl from Tube D+ 90 µl of TE) of Tube D	3 x 10^6
Tube F	1:10 dilution (10 µl from Tube E+ 90 µl of TE) of Tube E	3 x 10^5
Tube G	1:10 dilution (10 µl from Tube F+ 90 µl of TE) of Tube F	3 x 10^4
Tube H	1:10 dilution (10 µl from Tube F+ 90 µl of TE) of Tube G	3 x 10^3

4.4.3 Agglutination protocol

The streptavidin-coated microspheres obtained from the Polysciences Inc. come as a suspension that was composed of 1.36% solid-latex, with a biotin binding capacity of 0.7µg/ml; and the diameter of the microspheres were ~6.22 µm. Before performing the agglutination experiments, the microspheres were washed with PBS/BSA buffer. Normally, for N number of experiments, $[(N + 0.5) \times 30]$ µL of the microsphere were washed down to $(3N)$ µL of the final volume. The desired amount of microspheres was washed with PBS/BSA buffer in a microfuge tube. The solid microspheres were spun to the bottom of the tube by high-speed centrifugation. The excess liquid was removed from the microfuge tube with a pipette, taking care that microspheres at the bottom of the tube were not disturbed. This step was repeated two times. Once the microspheres were washed, the following protocol was performed for the all agglutination experiments presented in this thesis.

1. Pipette 3 µl of washed beads onto a glass slide and then add 2 µl of a DNA sample or negative control (TE) and mix by pipetting.

2. Incubate the mixture is at room temperature for 90 sec.

3. Observe the reaction mixture for agglutination.

Note: unless mentioned, the terms "microsphere" and/or "microspheres" in the text only mean the washed microsphere and/or washed microspheres.

4.5 Results

Various factors control the hybridization efficiency; one of them is the length of the oligos. The oligos has to be sufficiently long and possess a sufficiently high GC% content to generate a stable duplex DNA. On the other hand, very long oligos may be less favourable due to the random-coil nature of duplex DNA that directly affects the probe-packing density [70]. Hence, a sufficiently long set of two complementary single-stranded DNA oligos were selected for this research, keeping in mind a few considerations. The 40-base pair long oligos were selected such that when annealed/hybridized (1) it would not denature at the typical isothermal DNA amplification temperature of 65°C and (2) it would minimize the cost of DNA synthesis.

Furthermore, a 10-bp length of DNA is 34Å or 3.4 nm [66]. Hence, a 40-bp duplex DNA fragment (13.6 nm) would be long enough to connect two microspheres in close proximity (keeping in mind that ultimately the experiments were going to be performed in the microfluidic platforms, which would assist in confining the microspheres to close proximity).

4.5.1 Effect of washing the beads

The experiment was conducted by mixing 2 µl of Tube B DNA sample and 3 µl of washed or unwashed microspheres. For washed microspheres, 10 µl of microspheres were concentrated to the final volume of 3 µl. Similarly, for unwashed microspheres, 10 µl of microspheres were concentrated to the final volume of 3 µl. The experimental results (as shown in Figure 18) show that the washed microspheres produced larger agglutinates than the unwashed

microspheres. The TE buffer was used as the negative control for the experiment. We speculated that the difference in the amount of agglutination was due to the interference caused by sodium azide present in the unwashed microspheres [71]. Sodium azide is added to protein conjugated microspheres suspensions as a preservative in order to prevent bacterial growth [72].
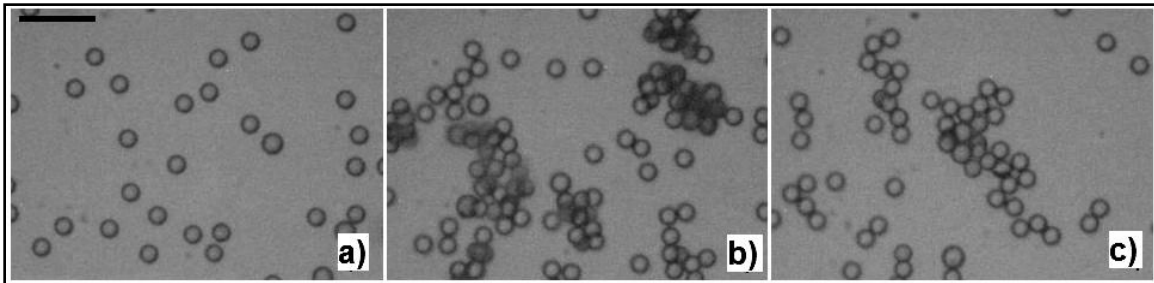
Figure 18: Agglutination results of; a) Washed microspheres with TE, b) Washed microspheres and DNA sample from Tube B, and c) Unwashed microspheres and DNA sample from Tube B. The scale bar represents 24 μm.

4.5.2 Microsphere agglutination

To evaluate streptavidin-coated microspheres agglutination, and to consider a positive control for the future experiments, the microspheres were incubated with Biotinylated 2-Log DNA ladder (New England Biolabs Ltd., USA). The DNA ladder consisted of biotinylated DNA fragments with lengths ranging from 100-10,000 base pairs (bp), with a majority of fragments containing two or more biotins/molecule. The agglutination results of the DNA ladder (positive control) was compared to the agglutination results obtained with the Tube B DNA sample in Figure 19. The experiment showed that the agglutinates produced with the positive control were approximately 20 times greater (~400-800 microspheres clumped together) as compared to the agglutinates (~20-40 microspheres)

produced with Tube B DNA sample. This difference in size of agglutinates was probably due to the length of the DNA fragments because the DNA fragments serve as the bridges that cross-link the microspheres. The length of the DNA fragments from Tube B was 40 bp, whereas, the length of DNA fragments in the DNA ladder varied between 100-10,000 bp. We speculate that the length of the DNA fragment significantly affected the amount of the cross-linking between the microspheres. Additionally, this experiment substantiated the ability of the microspheres to agglutinate because a considerable amount of agglutination was seen with the positive control.
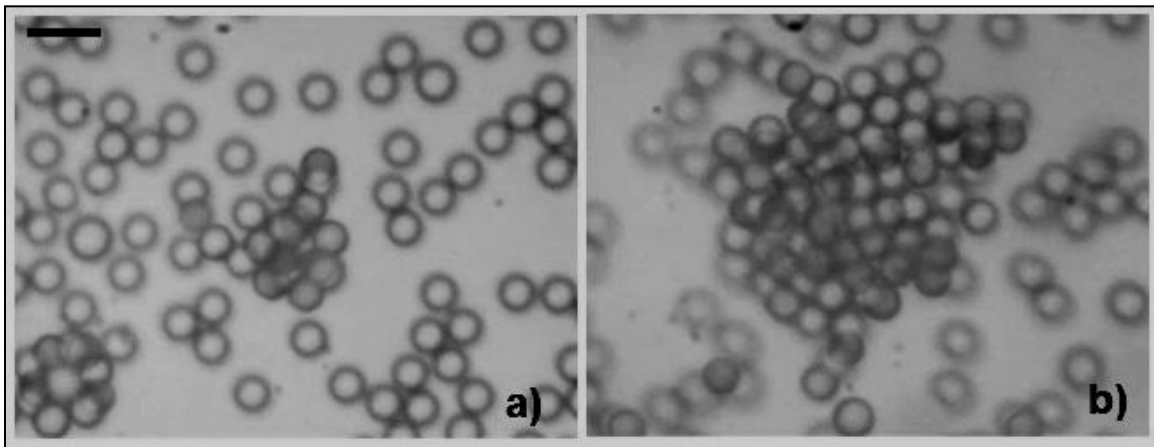
Figure 19: Agglutination results produced by; a) DNA sample from Tube B, and b) Biotinylated 2-Log DNA ladder. The scale bar represents 12 μm.

4.5.3 Effect of concentration of the DNA sample on agglutination

Determining the concentration that is required to achieve optimal agglutination was extremely crucial. A low concentration of the DNA sample will cause poor agglutination due to the insufficient number of DNA sample "bridges" that cross-link the microspheres. On the other hand, a high concentration DNA

sample will also cause little agglutination because the DNA sample will block all the receptor sites on the microspheres. The situation is depicted in Figure 20.
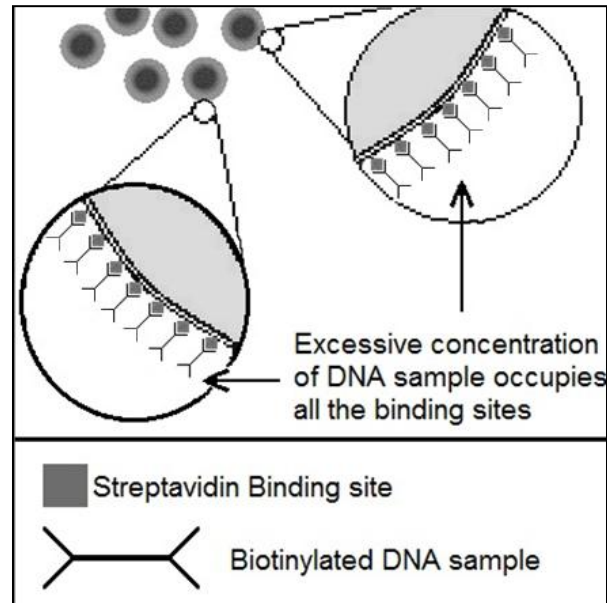
Figure 20: Effect of concentrating the DNA sample on the agglutination: Dual biotinylated DNA sample blocks all the streptavidin binding sites.

Hence, to determine the effect of the concentrating DNA sample on the agglutination, different DNA concentrations from Tubes A-H were tested. Figure 21 shows the agglutination results with different DNA sample concentrations. The DNA samples from Tube A and B showed the least amount of agglutination, whereas DNA sample from Tube F and G showed a greater amount of agglutination. The extent and amount of agglutination increased as the concentration of the DNA sample decreased from 3×10^{13} molecules/µl (Tube A) to 3×10^{4} molecules/µl (Tube G) and then started decreasing from 3×10^{3} molecules/µl (Tube H) onwards. Hence, we determined that, for all future experiments, the DNA sample from either Tube F or Tube G would be utilized, as

it provided the greatest amount of agglutination compared to other tested DNA

samples.
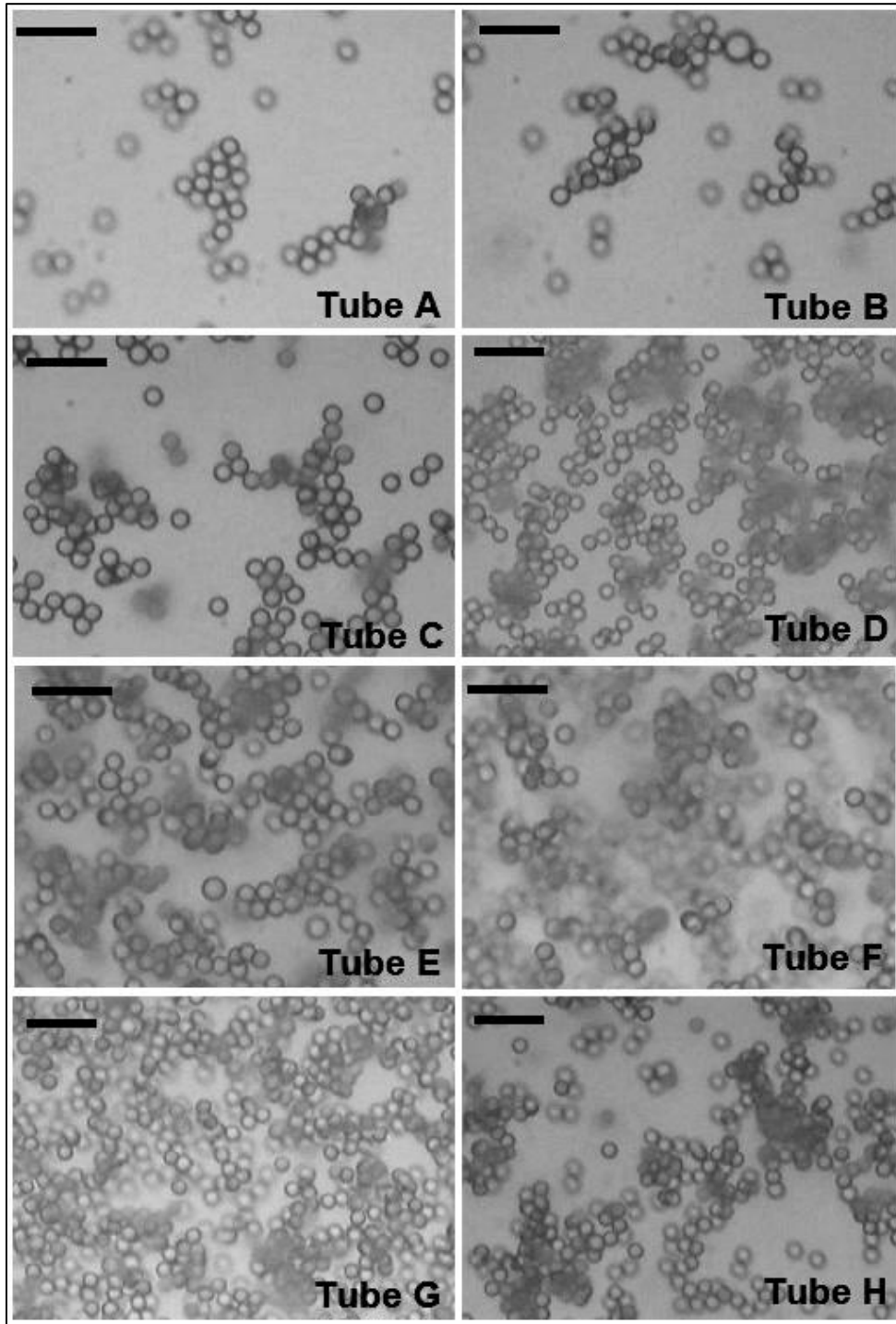
Figure 21: The agglutination results with different concentrations of DNA sample from the Tube A, B, C, D, E, F, G and H. The scale bars represents 24 µm.

4.5.4 Effect of concentrating microspheres

Different concentrations of microspheres were mixed with 2 µl of DNA sample from Tube F. Different volumes (30 µl, 15 µl, 10 µl and 5 µl) of microspheres were washed and concentrated to the final volume of 3 µl each and tested for agglutination. Contrary to the assumption that with the decrease in the microsphere concentration the interaction between the microspheres and the DNA sample would decrease and adversely affect the agglutination, all the concentrations of microspheres showed significant agglutination (as illustrated in Figure 22).
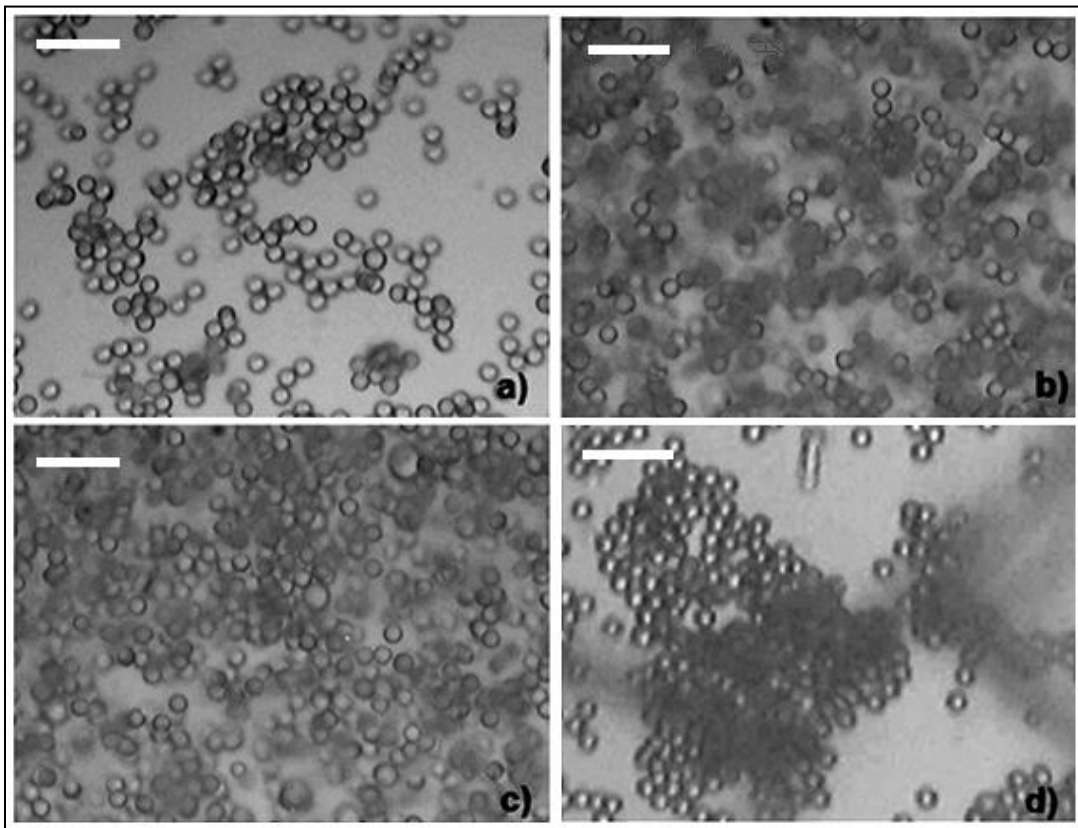
Figure 22: Agglutination results of the DNA sample from Tube F and 3 µl of washed microspheres. a) 5 µl of microspheres washed down to 3 µl, b) 10 µl of microspheres washed down to 3 µl, c) 15 µl of microspheres washed down to 3 µl, and d) 30 µl of microspheres washed down to 3 µl. The scale bars represent 24 µm.

The size of agglutinates was also observed to be similar in all the cases, only the amount of agglutinates lessened when the concentration of microsphere decreased. Volume of 5 µl washed beads showed a considerable amount of agglutination but fewer (almost 60% less) agglutinates in number compared to other concentrations. We could not visually distinguish between the extent of agglutination of 10 µl, 15 µl, and 30 µl of washed beads because all of these concentrations of microspheres produced similar agglutination. Therefore, we determined that 10 µl of microspheres would be washed and concentrated to the final volume of 3 µl for the future agglutination experiments.

4.6 Agglutination experiment with isothermally amplified DNA

An additional experiment was performed to substantiate the feasibility of detecting isothermal amplified DNA products with microsphere agglutination. The isothermal amplification product was generated by employing the USTAR TB isothermal Amplification diagnostic kit (Ustar Biotechnologies Ltd., China) [73]. The detection kit is primarily used for detecting *Mycobacterium tuberculosis* in sputum specimens collected from patients that generate typical biotin-labelled isothermal products, which in turn should agglutinate streptavidin-coated microspheres. The isothermal amplification was performed in accordance with the user's manual provided with the kit [73]. For the experiment, 2 µl of the isothermally amplified product (208 bp) was utilized to agglutinate 3 µl of washed microspheres. The DNA sample from Tube A was used as positive control for the

experiment. Figure 23 demonstrates the agglutination results obtained with the

isothermally amplified DNA product and the DNA sample from Tube A.
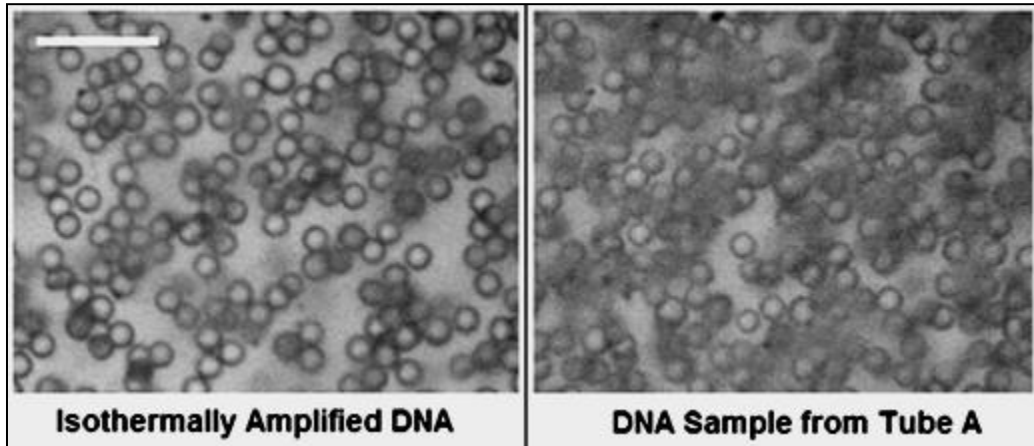
Figure 23: The agglutination results of isothermally amplified DNA and the DNA sample from Tube A. The scale bar represents 24 µm.

The results demonstrate that isothermally amplified biotin-labeled DNA

products agglutinate the streptavidin-coated microspheres. This result suggests

that an agglutination-based microfluidic discriminator may be utilized for

detecting isothermally amplified biotin-labeled DNA. The result also extends the

potential of developing a microfluidic device for detecting amplified DNA

products—including both isothermal amplified and PCR products.

5: PMMA MICROFLUIDIC DISCRIMINATOR: DETECTION OF AGGLUTINATION

This chapter discusses the various microfluidic system designs that discriminate between negative and positive agglutination conditions. "Positive agglutination" refers to a condition where the biotinylated DNA sample (target) has cross-linked the streptavidin-coated microspheres. "Negative agglutination" refers to a condition where no cross-linking of the streptavidin-coated microspheres occurs—i.e., individual microspheres. Hence, the microfluidic discriminator distinguishes between single and agglutinated microspheres, and it detects if a suitable biotinylated DNA sample is present. In addition, this chapter presents experimental results of the various microfluidic discriminator designs and highlights the design challenges faced during fabrication and experimentation.

All the designs discussed in this chapter were fabricated on PMMA substrates. The pattern of channels was registered onto the PMMA substrate using the 254nm DUV exposure technique (refer to page 20). The microwave bonding technique was employed to bond the channels (refer to page 23). For the experiments, 10 µl of microspheres were concentrated to 3 µl final volume; the DNA sample from Tube F was used to agglutinate these microspheres. The reaction mixture was incubated into the reaction reservoir for 90 seconds. To transport the contents from the reaction reservoir, through the discriminator

channel, and ultimately to the waste reservoir, a negative pressure was applied

at the waste reservoir using a handheld syringe or a syringe pump. As the

microspheres utilized in this research were fluorescent, for capturing the data, a

USB scope with UV illumination (Dino-Lite, AM313FVT) was used. Figure 24

shows the set-up for data acquisition.
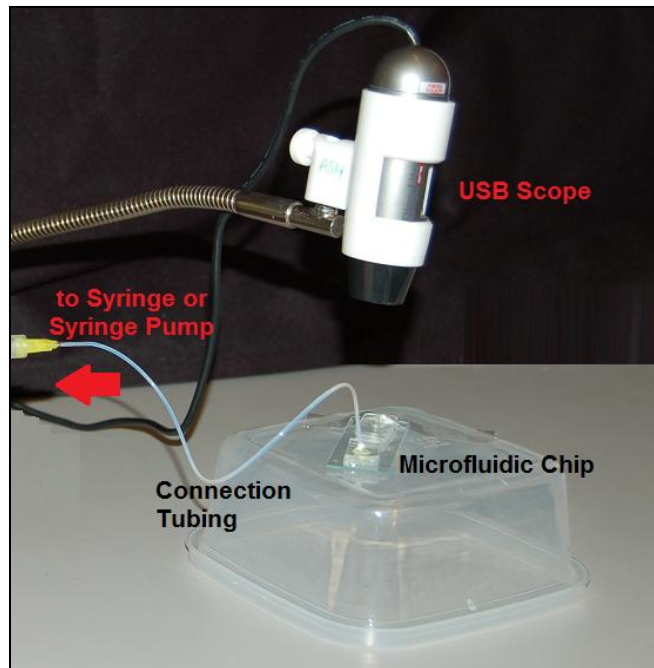
Figure 24: Set-up for capturing experimental data.

5.1 Design 1: "Constricting Channel"

The constricting channel design consisted of a 150-µm wide, 1.75-cm long

channel that transitioned into "the constricting channel", which was 3.25-cm long.

The transition between the 150-µm wide channel and constricting channel was

200-µm long (shown in Figure 25). Three different widths of the constricting

channel were designed (100 µm, 75 µm and 50 µm). The reaction and waste

reservoir were 6-mm in diameter. Before microwave bonding, holes with a

diameter of 3.0 mm and 1.2 mm were drilled into the reaction and waste

chambers, respectively, to provide "real world" connection to the microchannel.

The depth of the microchannel, measured using the Alphastep 500 profilometer

(Tencor Instruments Inc.), was 53 µm. This depth was achieved by a 10-minute

development in the IPA-H_2O bath after DUV exposure (refer to page 20).
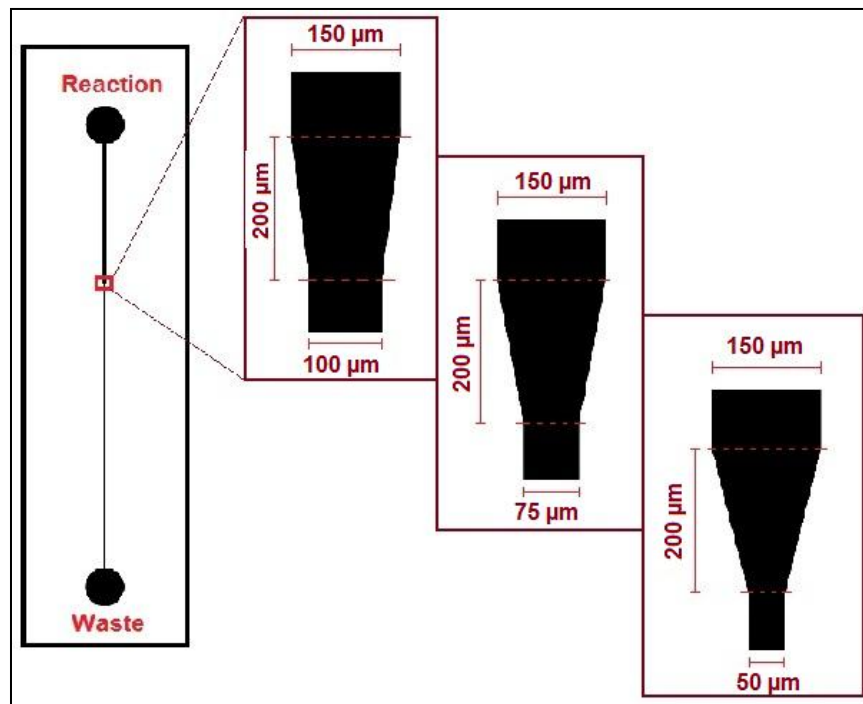
**Figure 25: The dimensional features of design 1: "constricting channel". The three inset
images show the different designs**

Figure 26 shows a photograph of the final microfluidic chip. We expected

that the application of negative pressure on the waste reservoir would transport

all the agglutinates from the reaction reservoir towards the waste reservoir;

during this process, the agglutinates would create a plug/ blockage at the

transition between the two channels.
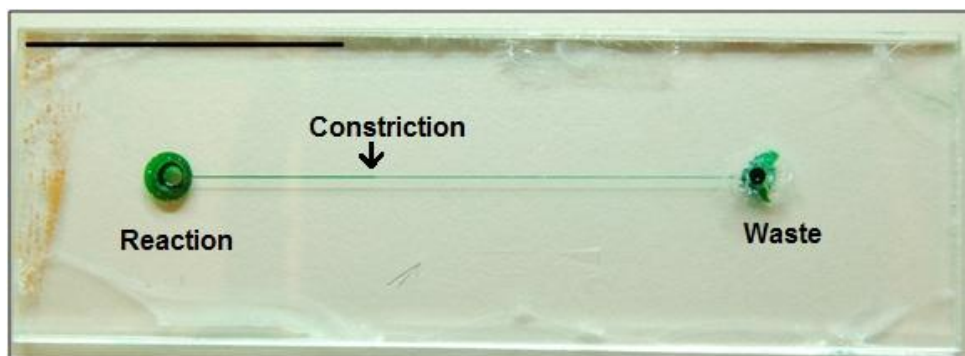
Figure 26: The final microfluidic chip for design 1. Green dye inserted for easy visualization the microchannel. The scale bas represents 2.54cm.

5.1.1 Results

For the 100-µm wide constricting channel, agglutinates were retained in the channel, but not at the expected transition region. The blockage was formed further downstream (~ 3 mm from the transition) in the constricting channel. The negative control (individual microspheres + TE) passed through the microchannel, and no blockage was observed. Figure 27 shows the results of the experiment.
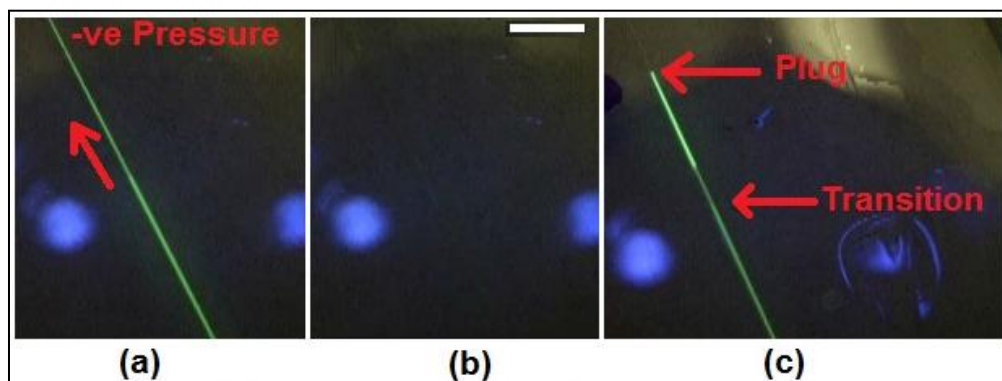
Figure 27: (a) shows the direction of the flow and the negative control (individual microsphere suspension) passing through the constricting channel, (b) The channel after the negative control is completely cleared, (c) shows the formation of the plug in the constricting channel. The scale bar represents 1.2 mm. The blue spots are the reflection of LEDs in the USB microscope used to capture data.

The remaining two constricting channels widths were also tested. The 75-µm wide constricting channel produced similar results as the 100-µm wide constricting channel—with the only difference that the distances the agglutinates travelled before blocking the constricting channel were different from the previous experiment. The agglutinates travelled approximately 1.5 cm from the transition zone before plugging the channel. Furthermore, the agglutinates blocked the 50-µm wide constricting channel, but the distances the agglutinates travelled before blocking were different from both the previous experiments. The negative control also blocked the 50-µm wide constricting channel, giving a false positive result.

5.1.2 Discussion

The 50-µm wide constricting channel was not able to discriminate between the agglutinated microspheres and the individual microspheres. We speculated that the false positive result was due to the discrepancies in the size of the microspheres or inconsistencies in the small constricting channel dimensions. However, the 100-µm and 75-µm wide constricting channels discriminated between the agglutinated and individual microspheres. The results were easily visualized as the microchannel retained the microspheres behind the blockage site. Therefore, the appearance of "piled up" fluorescent microspheres in the microchannel indicated that agglutinated microspheres had been retained, whereas, the microchannel remained "clear" or "empty", indicating that the individual microspheres had passed through and were not retained. These preliminary results provide proof-of-concept evidence that a properly designed

microfluidic channel could discriminate between agglutinated and individual microspheres.

5.1.3   Challenges

It was noticed that the plug was not created at the transition site between the 150-µm wide channel and the constricting channel; rather, the blockage occurred in the downstream constricting channel. It was observed in duplicate experiments, that the blockages occurred in different sites in the constricting channel. This challenge was addressed, "Design 2": a "serpentine" channel was designed and tested.

5.2 Design 2: "Serpentine Channel"

This design consisted of a 150-µm wide, 1.75-cm long channel and a serpentine section, which was 1-cm long. This serpentine section was intended to perform similarly as the constricting region. The width of the serpentine channel was 100 µm. After fabrication, the depth of the microchannel was measured to be 58 µm (10-minute development in the IPA-H_2O bath). Figure 28 illustrates the design of the microchannel.
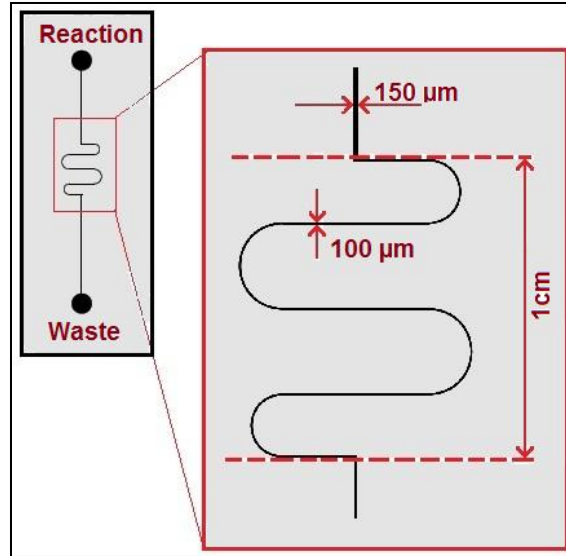
Figure 28: The design specifications of design 2: "serpentine channel"

Figure 29 shows the photograph of final microfluidic chip for design 2.
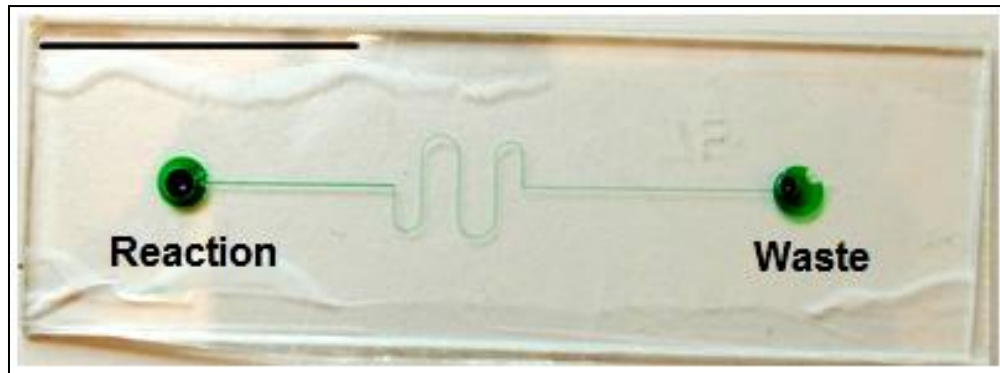
Figure 29: The final microfluidic chip for design 2. The green dye is inserted for easy visualization the microchannel. The scale bar represents 2.54 cm.

5.2.1 Results

Design 2 did not provide reliable discrimination between the agglutinated and individual microspheres. Although, one of the serpentine channel devices showed clear discrimination (as shown in Figure 30 and Figure 31), a duplicate experiment with a new microfluidic chip, provided a result similar to Design 1–the

blockage did not occur in the expected region (serpentine). Furthermore, both

false negatives and false positives were observed.
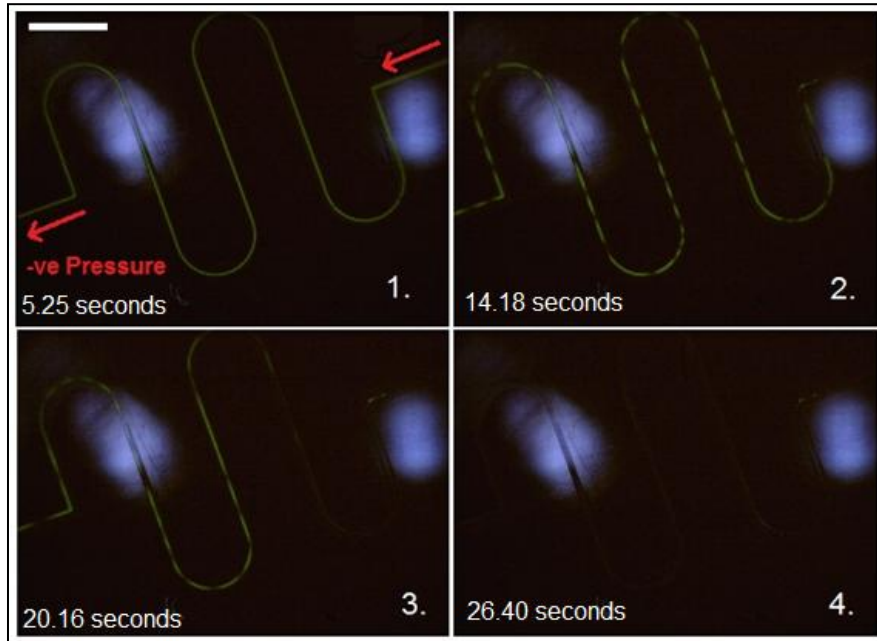
Figure 30: Discrimination results of the negative control. When the negative pressure was applied on the waste reservoir, the contents of the reaction reservoir were transported from the reaction reservoir, through the serpentine channel, and finally to the waste reservoir "without any blockage" in the serpentine channel. The arrow depicts the direction of the flow in the microchannel. The scale bar represents 2.5 mm.
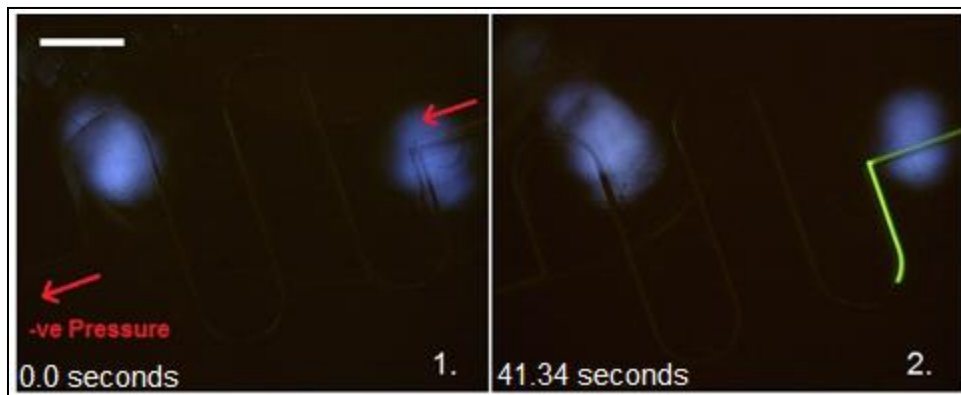
Figure 31: Discrimination results of the (DNA sample from Tube F + microspheres). When the negative pressure was applied on the waste reservoir, the agglutinates created a plug at the first turn of the serpentine channel. The arrow depicts the direction of the flow in the microchannel. The scale bar represents 2.5 mm.

5.2.2 Discussion

The microfluidic device, which demonstrated discrimination between agglutinated and single microspheres, was investigated in detail. We determined that the blockage occurred at the same location; i.e., the first turn of the serpentine channel. These results are in disagreement with the results of the other microfluidic devices, where blockages occurred at different locations. On close inspection of the microchannel, we discovered that there was a "pinch" or constriction at the first turn of the serpentine channel, shown in Figure 32.
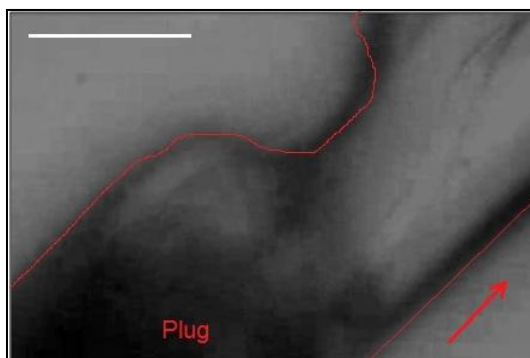
Figure 32: The plug created due to the "pinch" in the channel. The arrow represents the direction the flow and scale bar represents 50 μm.

This "pinch" occurred due to the feature deformation caused by the residual ethanol that was not removed from the microchannel during the microwave bonding (refer to page 23). This serendipitous result suggested a possible scheme in which the "pinch" or micro-constriction could be deliberately created to initiate agglutinate blockage at a specific location in the microchannel. Additionally, the incidences of false negatives were studied. False negatives occurred due to the shear stress created by the negative pressure, which was applied to the waste reservoir. It caused the agglutinates to compress and break

into smaller agglutinates (mostly singlets or doublets). Thus, at high hydrodynamic pressures, agglutinates pass through the channel as easily as individual microspheres.

Hence, in further experiments, a controlled negative pressure was applied by using an automated syringe pump. Additionally, the results were difficult to visualize because of small dimensions of the channels. Therefore, to address this issue, wider microchannels were fabricated in the next design.

5.3 Design 3: "The Pinch"

Contrary to both Design 1 and Design 2, in this design, aggregates were retained in the microchannel by creating constrictions in the flow path. In the previous designs, the focus was to obtain discrimination by changing the geometry of the channel (for instance, by replacing a straight channel with a serpentine channel). For Design 3, as shown in Figure 33, a 500-µm wide microchannel was designed with different constrictions in the middle.
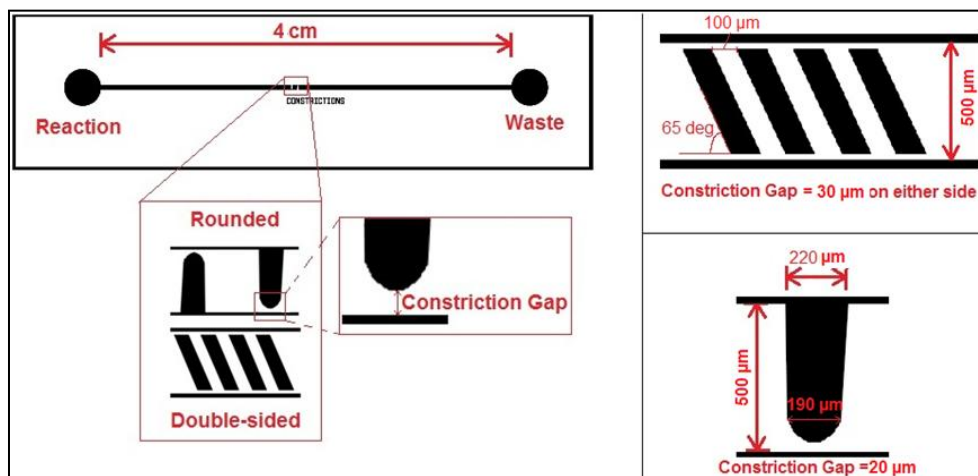
Figure 33: The specifications of Design 3: (top-right) is double-sided constriction, and (bottom-right) is the rounded constriction.

The agglutinates were expected to block the channel at the constriction and pile up; whereas, individual microspheres were expected to pass through the constriction, resulting in a clear channel. The depth of the channels, for this experiment, was 60 µm (10-minute development in the IPA-H$_2$O bath), and the constriction gap was 40 µm and 52 µm for the rounded and double-sided constrictions, respectively. For the experiment, negative pressure at the rate of 0.01 ml/min was applied at the waste reservoir by using a syringe pump. Figure 34 shows the fabricated microfluidic device for Design 3.
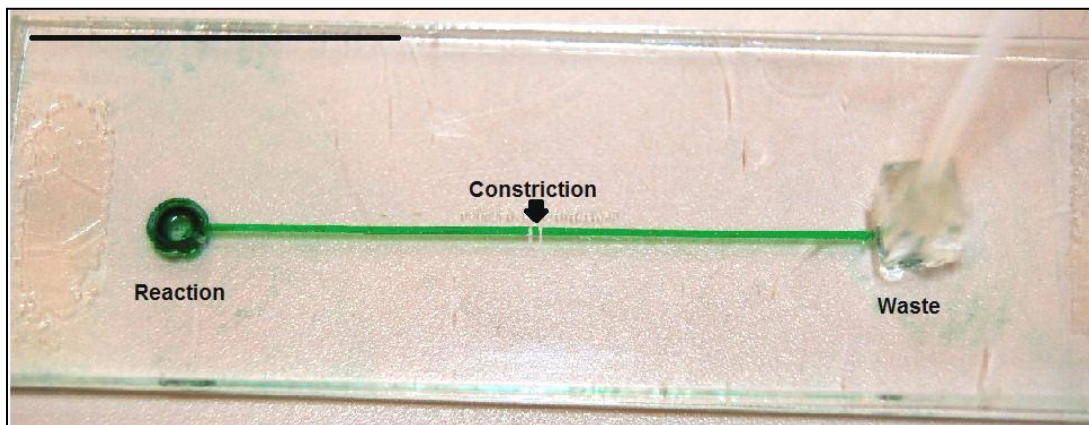

Figure 34: The final microfluidic device for Design 3. Green dye inserted for easy visualization of the microchannel. Scare bar represents 2.54 cm.

5.3.1 Results

Although, a significant amount of agglutination was noticed (as shown in Figure 35), no discrimination between agglutinated and individual microspheres was observed because the agglutinates were not blocked at the constriction. Furthermore, individual microspheres were retained due to air bubbles trapped in the microchannel.
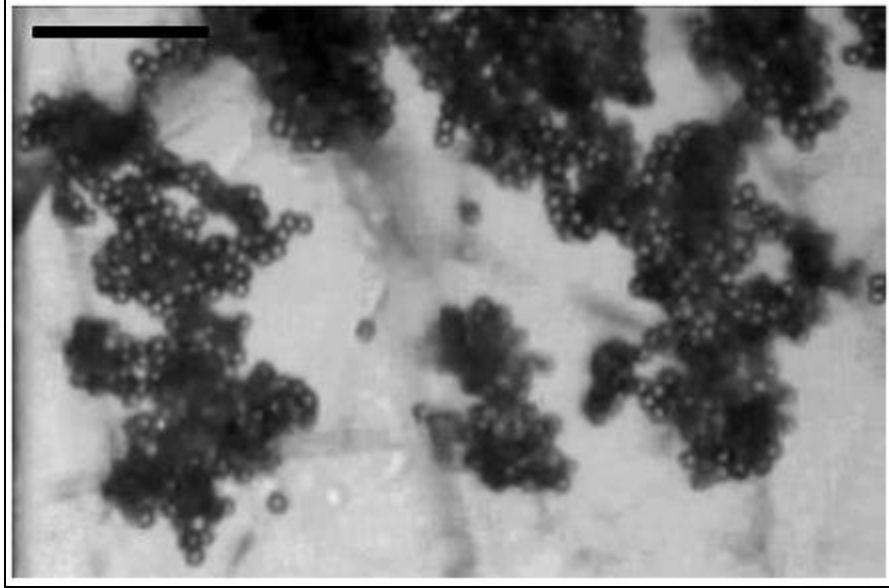
Figure 35: Illustration of the size of agglutinates produced in the experiment with Design 3. The scale bar represents 50 μm.

5.3.2 Discussion

Three main reasons for the failure of this design were considered. Firstly, after applying a controlled negative pressure (0.01 ml/min) the agglutinates were able to easily "compress" and squeeze through the constriction gap of 40 μm and 52-μm for rounded and the double-sided constrictions, respectively. Figure 36 shows the double-sided constriction, where the agglutinate squeezed through the constriction gap. The results showed that the agglutinates have high degrees of freedom and are extremely flexible. Agglutinates aligned themselves along with the hydrodynamic flow, thereby passing through the constriction gap.
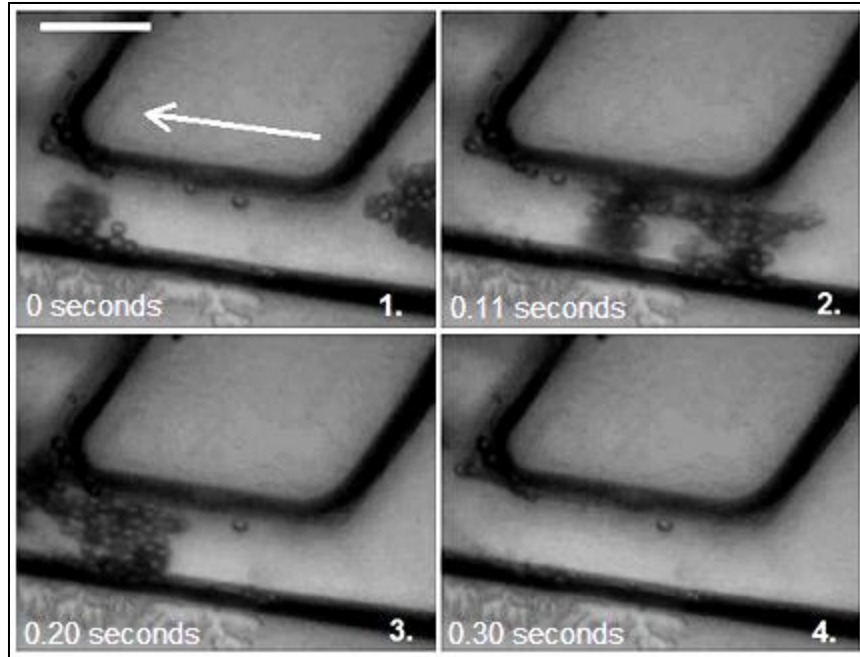
Figure 36: Illustration of an agglutinate aligning itself along the flow and squeezing through the constriction gap. The scale bar represents 50µm. The arrow represents the direction of flow.

Secondly, the constriction gap and the depth of the channels were functionally too large, given the degree of flexibility of the agglutinates. Therefore, another set of 35-µm deep microchannels were fabricated. This depth was almost one-half the depth of the first set of devices. This reduction was accomplished by reducing the development time in the IPA-H_2O bath from 10 to 3 minutes. The reduction in development time also resulted in the constriction gap to be 22 µm as compared to 40 µm for the rounded constriction.

The new set of microfluidic devices provided consistent discrimination with only a few minor exceptions – when air bubbles were trapped in the channels and higher flow rates (>5µl/min) resulted in blocking individual microspheres. Figure 37 and Figure 38 shows the retention of agglutinates. The experiment

was conducted with a flow rate of 5µl/min (produced by negative pressure applied by the syringe pump).
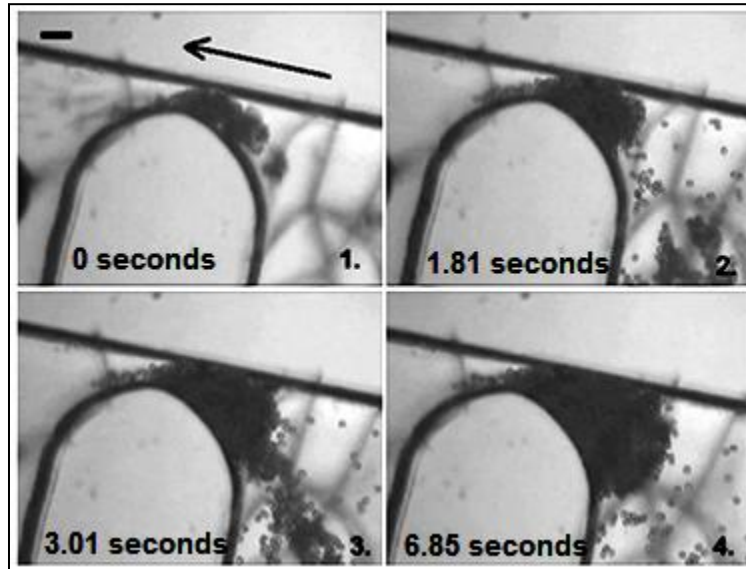
Figure 37: Illustration of the plug creation by retention of agglutinates. The arrow shows the direction of the flow. The scale bar represents 24 µm.
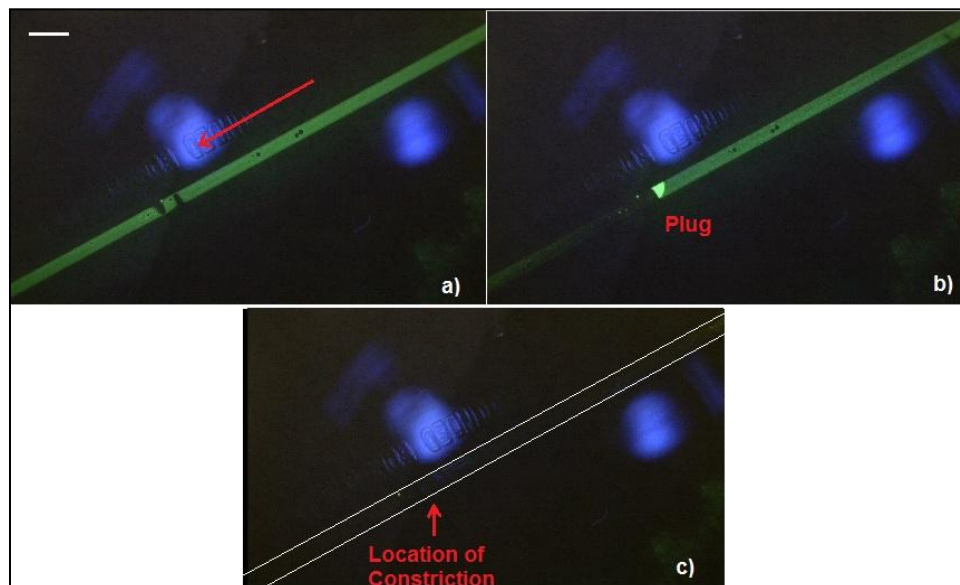
Figure 38: Results of agglutination: a) The arrow shows the direction of the flow, b) Shows the appearance of intense green fluorescence, indicating the retention of agglutinated microspheres, and c) Shows a clear channel indicating that individual microspheres flow through the constriction. The scale bar represents 500 µm.

Furthermore, air bubbles trapped in the channels caused individual

microspheres and agglutinated microspheres to slow down and form a plug at

the constriction. The air bubbles were present because the channels were filled

with PBS/BSA buffer before the experiment was initiated. The bubbles occurred

due to the frothiness of PBS/BSA buffer and/or trapped air in the channels.

Figure 39 demonstrates a situation where the air bubble blocked the flow of

individual microspheres, thereby providing a false positive result.
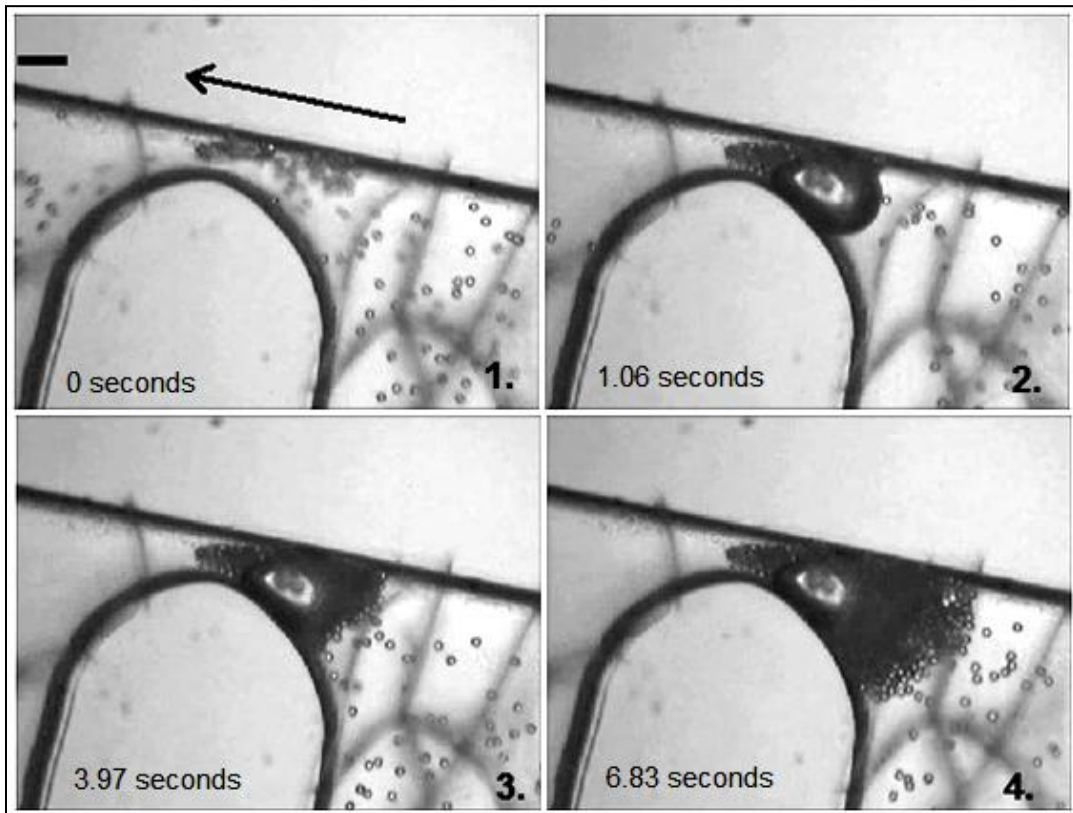
Figure 39: Illustration of an air bubble blocking the constriction gap and causing single microspheres to be blocked. 1) Shows single microspheres crossing the constriction gap. 2) Shows bubble blocking the constriction gap. 3) and 4) Show single microspheres piling up at the constriction due to the blockage caused by the bubble. The scale bar represents 24 μm. The arrow depicts the direction of the flow.

The flow rate also plays a vital role in obtaining effective discrimination. As mentioned before, at high flow rates, agglutinates break easily and even individual microspheres can cause blocking because a relatively high concentration of individual microspheres can flow through the pinched area (at the constriction gap) and block the constriction gap. This situation can be compared to a scenario where 1000 people running at the same speed try to pass through a small door simultaneously, thus causing a blockage at the door. To solve the problems caused by the flow rate, an experiment was conducted to find the optimal flow rate at which neither the agglutinates pass through the constriction nor the individual microspheres cause a blockage at the constriction.

5.3.3 Optimal flow rate

A volume of 3 µl unwashed microspheres were cross-linked with the DNA sample from Tube F. The observations are tabulated in Table 5.

Table 5: Effect of the flow rate on the agglutination experiment.

Flow Rate	Observation
> 20 µl/min	Agglutinates break into singlets or doublets
1 µl/min- 20 µl/min	Agglutinates still break into smaller agglutinates, but not into singlets
1 µl/min – 0.1 µl/min	agglutinates moved swiftly and did not dissociate
< 0.1 µl/min	It takes longer than 10 minutes to generate flow

The results show that at the flow rates between 0.1µl/min – 1µl/min agglutinates did not dissociate, but they were not retained at the constriction 22-µm gap. Hence, more than one constriction may be necessary (i.e., an array of constrictions) in the flow path to trap the agglutinates which flowed through an

early constriction. Additionally, for flow rates less than 5 µl/min, 3-5 minutes were needed to initiate flow. Therefore, to decrease flow initiation times, the length of the channel was reduced in the future designs.

5.4 Design 4:

In Design 4, a 500-µm wide, 2-cm long microchannel was designed with an array of posts in the middle. This array of posts (Figure 40) was expected to function as obstacles for the agglutinated microspheres and prevent them from flowing further through the channel.
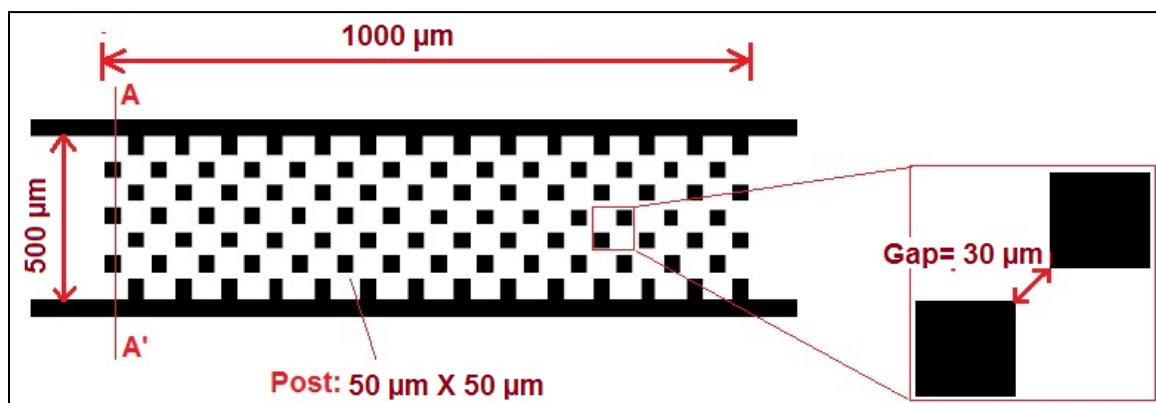
Figure 40: The specifications of the constriction in design 4.

5.4.1 Results

The experimental results showed no retention of agglutinated microspheres; both agglutinated and individual microspheres were carried to the waste reservoirs on the application of negative pressure (0.1 µl/ min). The channel and constrictions were observed under the profilometer to evaluate the possible cause. Figure 41 reveals that during the fabrication of the microfluidic

substrates, the height of post was reduced to approximately one-half the height

of the sidewall.
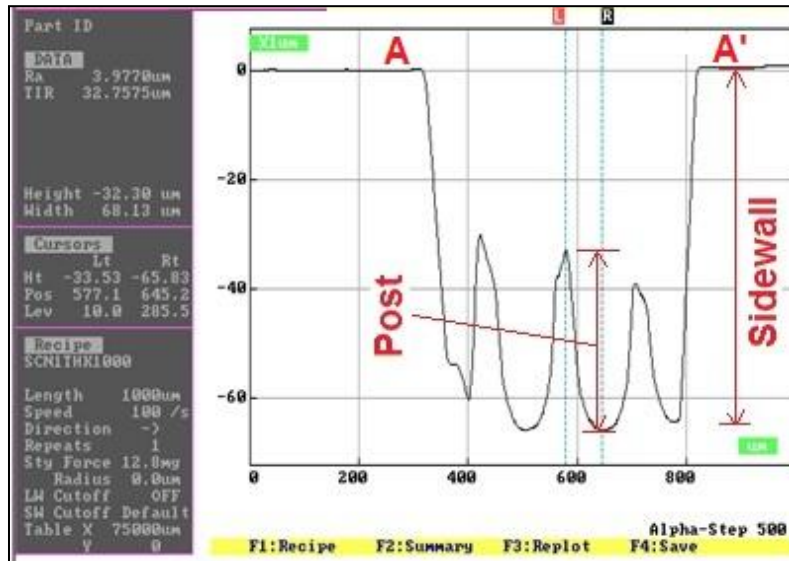
Figure 41: Profile measurements of cross-section AA'. The height of the middle post is 32.30 µm.

This height change was caused by the significant negative sidewalls due

to the non-collimated nature of the DUV light source used in the fabrication

process. The negative sidewalls produced by the non-collimated radiation source

generated severe undercuts of the features after the development in the IPA-

H_2O bath. Figure 42 shows the effect of a non-collimated radiation source.
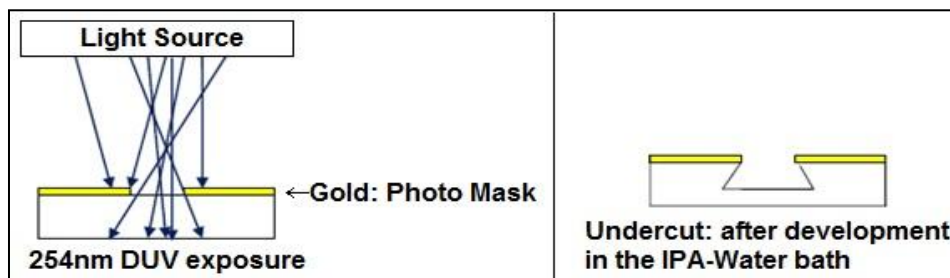
Figure 42: Schematic representation of the effect of the non-collimated light - negative side-walls.

Due to the difference in the height of posts and side walls, there was sufficient gap for the agglutinates to flow through the constriction. The fabrication of negative sidewalls can be eliminated by using a collimator. A honeycomb collimator was tried, but it significantly increased the irradiation time of the samples, due to the additional time necessary to compensate for the energy absorbed by the collimator. We determined that, after 48 hours of exposure (using the collimator), a 2-µm deep channel was produced after a 30-minute in IPA-H_2O bath. This long exposure time indicated that using a collimator was not a practical solution. Therefore, the design was modified by increasing the size of the posts from 50 µm to 200 µm. While the increased size of the post compensated for the undercut that occurred during the development in IPA-H_2O bath, the bonding of the PMMA microfluidic chip presented a different challenge. Microwave bonding is limited by the design complexity due to residual ethanol in the channels that blocked the constrictions, as illustrated in Figure 43.
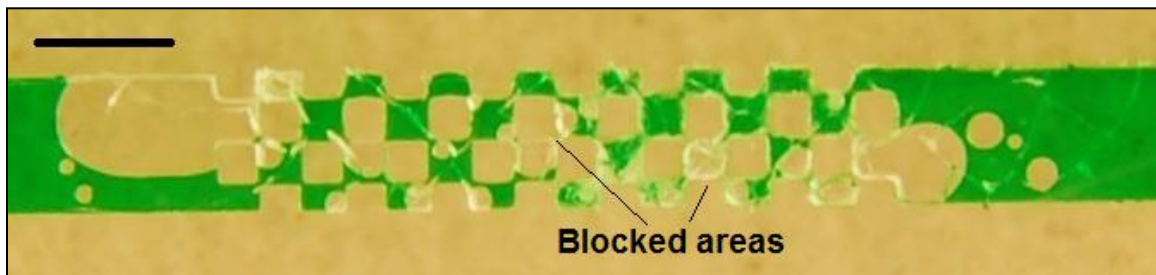
Figure 43: Illustration of discrepancies caused by the trapped ethanol during the Microwave bonding. The scale bar represents 500 µm.

With the microwave bonding, the yield was extremely low: only four out of ten microchannels survived after the bonding due to trapped residual ethanol in

the constriction channel, which in turn led to blockage after the heat treatment. Therefore, future designs were fabricated using PDMS instead of PMMA.

5.5 Considerations for the future designs: Summary of the designs fabricated on PMMA

After evaluating all the designs presented in this chapter, the following considerations were drawn for future designs.

1. At the flow rates between 0.1 µl/min – 1 µl/min, agglutinates do not break.

2. At flow rates between 0.1 µl/min – 1 µl/min, the constriction gap has to be smaller than 22 µm.

3. Agglutinates and / or microspheres gain velocity in the pinched area (at the constriction gap).

4. Air bubbles block individual or agglutinated microspheres at the constriction.

5. Agglutinates have a high degree of freedom—they tend to compress and bend during flow; therefore, to retain agglutinates, an array of constrictions in the flow path would be more effective than a single constriction in the channel.

6. The length of the channel should be small (~ 1 cm) to facilitate the rapid initiation of flow.

7. The depth of the channel should be less than 35 µm to prevent highly flexible agglutinates from compressing and flowing through the constriction.

6: DESIGN SIMULATIONS

Based on the conclusions drawn in the previous chapter, new designs were simulated using COMSOL Multiphysics® version 3.5a [74]. The purpose of simulating different designs with arrays of constrictions in microfluidic channel was to determine the ideal configuration, eliminating the problems encountered with the microfluidic designs covered in the previous chapter. This chapter presents simulation of flow velocities produced on the application of negative pressure. The simulation results of different designs are compared to determine the optimal design for the microfluidic discriminator.

6.1 Designs

Based on Design 4 (refer to page 63), three different designs were simulated to determine the geometry that will facilitate flow rates at which the agglutinates would not dissociate (0.1 µl/min – 1 µl/min). The specifications of all the simulated geometries are shown in Figure 44. The inlet flow of geometry is required to be maintained at 0.1µl/min; therefore, assuming depth of the channel to be 20 µm, the flow velocity can be calculated as,

$$Flow\ Velocity\ \left(\frac{m}{s}\right) = \frac{Flow\ rate\left(\frac{m^3}{s}\right)}{Area(m^2)}\ , \qquad \text{Equation 2}$$

$$where, \quad Flow\ rate = 0.1\left(\frac{\mu l}{min}\right) = 1.67 \times 10^{-12}\left(\frac{m^3}{s}\right)$$

$$and, \quad Area = (Width\ of\ channel) \times (Depth\ of\ channel)$$

$$Area = (275 \times 10^{-6}) \times (20 \times 10^{-6}) = 5.5 \times 10^{-9}(m^2)$$

$$Therefore, \quad Inlet\ velocity = Flow\ Velocity = 3.03 \times 10^{-4} \left(\frac{m}{s}\right)$$
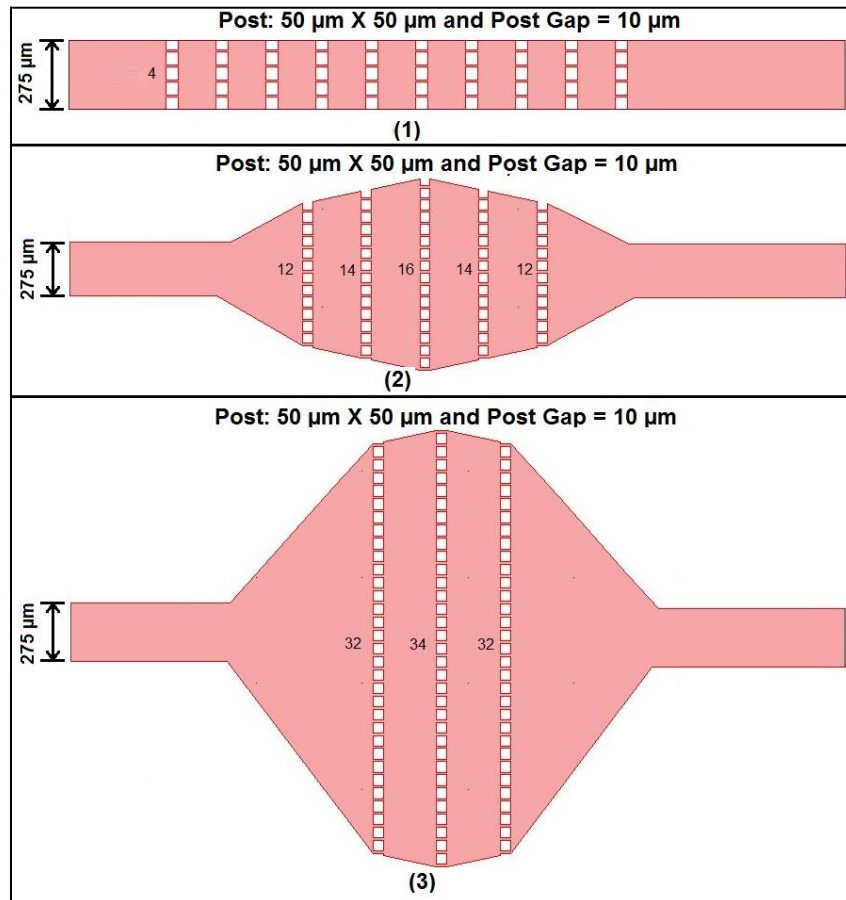
Figure 44: The specifications of the simulated geometry 1, 2 and 3. The number next to each column of posts represents the number of posts in that column.

6.1.1 Boundary and subdomain conditions

All the designs were simulated using the '*Incompressible Navier-Stokes'* application mode of the *MEMS module*. Table 6 tabulates the Boundary and subdomain settings for the simulations.

Table 6: Boundary and subdomain settings for the simulations.

Subdomain settings	Boundary Conditions
Density(ρ) = 1000 kg/m^3 Dynamic viscosity = 1 ×10^{-3} Pa.s Relative permittivity(ϵr) = 80 Mean free path = 1 × 10^{-6}	Inlet: 3.03 × 10^{-4} m/s Outlet: 'Zero pressure, with no viscous stress'. The remaining boundaries are set to 'No slip walls'

6.2 Simulations results

This section presents the simulation results for geometry-1, geometry-2 and geometry-3.

6.2.1 Geometry-1

The simulation results for geometry-1 showed that the flow velocity increased in the post gaps as compared to the applied input flow velocity. This occurred due to the "nozzle effect" that is created by splitting the main channel into four smaller channels. The velocity in the post gaps was 2.558 X10^{-3} m/s, which was 8.5 times greater than the inlet velocity 3.03 X 10^{-4} m/s. Figure 45 and Figure 46 show results for geometry-1.
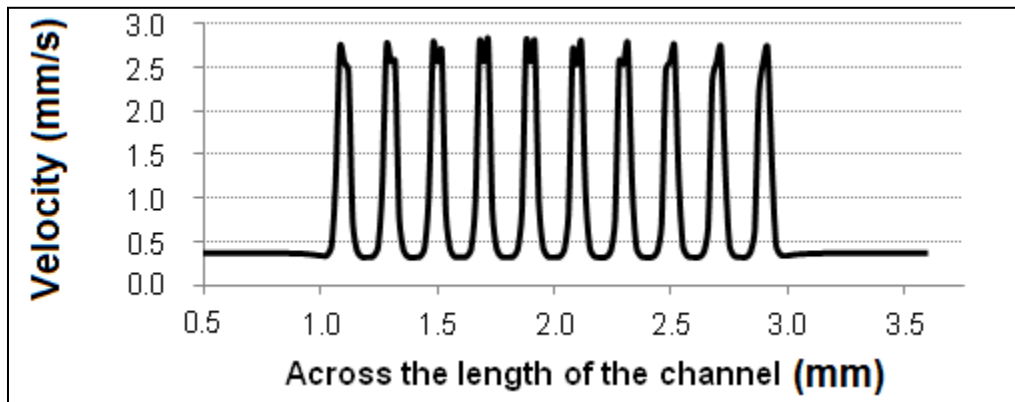
Figure 45: Flow velocity of the cross-section BB' of geometry-1.
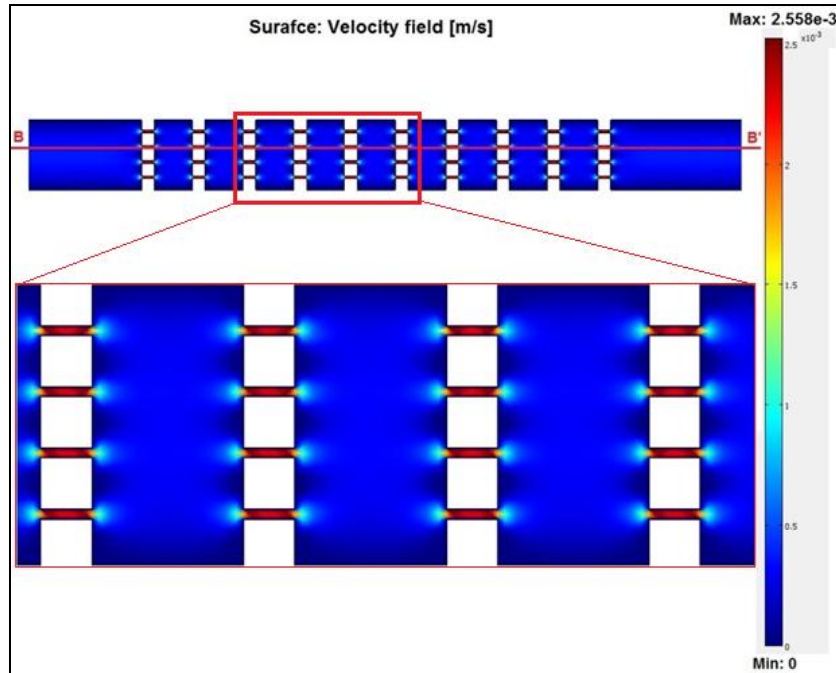
Figure 46: Simulation results of geometry-1. The color scale represents the color legend for surface velocity field, "blue" represents minimum velocity and "red" represents the maximum velocity.

Geometry-1 was not suitable for the microfluidic discriminator because the higher flow velocity in the post gaps allowed agglutinates to pass through and providing a greater chance for the agglutinates to dissociate.

6.2.2 Geometry-2

The simulation results for geometry-2 showed that by increasing the number of posts splitting the main channel, the velocity in post gaps was reduced. The maximum velocity in the post gaps of geometry-2 was 7.139×10^{-4} m/s, which was 3.6 times smaller than the maximum velocity in the post gaps of geometry-1. Figure 47 and Figure 48 show that the column with 16 posts had the lowest flow velocity in the post gaps in comparison to the velocity in post gaps of columns with 12 posts and 14 posts. This simulation result implied that by

increasing the number of posts in the columns, the flow velocity in the post gaps

could be reduced to the input flow velocity or lower.
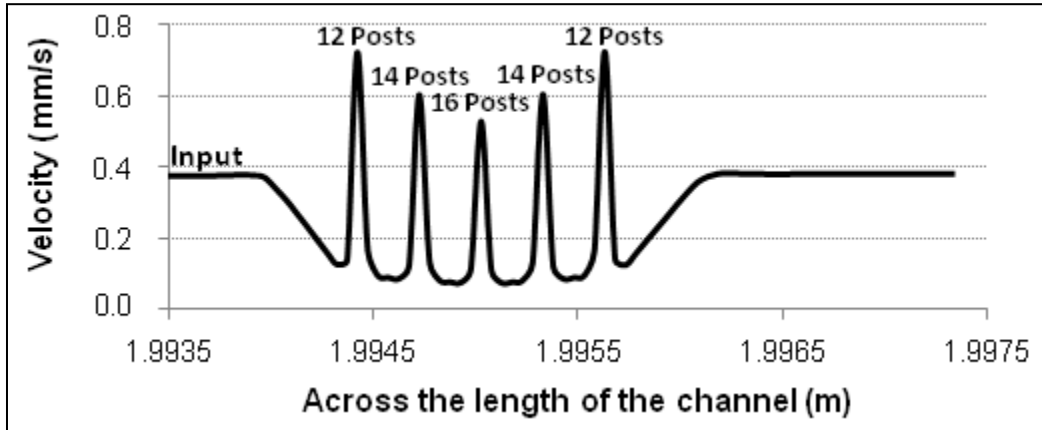
Figure 47: Velocity profile across the cross-section CC' of geometry-2.
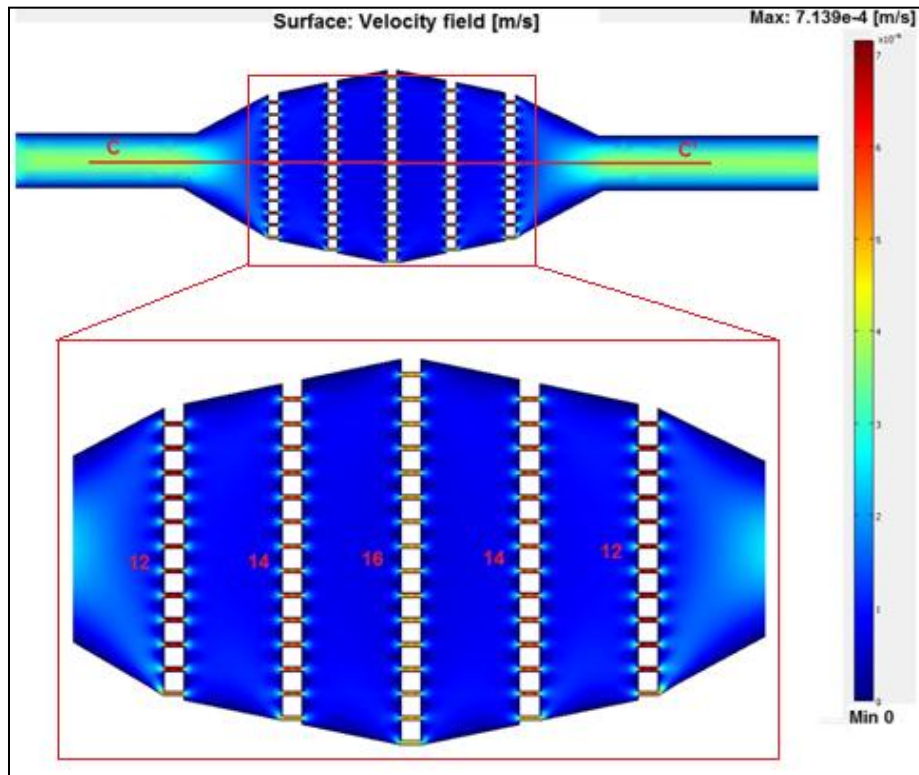
Figure 48: Simulation results of geometry-2. The colour scale represents the colour legend for surface velocity field, "blue" represents minimum velocity and "red" represents the maximum velocity. The number next to each column of posts represents the number of posts in that column.

6.2.3 Geometry-3

Simulation results of geometry-3 revealed that, by splitting the main channel into 32 channels, the array acted as a diffuser. In this geometry, the maximum flow velocity in the post gaps (2.49×10^{-4} m/s) was lower than the input flow velocity; consequently, this geometry was suitable for discriminating between agglutinated and individual microspheres. Figure 49 and Figure 50 show simulation results and the velocity field across the cross-section DD' of geometry-3. Based on the simulation results, the future designs were based upon geometry-2 and geometry-3.
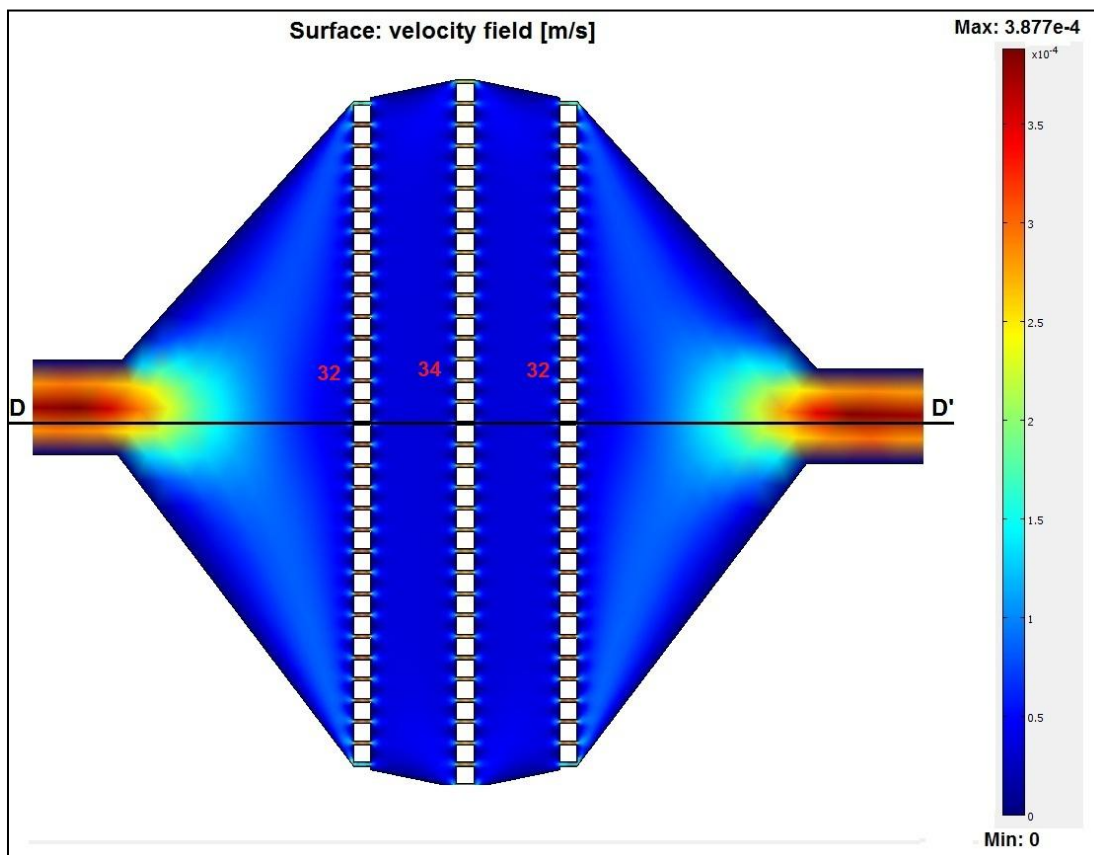
Figure 49: Simulation results of geometry3. The colour scale represents the colour legend for surface velocity field, "blue" represents minimum velocity and "red" represents the maximum velocity. The number next to each column of posts represents the number of posts in that column.
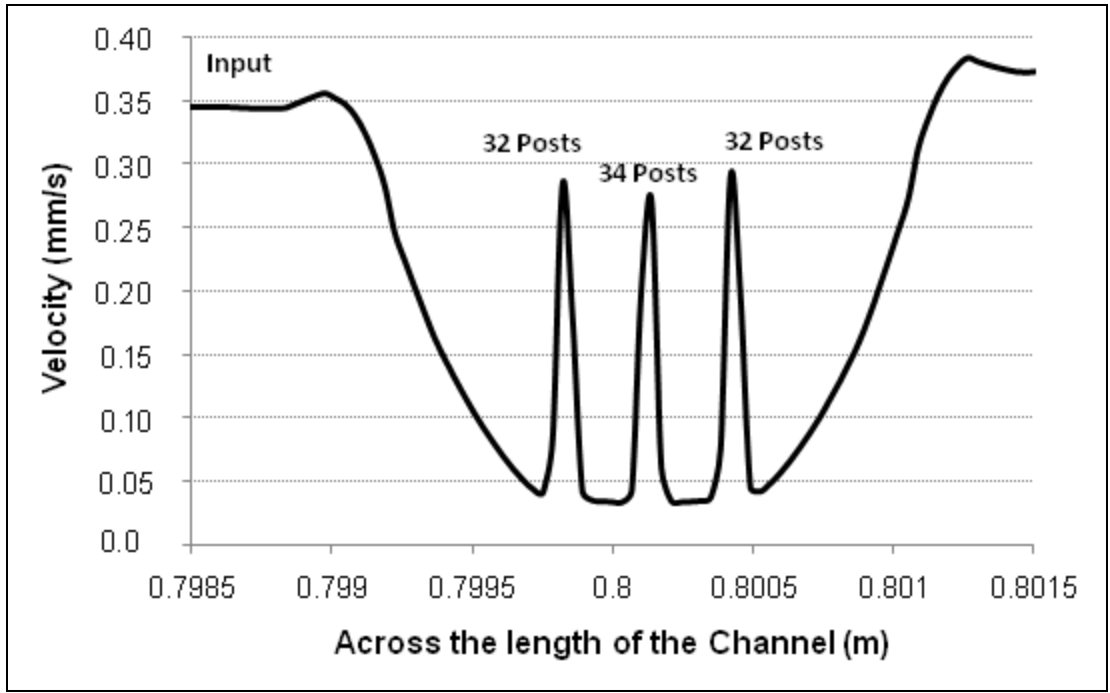
Figure 50: Velocity profile across the cross-section DD' of geometry-3.

7: PDMS BASED MICROFLUIDIC DISCRIMINATOR

Based on the simulation results from the previous chapter; this chapter presents experimental results of the different microfluidic discriminator designs. This chapter focuses on the fabrication and testing of the new designs. Furthermore, the chapter discusses, in detail, the challenges encountered in discriminating agglutinated and individual microspheres, and it presents potential solutions. Finally, the chapter presents the final microfluidic discriminator design and experimental results.

The designs described in this chapter were fabricated using soft lithography of the PDMS substrate (refer to page 24). The bonding of the microfluidic devices was accomplished using Corona discharge (refer to page 26).

For the agglutination experiments, the microchannels were filled with PBS/BSA buffer by applying a positive pressure (0.5 µl/min) on the waste reservoir (using a syringe pump). This flow rate eliminated trapped air bubbles in the microchannels. Additionally, at 0.5 µl/min, new bubbles were not generated. Figure 51 depicts the bubbles blocking the post gaps, which could cause false positive results. A volume of 10 µl of unwashed microspheres was concentrated to 3 µl of the final volume, and the DNA sample from Tube G was used to cross-link the microspheres. The reaction mixture was incubated in the reaction reservoir for 90 seconds. Finally, the contents from the reaction reservoir were

transported to the waste reservoir by applying a negative pressure on the waste reservoir by using a syringe pump.
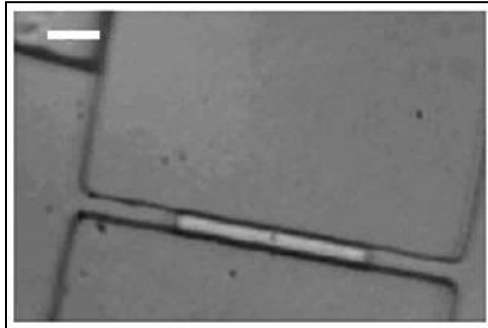
Figure 51: Illustration of a bubble blocking the post gap. The scale bar represents 14 μm.

7.1 Microfluidic discriminator: "The Filter"

The filter design consisted of reaction and waste reservoirs along with a filter section. Reaction and waste reservoirs were connected to the filter section with 200-μm wide and 3-mm long microchannels, respectively. The reservoirs were 3-mm in diameter. Figure 52 depicts the schematic of the filter design.
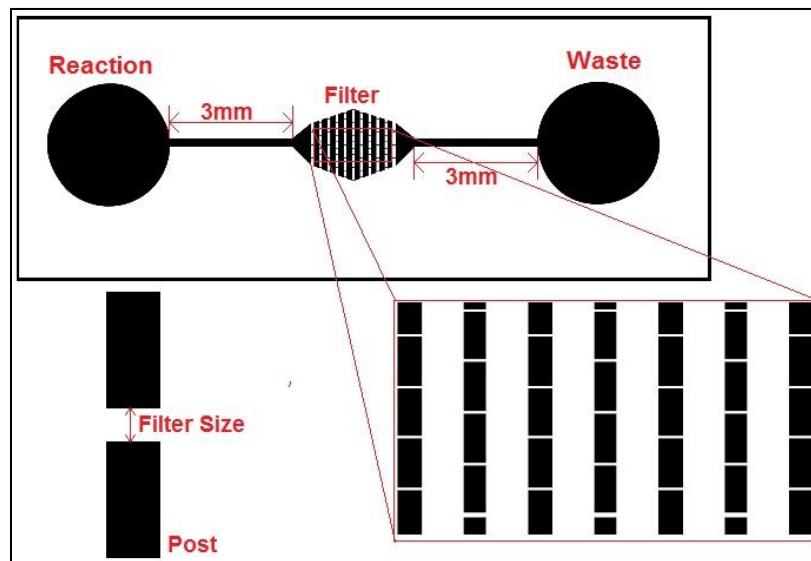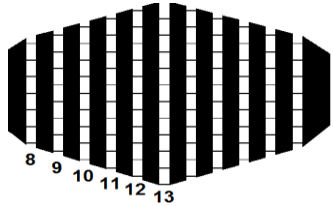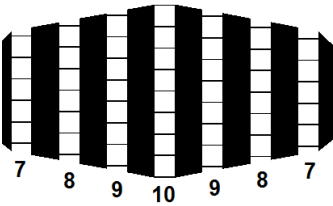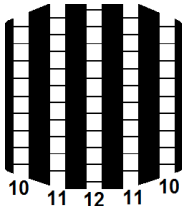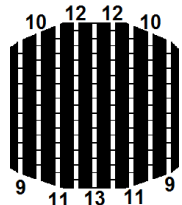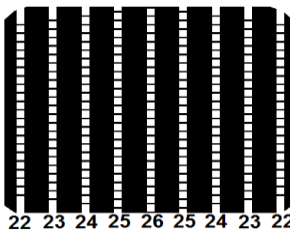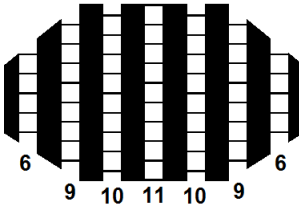
Figure 52: Schematic of the filter design.

Different designs with varying post and filter sizes were fabricated. Table 7 summarizes the fabricated designs.

Table 7: Description of the fabricated filter designs. The number next to each column represents the number posts in the column.

Channel number	Post size (Height X Width)	Filter size	Filter details
1	150 µm X 75 µm	7 µm	
2	150 µm X 150 µm	7 µm	
3	150 µm X 150 µm	10 µm	
4	150 µm X 75 µm	10 µm	
5	50 µm X 50 µm	10 µm	
6	150 µm X 150 µm	12 µm	

Since, PDMS is a flexible polymer and different design features would produce variable flexibility. For example, a high aspect ratio feature would be more flexible than a low aspect ratio feature. Therefore, bonding of the filter design could be a concern, because when pressure is applied to bond corona activated surfaces, posts could get deformed which, in turn, could affect the post gap. Therefore, the different sizes of the posts (listed in Table 7) were designed to determine that which post size is effectively fabricated, without any comprise in the post gaps.

7.1.1 Filer design fabrication: 10-µm deep microchannel

For fabricating 10-µm deep microchannels, the SU-8 master was prepared with the intended feature height of 10 µm (Appendix B provides the process parameters required to produce the intended feature height). Figure 53 shows the final microfluidic device for channel 2 (refer to Table 7). The fabricated microchannels were 10.83-µm deep.
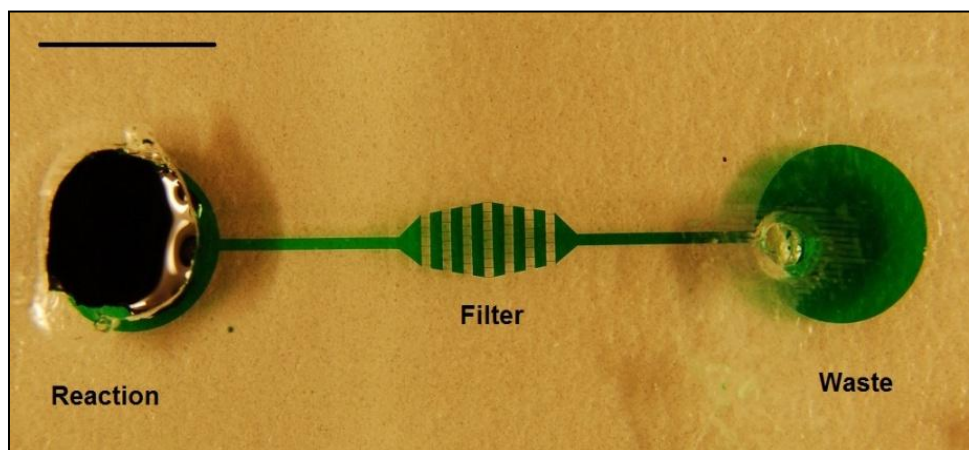
Figure 53: Final fabricated microfluidic device for channel 2. Green dye inserted for clear visualization of the design. The scale bar represents 3 mm.

77

7.1.2 Results

All six channel designs were successfully fabricated without any discrepancies. Channel-1 was tested for the discrimination between agglutinated and un-agglutinated products. The results of channel-1 showed that the 7-µm filter size was not suitable for discrimination given that the individual microspheres clogged the filter on application of negative pressure (1 µl/min) on the waste reservoir. Figure 54 shows that the 7-µm gap between the filter posts was too narrow for the microspheres (6-µm diameter) to pass through the gap. Consequently, channel-1 and channel-2 were not used for subsequent experiments.
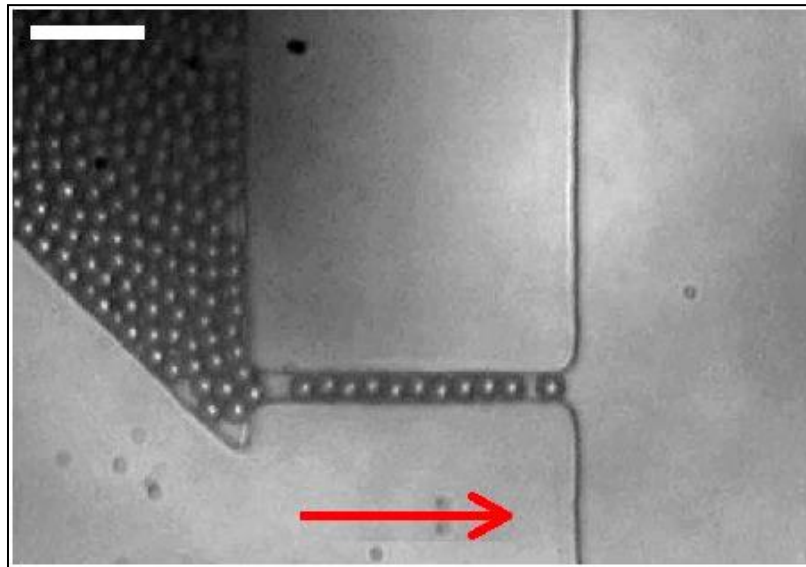
Figure 54: Single microspheres blocking 7-µm wide filter gap. The arrow shows the direction of the flow. The scale bar represents 20 µm.

Channel-5 (10-µm filter gap) was also tested for the discrimination experiment. Channel-5 did not discriminate between agglutinated and individual microspheres upon the application of negative pressure (0.1 µl/min), mainly

because the extent of agglutination was less than the agglutination in other experiments as described in chapter 5. In this case, the agglutinates were comprised of 3 -10 cross-linked microspheres; whereas, agglutinates in the previous experiments were composed of several hundred cross-linked microspheres (see Figure 55). We intuitively deduced that this difference in the extent of agglutinate size was due to the difference in the depth of the channels. In Figure 55, it can be visually determined that the size of agglutinates in a 60-μm deep channel is greater than the size of the agglutinates produced in 10.83-μm deep channel.
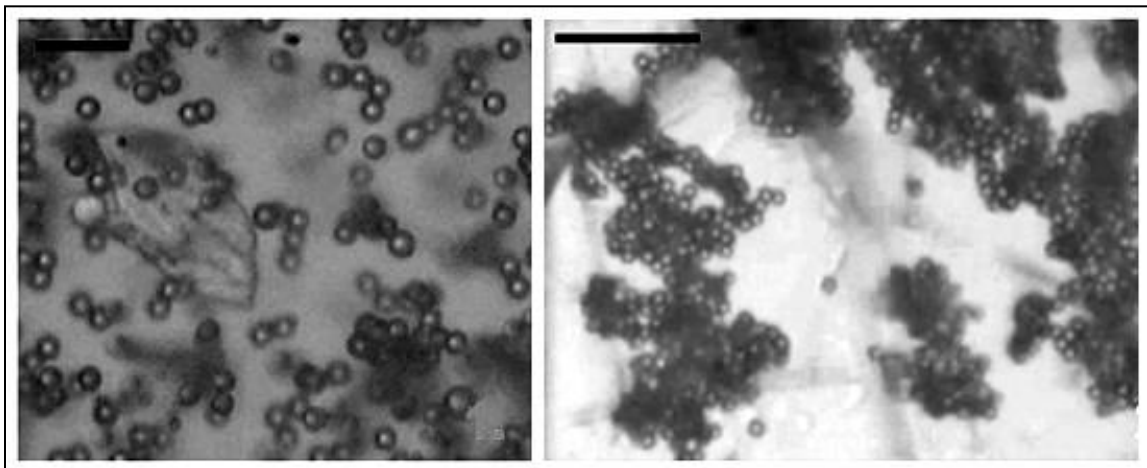
Figure 55: Amount of agglutination: in the 10.83-μm deep channel (left) and in the 60-μm deep channel (right). The scale bars on the left and right represent 24 μm and 50 μm, respectively.

The small agglutinates easily passed through the filter like the individual microspheres, thereby, resulting in no discrimination (as illustrated in Figure 56). Therefore, in the subsequent experiment, the depth of the channel was increased to 20 μm, keeping in mind that the depth of the channel should be less than 35 μm for effective discrimination (refer to page 66).
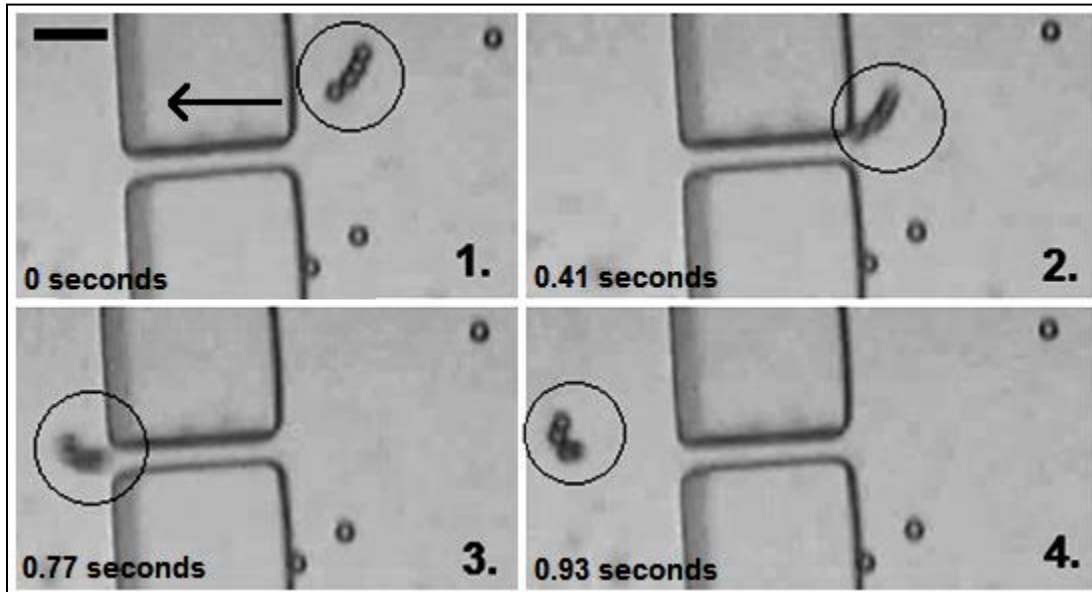
Figure 56: Illustration of an agglutinate composed of four microspheres passing through the 10-μm filter gap. The arrow depicts the direction of the flow and the scale bar represents 24 μm.

7.1.3 Filer design fabrication: 20-μm deep microchannel

For the filter design, a new SU-8 master, was fabricated with a feature height of 20 μm by following the process described in the processing guidelines provided by the manufacturer [65]. Appendix C summarizes the process specifications for producing 20-μm thick SU-8 mold. The final height achieved was 19.8 μm.

7.1.4 Results

In this trial, channels 3, 5, and 6 were tested. All the tested channels showed discriminated between agglutinated and individual microspheres. Figure 57 depicts the discrimination of agglutinated and individual microspheres.
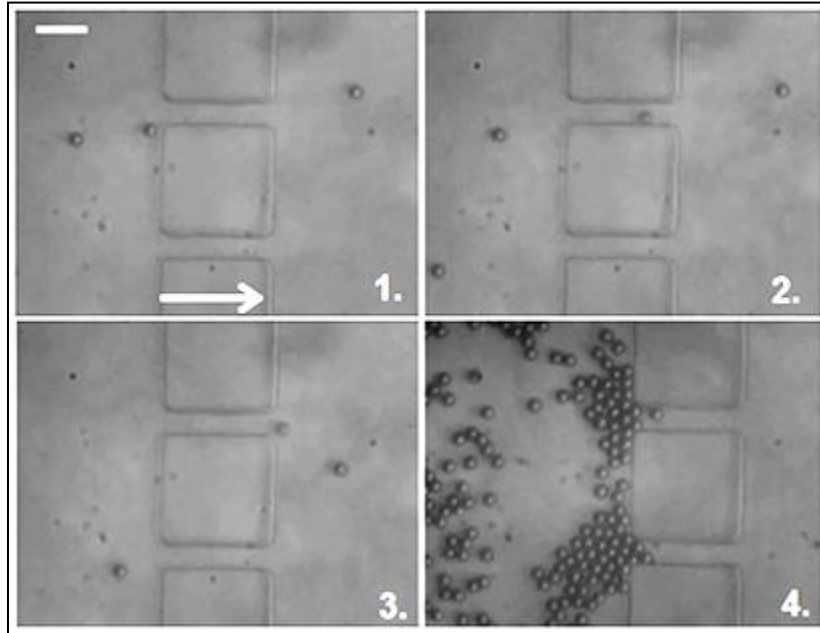
Figure 57: Panels 1, 2, and 3 show that single beads did not block the filter gap of 10-µm, whereas, panel 4 shows agglutinates blocking at the filter gap. The arrow represents the direction of flow and the scale represents 25 µm.

Also, the extent of agglutination in the channels was greater than the agglutination seen in the 10.83-µm deep channels. Figure 58 compares the size of agglutinates in both cases.
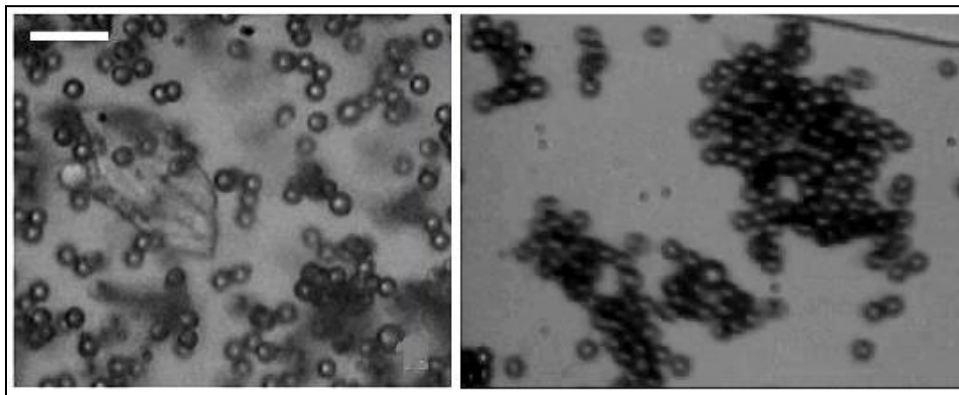
Figure 58: Comparison of the size of agglutinates in 10.83-µm deep channel (left) and 19.8-µm deep channel (right). Scale bar represents 24 µm.

Comparing the agglutination results for the 10.83-μm, 19.8-μm, and 60-μm deep microchannels, a correlation between the depth of the channels and size of agglutinates was observed. The deeper channels allowed the microspheres to form larger (in size) agglutinates. Intuitively, deeper channels provided extra space for agglutinate formation. Thus, the depth of the channel was a significant factor in the design of the microfluidic discriminator as it influenced the size of the agglutinates. Evident from the results of this and the previous experiment is that the greater size of agglutinates eliminated the likelihood of agglutinates escaping through the gaps (similar to individual microspheres), thus, enhancing effective discrimination. Therefore, in subsequent experiments, an optimal channel depth range was determined to enable larger agglutinates to be formed and retained.

A few exceptions were also observed during the trials. We observed that larger microspheres caused blockages. All the microspheres were not exactly 6 μm in diameter, in a few incidences, microspheres with diameters greater than 6 μm were observed, which in turn blocked the channel (Figure 59) and thereby produced false-positive results. This problem was mostly observed in channels with 10-μm filter gap. As a result, a 12-μm filter gap was chosen to compensate for the variation in microsphere diameter.
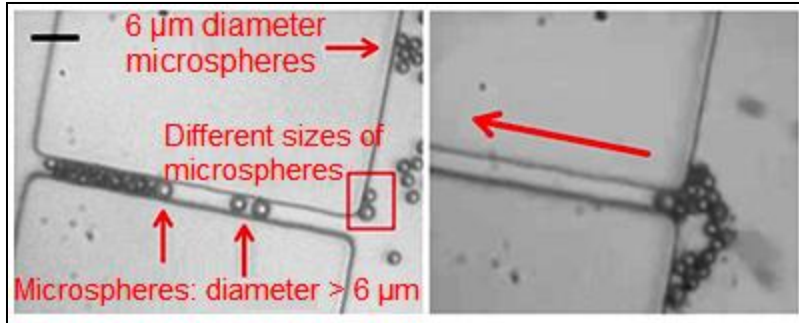
Figure 59: Illustration of different sizes of microspheres (left), and the blockage caused by the "large" microsphere (right). The arrow (right) shows the direction of flow. The scale bar represents 20 µm.

In addition to variations in the size of microspheres, residual PDMS in channels also formed blockages, providing false results. The issue of residual PDMS was resolved by thoroughly cleaning the channels before bonding and performing a microscopic examination of microfluidic channels to eliminate those samples that had fabrication blockages. In future experiments, the samples were thoroughly cleaned with IPA, rinsed with water, and then blow dried with N_2 before bonding. Figure 60 shows residual PDMS blocking the filter gap and causing plug formation.
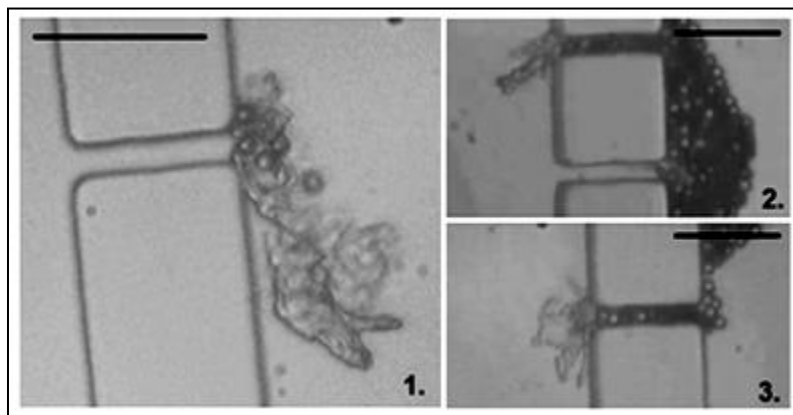
Figure 60: Picture 1: Residual PDMS blocking the filter gap, the scale bar represents 75 µm. Picture 2 & 3: Plug formed by single microspheres due to the clogging of filter gaps by the residual PDMS. The scale bars represent 50 µm.

7.2 Microfluidic Discriminator: The final design

In the final discriminator design, simulated geometry-3 (refer to page 72) was fabricated. The length of the channel and the shape of the reservoirs were modified as shown in previous filter designs (Figure 61). The teardrop-shaped reservoirs were designed to reduce dead volume (compared to round reservoirs) and to facilitate a greater mass of agglutinates entering the channel (Figure 62). Furthermore, the number of post columns was reduced to three in the new design, as the retention of agglutinated microspheres predominantly occurred at the first column.
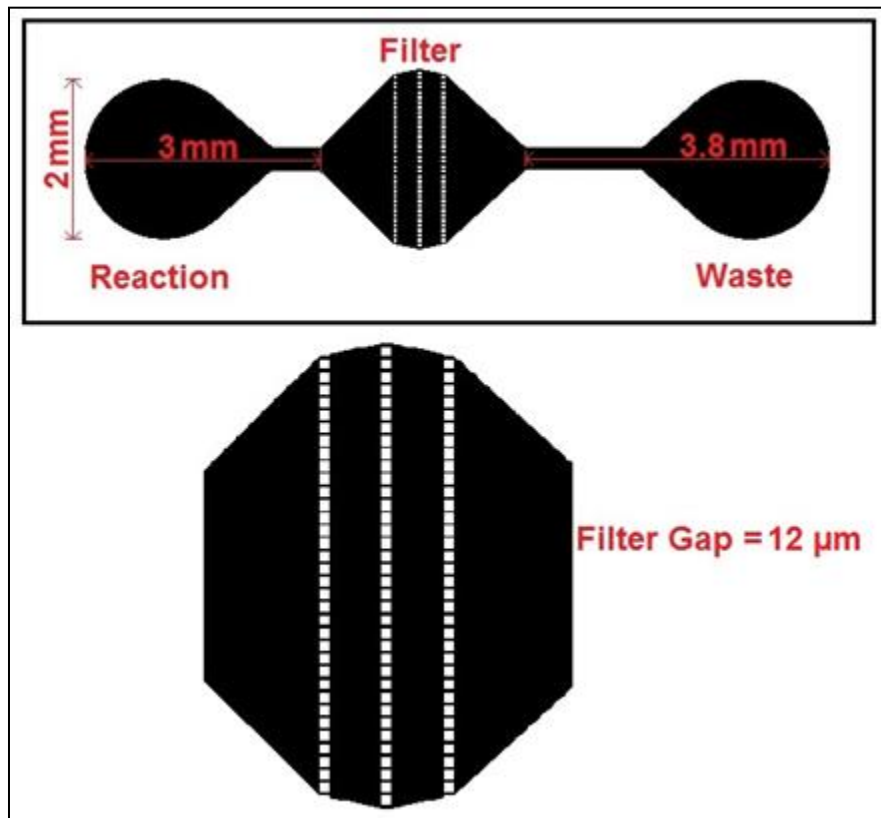
Figure 61: Schematic of the final microfluidic discriminator design. The number next to each column represents the number posts in the column.
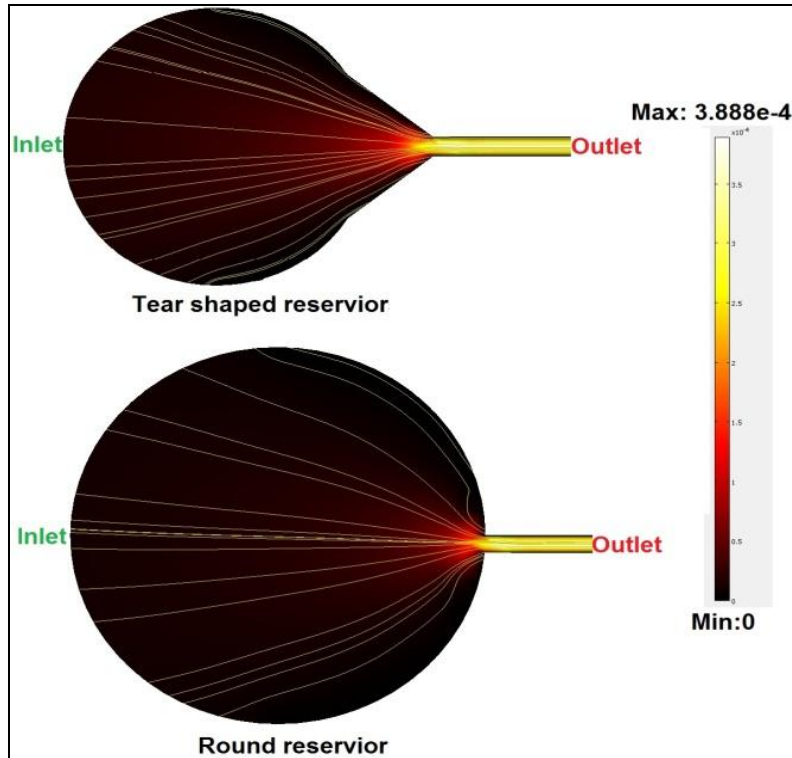
Figure 62: Comparison of the computer simulation of flow rates of the teardrop-shaped and round reservoirs when negative pressure (0.1 µl/min) was applied at the outlet. The concentration of flow lines indicate the velocity field in the area. Higher concentration of flow lines mean greater field velocity and *vice versa*.

7.2.1 Results

We observed that modifying the final design improved the results compared to the previous filter designs. Firstly, the teardrop-shaped reservoirs helped reduce the dead volume in the reservoir and enabled greater amount of agglutinates and microspheres into the channels. This feature minimized the volume of reagents (microspheres and the DNA sample) required to create a visible plug because, with the reduction of the dead volume in the reservoir, all contents of the reservoir could be transported into the channel. Secondly, filter dimensions facilitated easy visualization the retained agglutinates. Figure 63

illustrates the retention of the agglutinates; the experiment was performed with 2 µl of DNA sample from Tube F and 3 µl of washed microspheres.
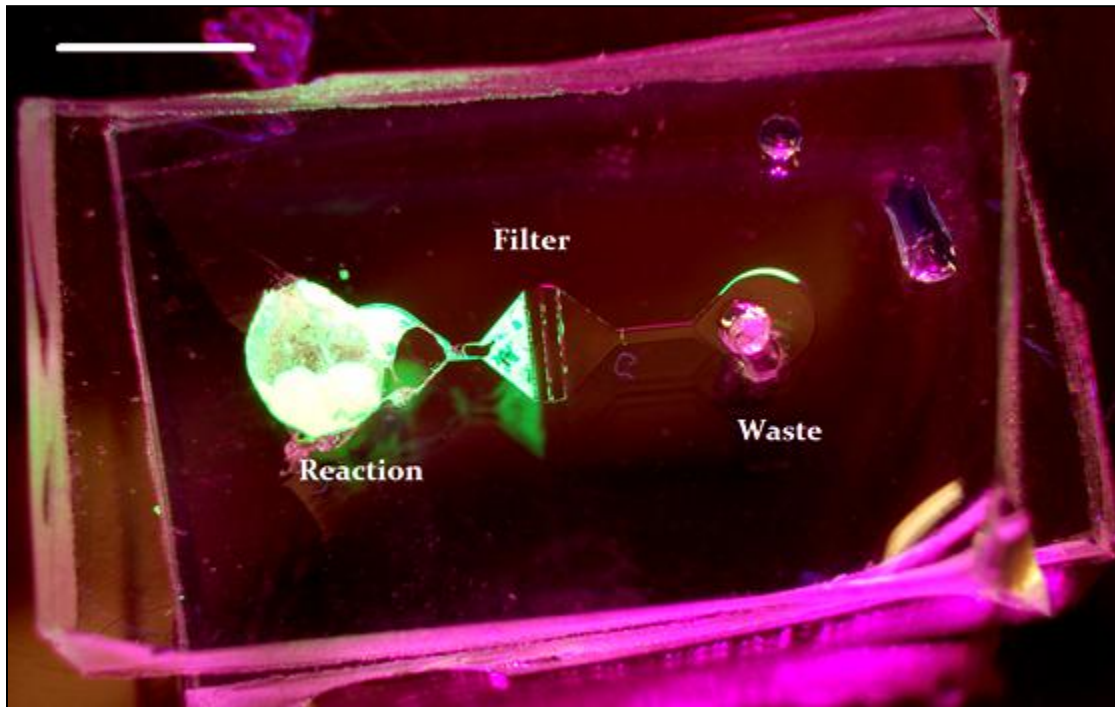
Figure 63: Illustration the retention of agglutinated microspheres in the final microfluidic discriminator design. The scale bar represents 3 mm.

Thirdly, the agglutinates maintained the applied flow velocity (0.1 µl/min) in the filter gaps, unlike the previous designs where the agglutinates gained velocity in the filter gaps and, often, fragmented or dissociated due to hydrodynamic shear caused by the increased velocity of flow.

7.2.2 Optimal depth

As mentioned in section 7.1.4, the depth of the channel influenced the size of the agglutinates that formed inside the channels, which, in turn, affected the effectiveness of discrimination between the agglutinates and the individual

microspheres. Therefore, to determine an optimal depth range of the channel, two new depths (25 μm and 30 μm) of the channel were tested, and the results were compared to the results of channels where the depth was 20 μm. The fabrication process specification used to produce 25 μm and 30 μm deep channels are given in Appendix D and E, respectively. The final fabricated channels were 24.63 μm and 32.35 μm deep. Both the channels showed discrimination, the results indicated that the extent of agglutination in the 20-μm and the 24.63-μm deep channels was similar and no difference in results of the two depths was noticed. However, in 32.35-μm deep channels, the size of the agglutinates was greater in comparison to 20-μm and 24.63-μm deep channels.
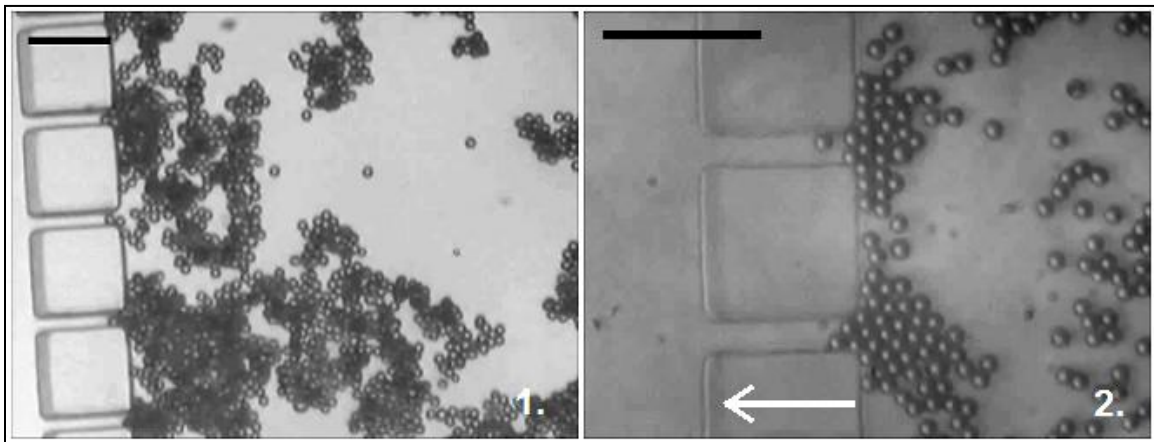
Figure 64: Comparison of the size of agglutinates that blocked the filter gap of 12 μm in: 1) 30.35-μm, and 2) 19.83-μm deep microchannels. The arrow depicts the direction of flow, and both the scale bars represent 50 μm.

The enhanced size of agglutinates in 32.35-μm deep channels was an improvement on the discrimination results of 20-μm and 24.63-μm deep channels because the greater size of agglutinates ensured that, even if the agglutinates broke up into smaller agglutinates (due to the hydrodynamic shear), they were

big enough to create a blockage at the filter gaps. Thus, 32.35 µm deep channels provided the most favourable discrimination results amongst all the microchannels with different depths.

7.3 Summary

After evaluating all the filter designs presented in this chapter, the following conclusions were drawn.

1. Before bonding, microfluidic substrates should be thoroughly cleaned with IPA and water.

2. Bubbles should be removed by filling the channel with PBS/BSA buffer, by applying positive pressure (0.5 µl/min) at waste reservoir.

3. A 12-µm filter gap provide superior results than 7-µm and 10-µm filter gaps because the former compensates for the variation in the size of microspheres compared to the latter ones.

4. A 32.35-µm deep microchannel allowed the formation of the larger agglutinates, thus more efficient discrimination ensues, in comparison to the discrimination generated by the 20-µm and 24.63-µm deep microchannels.

5. Teardrop-shaped reservoirs enable greater volumes of agglutinates entering the microfluidic channels in comparison to the round reservoirs, providing an opportunity to reduce the reaction volume.

6. The increased dimensions of the filter (in the final design) allow easy visualization of the retained agglutinates.

8: CONCLUSION AND FUTURE WORK

8.1 Contribution

This thesis describes a microfluidic system that, under specific physical and biochemical conditions (which can be easily controlled), can simultaneously retain agglutinated microspheres and allow individual microspheres to pass through. This microfluidic discrimination method is a novel and non-subjective screening method for DNA-mediated particle agglutination, which, in turn, may be used as the detection component of an integrated pathogens diagnostic platform. The novel device described in this work performs the discrimination easily and in a highly reproducible manner at a low cost and without the use of any specialized hardware. The microfluidic system is inexpensive, portable, easy-to-use, and disposable. Furthermore, a protocol for the agglutination experiments was developed, and the knowledge gained from this research can help adapt this protocol for detecting different target DNA samples.

8.2 Future work

During the course of the work explained in this thesis, several possible process improvements were identified for future work. Future improvements can be separated into two main categories: improvements in the fluid handling system and improvements related to the PMMA fabrication process.

Successful discrimination requires that the DNA sample to be mixed and incubated with microspheres, and eventually transported to the filter. With the current settings, this fluid handling was performed using pipettes, and the negative pressure was applied using a syringe pump that was operated electrically. To miniaturize the system and finally integrate it into a disease detection device (refer to page 8), this fluid handling operation must be miniaturized. Although MEMS technology has offered several micro-pump designs for such applications, all of them require considerable amounts of electrical power; moreover, these pumps have not been reliable. Therefore, in the future, a novel pumping technique called "Wicking Pump" will be explored. In this scheme, a highly-absorbent material will be used to wick the fluid from the microfluidic channel and create a pressure differential within the channel. This pressure differential will move the fluid, based on the extent of the material absorbency and the fluid volume. Further, the wicking action can be created using a blister pack containing a small volume of fluid in combination with the absorbent material. On the application of pressure with a finger, the blister pack will open, and the wicking action will be initiated. Such a wicking pump set can be combined with unidirectional stopper-valves and configured to move fluid in defined stages into multiple chambers. Furthermore, the mixing of the DNA sample with the microspheres can be enhanced by chaotic mixing. The chaotic mixing can be achieved by making edges of the microchannel irregular.

Additionally, to improve present PMMA microfluidic technology, the problems caused by negative side walls during DUV exposure and microwave

bonding need to be improved to facilitate the fabrication of complex microfluidic channels. As mentioned earlier, the problem of negative sidewalls is caused due to the non-collimated nature of the light during the DUV exposure. This problem can be eliminated by using a light collimator, but, with the present in-house exposure system, it is not a practical solution. The present exposure system utilizes twelve 25 watt germicidal lamps. These germicidal lamps are normally used for killing pathogenic organisms on exposed surfaces and for producing ozone for water disinfection. The strongest peak in the emission spectrum of these lamps is located at 254 nm while their radiation is non-collimated. Therefore, most of the energy from these lamps is absorbed by the collimator itself. Consequently, to compensate for lost energy, the exposure time has to be increased to 48 hours, in comparison to 16 hours (without collimator). A possible solution for this problem is to reconfigure the exposure system with high wattage lamps to increase the input dosage of energy and to use a vacuum inside the exposure chamber to accelerate the exposure process when using a collimator.

Furthermore, to improve the microwave bonding process, a reliable mechanism for removing ethanol has to be developed. At present, a rolled Kimwipe was used to remove the ethanol from the channels by the wicking action, but this method is not helpful when complex geometry (like filter design for the microfluidic discriminator) has to be bonded. This problem can be solved by developing a small suction pump that forcefully removes ethanol from the nooks and corners of the channels.

8.3 Conclusion

This thesis described the fabrication and design of a microfluidic system, developed to distinguish between agglutinated or individual streptavidin-coated microspheres for detecting biotin-labeled DNA. A working microfluidic system was developed and tested for functionality using a microsphere agglutination technique, and the results were seen as the retention of fluorescent agglutinated microspheres—which can be easily extended to the retention of pigmented agglutinated microspheres. The development of the microfluidic system was a two-part process consisting of the development of the microsphere agglutination protocol and the design and fabrication of the discriminator microfluidic system. The microfluidic system was fabricated on PMMA and PDMS. Four iterations of PMMA microfluidic designs were fabricated before concluding that the PMMA microfluidic fabrication process was not suitable for the intricate microfluidic design required for discriminating between agglutinated and individual microspheres, because inefficient microwave bonding and less than optimum channel etching.

The final design was established once an ideal configuration for the filter was determined by the computer simulations of different arrays of the constrictions, which were designed to retain the agglutinates and not individual microspheres. The final microfluidic design was fabricated with PDMS soft lithography process. Furthermore, the PDMS fabrication underwent two redesigns before effective discrimination could be obtained. Effective discrimination was accomplished by fabricating a platform that would allow the

formation of big agglutinates (~200-600 microspheres), maintaining the flow

velocity throughout the channel such that these agglutinates did not dissociate

under the hydrodynamic shear, and retaining the agglutinates at the filter while

allowing single microspheres to pass through.

The end result was a working microfluidic system that detects amplified

biotinylated DNA—a typical end product in diagnostic pathogen detection. While

improvements can be implemented to the work presented in this thesis, it forms a

basis for the development of a marketable biosensor prototype. This research

addresses the target area of biomedical technologies, by integrating molecular

biochemistry, analytical biochemistry, and microfluidic engineering. Further, the

work described in this thesis, along with DNA amplification, can be utilized to

develop disposable and handheld POCT systems to detect disease and

bioterrorism pathogens.

APPENDIX A: RECIPES FOR THE REAGENTS USED IN THE RESEARCH

Table A- 1: Recipe for Tris- EDTA (TE) buffer.

Recipe for TE				
Volume	**Reagent**	**Manufacturer**	**Lot #**	**Final concentration**
10 ml	1M Tris-HCl pH 8.0	Bioshop Canada Inc.	7G4741	10mM
2 ml	0.5M EDTA pH 8.0	Bioshop Canada Inc.	0D15736	1 mM
988 ml	ddH$_2$O			

Table A- 2: Recipe for PBS/BSA binding buffer.

Recipe for PBS/BSA Binding Buffer		
- Prepare 0.1M phosphate buffer (pH 7.4) by adding 0.1M NaH$_2$PO$_4$ to 0.1M Na$_2$HPO$_4$, until pH reaches7.4. - Place 20 ml of the 0.1M phosphate buffer (pH 7.4) in a 100-ml graduated cylinder. - Add 0.88g NaCl and 1g bovine serum albumin (BSA) and make up the volume to 100ml. - Check the pH of the final solution. If necessary, adjust the pH to 7.4 by adding dilute HCl or NaOH.		
Reagents	**Manufacturer**	**Lot #**
NaH$_2$PO$_4$	BDH Inc.	108718/2882
Na$_2$HPO$_4$	BDH Inc.	107207/28667
NaCl	EMD Chemicals Inc.	47253741
BSA	Bioshop Canada Inc.	YT33304

APPENDIX B: FABRICATION PROCESS SPECIFICATIONS: 10 μM FEATURE HEIGHT IN SU-8 MASTER

Table B- 1: Process parameters for producing 10μm high SU-8 features.

Process	Specifications
Spin coat SU-8 2010	5 seconds @ 500rpm, and 40 seconds @ 4000rpm
Edgebead removal	Not done(not required)
Soft Bake	5 minutes @ 90°C on hotplate
Expose	10 seconds @ 400-nm UV
Post bake	5 minutes @ 90°C on hotplate
Develop	3 minutes in SU-8 Developer(MicroChem, MA, USA)
Hard Bake	5 minutes @ 90°C on hotplate

APPENDIX C: FABRICATION PROCESS SPECIFICATIONS: 20 µM FEATURE HEIGHT IN SU-8 MASTER

Table C- 1: Fabrication process specifications for producing 20µm thick SU-8 mold.

Process	Specifications
Spin coat SU-8 2010	5 seconds @ 500rpm, and 40 seconds @ 1100rpm
Edgebead removal	Not done (not required)
Soft Bake	3.5 minutes @ 95°C on hotplate
Expose	10 seconds @ 400-nm UV
Post bake	3.5 minutes @95°C on hotplate
Develop	3 minutes in SU-8 Developer (MicroChem, MA, USA)
Hard Bake	5 minutes @ 95°C on hotplate

APPENDIX D: FABRICATION PROCESS SPECIFICATIONS: 25 µM FEATURE HEIGHT IN SU-8 MASTER

Table D- 1: Fabrication process specifications for producing 25µm thick SU-8 mold.

Process	Specifications
Spin coat SU-8 2025	5 seconds @ 500rpm, and 40 seconds @ 3500rpm
Edgebead removal	Not done (not required)
Soft Bake	3.5 minutes @ 95°C on hotplate
Expose	10 seconds @ 400-nm UV
Post bake	3.5 minutes @95°C on hotplate
Develop	3 minutes in SU-8 Developer (MicroChem, MA, USA)
Hard Bake	5 minutes @ 95°C on hotplate

APPENDIX E: FABRICATION PROCESS SPECIFICATIONS: 30 µM FEATURE HEIGHT IN SU-8 MASTER

Table E- 1: Fabrication process specifications for producing 30µm thick SU-8 mold.

Process	Specifications
Spin coat SU-8 2025	5 seconds @ 500rpm, and 40 seconds @ 3000rpm
Edgebead removal	Not done (not required)
Soft Bake	3.5 minutes @ 95°C on hotplate
Expose	10 seconds @ 400-nm UV
Post bake	3.5 minutes @95°C on hotplate
Develop	3 minutes in SU-8 Developer (MicroChem, MA, USA)
Hard Bake	5 minutes @ 95°C on hotplate

APPENDIX F: EFFECT OF CHAOTIC MIXING ON AGGLUTINATION

The amount of agglutination can be enhanced by continuously mixing the DNA sample with the microspheres. The continuous mixing can be achieved by chaotic mixing. To verify this, agglutination experiment was conducted in the silk screen fabricated 150-µm wide microchannel [75]. The irregular edges of the microchannel cause chaotic mixing of the reaction and thus, enhance the amount of agglutination. The bleeding of the ink, during the fabrication process, caused these irregular edges. Figure F-1 shows the comparison of agglutination in PMMA microfluidic devices fabricated by DUV exposure and silkscreen fabrication techniques.

Irregular channel edges   Straight channel edges
(Silk screen fabrication)   (DUV exposure fabrication)
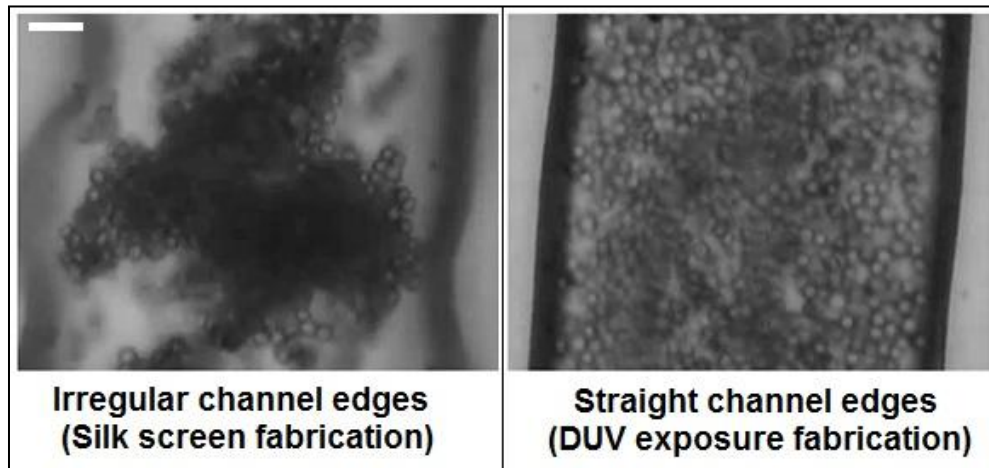
Figure F-1: The comparison of the size of the agglutinates formed by 2 µl of DNA sample from Tube A and 3 µl of washed microspheres in silk screen fabricated 150-µm wide, 58-µm deep microchannel (left) and in 150-µm wide, 61-µm deep microchannel fabricated by DUV exposure technique (right). Scale bar represents 24 µm.

The results showed that size of agglutinates in the silk screen fabricated microchannel were ~10 times greater than agglutinates in the microchannel fabricated using DUV exposure. Almost 50% of the microspheres in the microchannel fabricated by DUV exposure remained as singlets, whereas, in the silk screen fabricated microchannel almost, 99% of microspheres formed agglutinates and only 1% of microspheres remained singlet. Therefore, in the future, this chaotic mixing effect can be incorporated in the final microfluidic discriminator design to provide enhanced agglutination, and, consequently, improve discrimination results.

REFERENCES

[1]   C. P. Price, A. S. John, and J. M. Hicks, *Point-of-care testing*: AACC Press, 2004.

[2]   I. Schimke, "Quality and timeliness in medical laboratory testing," *Anal Bioanal Chem,* vol. 393, pp. 1499-1504, Mar 2009.

[3]   G. J. Kost, L. E. Kost, A. Suwanyangyuen, S. K. Cheema, C. Curtis, S. Sumner, J. Yu, and R. Louie, "Emergency Cardiac Biomarkers and Point-of-Care Testing: Optimizing Acute Coronary Syndrome Care Using Small-World Networks In Rural Settings," *Point Care,* vol. 9, pp. 53-64, Jun 2010.

[4]   R. Daw and J. Finkelstein, "Lab on a chip," *Nature,* vol. 442, p. 367, 2006.

[5]   C. H. Ahn, J. Choi, G. Beaucage, J. H. Nevin, J. Lee, A. Puntambekar, and J. Y. Lee, "Disposable smart lab on a chip for Point-of-care clinical diagnostics," in *IEEE*, 2004, pp. 154-173.

[6]   R. Ehrnstrom, "Miniaturization and integration: challenges and breakthroughs in microfluidics," *Lab Chip,* vol. 2, pp. 26N-30N, May 2002.

[7]   M. A. Burns, B. N. Johnson, S. N. Brahmasandra, K. Handique, J. R. Webster, M. Krishnan, T. S. Sammarco, P. M. Man, D. Jones, D. Heldsinger, C. H. Mastrangelo, and D. T. Burke, "An integrated nanoliter DNA analysis device," *Science,* vol. 282, pp. 484-487, Oct 16 1998.

[8]   E. Verpoorte, "Microfluidic chips for clinical and forensic analysis," *Electrophoresis,* vol. 23, pp. 677-712, Mar 2002.

[9]   T. Dinh, G. Griffin, D. Stokes, and A. Wintenberg, "Multi-functional biochip for medical diagnostics and pathogen detection," *Sensors and Actuators Biochem Biophys Res Commun,* vol. 90, pp. 104-111, 2003.

[10]   L. J. Kricka, "Microchips, microarrays, biochips and nanochips: personal laboratories for the 21st century," *Clin Chim Acta,* vol. 307, pp. 219-223, May 2001.

[11]   B. L. Ziober, M. G. Mauk, E. M. Falls, Z. Chen, A. F. Ziober, and H. H. Bau, "Lab-on-a-chip for oral cancer screening and diagnosis," *Head Neck,* vol. 30, pp. 111-121, Jan 2008.

[12]   I. Lauks, "Microfabricated biosensors and microanalytical systems for blood analysis," *Acc. Chem. Res.,* vol. 31, pp. 317-324, 1998.

[13]   G. M. Whitesides, "The origins and the future of microfluidics," *Nature,* vol. 442, pp. 368-373, Jul 27 2006.

[14]   S. Shoji and M. Esashi, "Microflow device and systems," *J. Micromech. Microeng.,* vol. 4, pp. 157-171, 1994.

[15]   W. Schomburg, J. Fahrenberg, D. Maas, and R. Rapp, "Active valves and pumps for microfluidcs," *J. Micromech. Microeng.,* vol. 3, pp. 216–218, 1993.

[16] M. Koch, N. Harris, A. G. R. Evans, N. M. White, and A. Brunnschweiler, "A novel micromachined pump based on thick-film piezoelectric actuation," *Sensors and Actuators A: Physical,* vol. 70, pp. 98-103, 1998.

[17] A. V. Lemoff and A. P. Lee, "An AC magnetohydrodynamic micropump," *Sensors and Actuators B: Chemical,* vol. 63, pp. 178-185, 2000.

[18] C. H. Ahn and J.-W. Choi, "Microfluidic Devices and Their Applications to Lab-on-a-Chip," in *Springer Handbook of Nanotechnology*, B. Bhushan, Ed., ed: Springer Berlin Heidelberg, 2010, pp. 503-530-530.

[19] N. L. Jeon, D. T. Chiu, C. J. Wargo, H. Wu, I. S. Choi, J. R. Anderson, and G. M. Whitesides, "Design and Fabrication of Integrated Passive Valves and Pumps for Flexible Polymer 3-Dimensional Microfluidic Systems," ed: Springer Verlag (Germany), 2002.

[20] D. J. Beebe, R. J. Adrian, M. G. Olsen, M. A. Stremler, H. Aref, and B.-H. Jo, "Passive mixing in microchannels: Fabrication and flow experiments," *Mécanique & Industries,* vol. 2, pp. 343-348.

[21] A. D. Stroock, S. K. W. Dertinger, A. Ajdari, I. Mezić, H. A. Stone, and G. M. Whitesides, "Chaotic Mixer for Microchannels," *Science,* vol. 295, pp. 647-651, 2002.

[22] T. A. Desai, D. J. Hansford, and M. Ferrari, "Micromachined interfaces: new approaches in cell immunoisolation and biomolecular separation," *Biomolecular Engineering,* vol. 17, pp. 23-36, 2000.

[23] F. J. Martin and C. Grove, "Microfabricated Drug Delivery Systems: Concepts to Improve Clinical Benefit," *Biomedical Microdevices,* vol. 3, pp. 97-108-108, 2001.

[24] F. Benito-Lopez, S. Coyle, R. Byrne, A. Smeaton, N. E. O'Connor, and D. Diamond, "Pump Less Wearable Microfluidic Device for Real Time pH Sweat Monitoring," *Procedia Chemistry,* vol. 1, pp. 1103-1106, 2009.

[25] T. Nagakura, K. Ishihara, T. Furukawa, K. Masuda, and T. Tsuda, "Auto-regulated osmotic pump for insulin therapy by sensing glucose concentration without energy supply," *Sensors and Actuators B: Chemical,* vol. 34, pp. 229-233, 1996.

[26] P. C. H. Li and P. H. Li, *Microfluidic lab-on-a-chip for chemical and biological analysis and discovery*: Taylor & Francis/CRC Press, 2006.

[27] Y. Chen, L. Zhang, and G. Chen, "Fabrication, modification, and application of poly(methyl methacrylate) microfluidic chips," *Electrophoresis,* vol. 29, pp. 1801-1814, 2008.

[28] K.-S. Yun and E. Yoon, "Fabrication of complex multilevel microchannels in PDMS by using three-dimensional photoresist masters," *Lab on a Chip,* vol. 8, pp. 245-250, 2008.

[29] H. Becker and L. E. Locascio, "Polymer microfluidic devices," *Talanta,* vol. 56, pp. 267-287, 2002.

[30] M. Haiducu, M. Rahbar, I. G. Foulds, R. W. Johnstone, D. Sameoto, and M. Parameswaran, "Deep-UV patterning of commercial grade PMMA for low cost, large-scale microfluidics," *J. Micromech. Microeng.,* vol. 18, p. 8, 2008.

[31] Z. Wu, N. Xanthopoulos, F. Reymond, J. S. Rossier, and H. H. Girault, "Polymer microchips bonded by O2-plasma activation," *Electrophoresis,* vol. 23, pp. 782-790, 2002.

[32] Y. Wang and M. Ferrari, "Surface modification of micromachined silicon filters," *Journal of Materials Science,* vol. 35, pp. 4923-4930-4930, 2000.

[33] M. J. Heller, "DNA microarray technology: devices, systems, and applications," *Annu Rev Biomed Eng,* vol. 4, pp. 129-153, 2002.

[34] P. J. Asiello and A. J. Baeumner, "Miniaturized isothermal nucleic acid amplification, a review," *Lab Chip,* vol. 11, pp. 1420-1430, Apr 21 2011.

[35] S.-J. Wu, A. Chan, and C. I. Kado, "Detection of PCR amplicons from bacterial pathogens using microsphere agglutination," *Journal of Microbiological Methods,* vol. 56, pp. 395-400, 2004.

[36] H. Cai, Y. Xu, P.-G. He, and Y.-Z. Fang, "Indicator Free DNA Hybridization Detection by Impedance Measurement Based on the DNA-Doped Conducting Polymer Film Formed on the Carbon Nanotube Modified Electrode," *Electroanalysis,* vol. 15, pp. 1864-1870, 2003.

[37] T.-Y. Lee and Y.-B. Shim, "Direct DNA Hybridization Detection Based on the Oligonucleotide-Functionalized Conductive Polymer," *Analytical Chemistry,* vol. 73, pp. 5629-5632, 2001.

[38] L. He, M. D. Musick, S. R. Nicewarner, F. G. Salinas, S. J. Benkovic, M. J. Natan, and C. D. Keating, "Colloidal Au-Enhanced Surface Plasmon Resonance for Ultrasensitive Detection of DNA Hybridization," *Journal of the American Chemical Society,* vol. 122, pp. 9071-9077, 2000.

[39] H. Peng, L. Zhang, T. H. M. Kjällman, and C. Soeller, "DNA Hybridization Detection with Blue Luminescent Quantum Dots and Dye-Labeled Single-Stranded DNA," *Journal of the American Chemical Society,* vol. 129, pp. 3048-3049, 2007.

[40] H. Cai, Y. Xu, N. Zhu, P. He, and Y. Fang, "An electrochemical DNA hybridization detection assay based on a silver nanoparticle label," *Analyst,* vol. 127, pp. 803-808, 2002.

[41] J. C. Pommerville, *Alcamo's Fundamentals of Microbiology: Body Systems*: Jones and Bartlett Publishers, 2009.

[42] E. Verpoorte, "Focus Beads and chips: new recipes for analysis," *Lab on a Chip,* vol. 3, pp. 60-68, 2003.

[43] C. M. Plotz and J. M. Singer, "The latex fixation test. I. Application to the serologic diagnosis of rheumatoid arthritis," *Am J Med,* vol. 21, pp. 888-892, Dec 1956.

[44] M. B. Meza, "Bead-based HTS applications in drug discovery," *Drug Discovery Today,* vol. 5, pp. 38-41, 2000.

[45] L. B. Bangs, "New developments in particle-based immunoassays: Introduction," *Pure & Appl. Chem.,* vol. 68, pp. 1873-1879, 1996.

[46] D. A. A. Vignali, "Multiplexed particle-based flow cytometric assays," *Journal of Immunological Methods,* vol. 243, pp. 243-255, 2000.

[47] A. S. Brodsky, A. P. Johnston, M. Trau, and P. A. Silver, " Analysis of RNA protein interactions by flow cytometry," *Curr. Opin. Mol. Ther.,* vol. 5, pp. 235-240, 2003.

[48] Z. J. Attar, M. L. Chance, S. el-Safi, J. Carney, A. Azazy, M. El-Hadi, C. Dourado, and M. Hommel, "Latex agglutination test for the detection of urinary antigens in visceral leishmaniasis," *Acta Tropica,* vol. 78, pp. 11-16, 2001.

[49] T. R. Kline, M. K. Runyon, M. Pothiawala, and R. F. Ismagilov, "ABO, D Blood Typing and Subtyping Using Plug-Based Microfluidics," *Analytical Chemistry,* vol. 80, pp. 6190-6197, 2008.

[50] M. Ramasubramanian and S. Alexander, "An integrated fiberoptic–microfluidic device for agglutination detection and blood typing," *Biomedical Microdevices,* vol. 11, pp. 217-229-229, 2009.

[51] N. Pamme, R. Koyama, and A. Manz, "Counting and sizing of particles and particle agglomerates in a microfluidic device using laser light scattering: application to a particle-enhanced immunoassay," *Lab on a Chip,* vol. 3, pp. 187-192, 2003.

[52] X. Song, J. Shi, and B. Swanson, "Flow Cytometry-Based Biosensor for Detection of Multivalent Proteins," *Analytical Biochemistry,* vol. 284, pp. 35-41, 2000.

[53] I. V. Surovtsev, M. A. Yurkin, A. N. Shvalov, V. M. Nekrasov, G. F. Sivolobova, A. A. Grazhdantseva, V. P. Maltsev, and A. V. Chernyshev, "Kinetics of the initial stage of immunoagglutionation studied with the scanning flow cytometer," *Colloids and Surfaces B: Biointerfaces,* vol. 32, pp. 245-255, 2003.

[54] R. Chunara, M. Godin, S. M. Knudsen, and S. R. Manalis, "Mass-based readout for agglutination assays," *Applied Physics Letters,* vol. 91, pp. 193902-193903, 2007.

[55] O. Deegan, K. Walshe, K. Kavanagh, and S. Doyle, "Quantitative detection of C-reactive protein using phosphocholine-labelled enzyme or microspheres," *Analytical Biochemistry,* vol. 312, pp. 175-181, 2003.

[56] W. J. Litchfield, A. R. Craig, W. A. Frey, C. C. Leflar, C. E. Looney, and M. A. Luddy, "Novel shell/core particles for automated turbidimetric immunoassays," *Clin Chem,* vol. 30, pp. 1489-1493, Sep 1984.

[57] R. W. Johnstone, I. G. Foulds, and M. Parameswaran, "Self-sacrificial surface micromachining using poly(methyl methacrylate)," *J. Micromech. Microeng.,* vol. 18, p. 7, 2008.

[58] R. Truckenmuller, P. Henzi, D. Herrmann, V. Saile, and W. K. Schomburg, "A new bonding process for polymer micro- and nanostructures based on near-surface degradation," presented at the Micro Electro Mechanical Systems, 2004. 17th IEEE International Conference on MEMS, 2004.

[59] U. L. Systems. (May 2, 2011). *VLS 3.60*. Available: http://www.ulsinc.com/english/downloads/vls360.pdf

[60] M. Haiducu, "Low-cost microfluidics on commercial grade Poly(Methyl Methacrylate) (PMMA) using deepUV patterning," Masters of applied science, School of engineering science, Simon Fraser university, Burnaby, 2009.

[61] M. Rahbar, S. Chhina, D. Sameoto, and M. Parameswaran, "Microwave-induced, thermally assisted solvent bonding for low-cost PMMA

microfluidic devices," *Journal of Micromechanics and Microengineering,* vol. 20, p. 015026, 2010.

[62] J. C. McDonald, D. C. Duffy, J. R. Anderson, D. T. Chiu, H. Wu, O. J. A. Schueller, and G. M. Whitesides, "Fabrication of microfluidic systems in poly(dimethylsiloxane)," *Electrophoresis,* vol. 21, pp. 27-40, 2000.

[63] H. Makamba, J. H. Kim, K. Lim, N. Park, and J. H. Hahn, "Surface modification of poly(dimethylsiloxane) microchannels," *Electrophoresis,* vol. 24, pp. 3607-3619, 2003.

[64] K. Haubert, T. Drier, and D. Beebe, "PDMS bonding by means of a portable, low-cost corona system," *Lab on a Chip,* vol. 6, pp. 1548-1549, 2006.

[65] Microchem. (2011, May 1,2011). *Processing guidelines for: SU-8 2000.5, SU-8 2002, SU-8 2005, SU-8 2007, SU-8 2010 and SU-8 2015SU-.* Available: http://www.microchem.com/products/pdf/SU-82000DataSheet2000_5thru2015Ver4.pdf

[66] G. Karp, *Cell and Molecular Biology: Concepts and Experiments*: John Wiley & Sons, 2009.

[67] R. J. McMahon, *Avidin-biotin interactions: methods and applications*: Humana, 2008.

[68] J. DeChancie and K. N. Houk, "The origins of femtomolar protein-ligand binding: hydrogen-bond cooperativity and desolvation energetics in the biotin-(strept)avidin binding site," *J Am Chem Soc,* vol. 129, pp. 5419-5429, May 2 2007.

[69] (April 28, 2011). *Oligo calculator*. Available: http://www.bioinformatics.org/JaMBW/3/1/9/index.html

[70] I. Willner and E. Katz, *Bioelectronics: from theory to applications*: Wiley-VCH, 2005.

[71] Polysciences. (May 1, 2011). *Streptavidin and Biotin Conjugated Microspheres: Technical Data Sheet 616*. Available: http://www.polysciences.com/SiteData/docs/TDS%20616/cbd811c649141ed4402d71db2fd159ff/TDS%20616.pdf

[72] H. C. Lichstein and M. H. Soule, "Studies of the Effect of Sodium Azide on Microbic Growth and Respiration: IV. The Effect of Sodium Azide on Glucose Fermentation and Lactic Acid Production by Streptococci and Lactobacilli," *J Bacteriol,* vol. 47, pp. 253-257, Mar 1944.

[73] U. Biotechnologies. (May 12, 2011). *Mycobaterium Tuberculosis (TB) Isothermal Amplification Diagnostic Kit*. Available: http://www.bioustar.com/en/manage/orderNewProduct.jsp?pid=73

[74] COMSOL. (May 6, 2011). *Comsol version 3.5a*. Available: http://www.uk.comsol.com/shared/downloads/products/releasenotes_35a.pdf

[75] A. A. Kaleibar, M. Rahbar, M. Haiducu, and A. M. Parameswaran, "Patterning of PMMA microfluidic parts using screen printing process," San Francisco, California, USA, 2010, pp. 75930E-75938.